RESEARCH ON APPLYING THE SELF-PIERCE RIVETING (SPR) FOR DIE CASTING ALUMINUM ALLOYS

by

Xuzhe Zhao

A Dissertation

Submitted to the Faculty of Purdue University

In Partial Fulfillment of the Requirements for the Degree of

Doctor of Philosophy

Department of Technology

West Lafayette, Indiana

May 2019

THE PURDUE UNIVERSITY GRADUATE SCHOOL
STATEMENT OF COMMITTEE APPROVAL

Dr. Xiaoming Wang, Chair

Department of Engineering Technology

Dr. Haiyan Zhang

Department of Engineering Technology

Dr. Milan Rakita

Department of Engineering Technology

Dr. Yeouli Chu

Ryobi Die Casting

Approved by:

Dr. Kathryne A. Newton

Head of the Graduate Program

All my research and contribution at Purdue will be dedicated to my wife, Chengxin, and all other family members behind me in the past 4 years. Without their support, I will not have the current achievement. And I am very glad to be their son, husband and father.

ACKNOWLEDGMENTS

I will give my sincere respect to Dr. Qingyou Han. He played as a mentor, a friend, and a family member to provide support for my study and routine life at Purdue. He will be a lifelong mentor that I wish to share my rest of life.

The faculties at mechanical engineering technology department gave a great help for my school career. They were friendly and helpful to assist me for each of my requests. Without their help, I will not have my current achievements.

Dr. Yeouli Chu and Patrick Cheng from Ryobi Die Casting provided a great help in past two years. My two summer internships at Ryobi was significant to my life. The experience at Ryobi is hardly to be ignored for my career.

TABLE OF CONTENTS

LIST OF TABLES

LIST OF FIGURES

LIST OF ABBREVIATIONS

SPR	Self-Pierce Riveting
RSW	Resistance Spot Welding
UTS	Ultimate Tensile Strength
YS	Yielding Strength
T_{min}	The minimal remaining bottom material thickness
Mg_2Si	Magnesium Silicide
SEM	Scanning Electron Microscopy
S/P	Small Crack fraction
L/P	Large Crack Fraction
FEA	Finite Element Analysis

GLOSSARY

Self-Pierce Riveting– A cold forming technique, which is used for joining two or multiple material sheets mechanically by a rivet.

Rivet Head Height– The distance between the top cap of the rivet and top sheet material. It is a significant parameter to determine the quality of a SPR joint.

The Remaining Bottom Material Thickness– The remaining distance of the bottom sheet after joining.

Interlock Distance– The distance that the rivet shank inserts into the bottom sheet.

Shear Test– A joint formed by two one times four inches material plates is pulled under tension until the joint fails.

Shear Strength– The strength of a joint can withstand under the SPR shear test. Shear strength is usually expressed by load verse displacement.

Fatigue Strength– The strength of a joint can withstand under the SPR fatigue test. Fatigue strength is usually expressed by load verse number of cycle.

Material Stack– A stack is formed by two or multiple material sheets.

Rivetability– To describe the availability of a material sheet by using riveting. It could be related to the mechanical properties and the microstructure of the material.

Castability– The ability to obtain a qualified casting. For aluminum alloys, castability usually describes the fluidity of the material during casting.

Joint Strength– The magnitude of resistance to against joint failure. Joint strength in this research is determined by the shear test.

ABSTRACT

Author: Zhao, Xuzhe. Ph.D.
Institution: Purdue University
Degree Received: May 2019
Title: Research on Applying the Self-Pierce Riveting (SPR) for Die Casting Aluminum Alloys
Major Professor: Xiaoming Wang

Self-pierce riveting as a relative new technology has been used by automotive industry for decades. Because of the several benefits of the SPR technique, it has been widely used for joining the similar or dissimilar materials to satisfy the light-weighting requirements of automobile. There were many researchers and automotive manufacturers that had been investigated the SPR by experiments and applied this technique to their products. The SPR was designed for joining the materials with sufficient ductility because the joining process was going to introduce the large plastic deformation on the joint button area. Die casting aluminum alloy products became more and more popular to be used for structural components. However, the casting aluminum components have relative low ductility than the wrought alloy product. The cracking problems were easy to occur during the riveting process.

In terms of the cracking issues on die casting aluminum products, an analysis was conducted in this study to investigate the influence of composition on cracking problem. And the cracking mechanism was also analyzed and summarized. Corresponding to the influence of silicon content difference and silicon morphology, heat treatment was used to modify the eutectic silicon morphology of the casting aluminum alloys to improve the rivetability. Once the silicon network was broken by the heat treatment, the rivetability of die casting aluminum was drastically increased and the cracks on joint button were also suppressed. Under the effect of heat treatment, the joint performance was tightly related to the variation of the eutectic silicon phase and the cracks on the joint button. The joint strength was obtained by shear test to investigate the influence of heat treatment and die depth. A novel cracking statistics has been generated and used to calculate the cracks on

the joint button. Eventually, a comprehensive joint performance was obtained by taking into consideration of joint strength, heat treatment and die depth.

Finally, the simulation of the SPR process was conducted and analyzed by FORGE. The die depth as the variable was used to investigate the strain and fracture distribution in cross-section view of the joint. In terms of the initial results of the simulation, the die cavity with various sidewall incline angles was simulated to find the optimal die cavity geometry in order to improve the rivetability of the bottom material sheet.

CHAPTER 1. INTRODUCTION

1.1 Background

Nowadays, automotive industry is always seeking for the solutions to accommodate the new environmental regulations from governments in the world wide. Because a large amount of chemicals, such as carbon dioxides, mainly exhausted by the millions of automobiles. The governments have to setup the regulations to control the exhaust from automobiles in consideration of the sustainability of earth. Instead of developing the new energy vehicles, the light-weighting technology plays a significant role to solve the excessive exhaust issue from the traditional gasoline vehicles. The research was conducted by Aluminum Association Inc. (Hadley, Das, & Miller, 2000) indicated that the 10% reduction of vehicle mass could save 6-8% gasoline. And 100 pounds reduction from the total weight of vehicle could save 3.4 5.3 miles in 1000 miles driving.

The light-weighting technology has been developed for several decades. The most effective way of applying light-weighting concept for automobiles is replacing the current materials by the lighter one. As one of the strong candidates, aluminum alloys become to the most compatible material. Aluminum alloy products are mainly composed of the wrought and casting parts. The wrought aluminum parts have enough ductility and strength, and they have been used for many fields, including automotive manufacturing, aircraft manufacturing and home appliances etc. The casting aluminum parts compared to the wrought parts have the less ductility and lower strength. But casting aluminum alloys with the excellent castability have been widely used for industry to fabricate the complex structural components.

Welding is always the first and the foremost choice to join the different parts together for automobile. However, the weldability of the aluminum alloy parts is worse than the steel parts. Self-piercing riveting (the SPR) was developed to join the materials in a mechanical forming method. However, the riveting process will introduce the severe plastic deformation to the joined materials. The casting aluminum alloy parts with the

poor ductility could experience the quality issues, include cracking, low joint strength etc. In order to successfully apply the SPR to the brittle materials, the research and study of the SPR process need to be conducted in advance.

1.2 Self-Pierce Riveting

Self-piercing riveting as a young joining technique has been used for the industries for decades. It was originally invented in 1960s and rapidly developed in the past two decades (D. Li et al., 2017). Due to the lightweight trend for automotive industries, the SPR was accepted and applied for joining the structural and other components in automobile because of the benefits in weight and simplicity. In 1972, Hulbert studied the SPR and compared with the traditional riveting (Hulbert, 1972). In 1975, Bifurcated and Tubular Rivet Co. Ltd. used the SPR system to successfully join the handle on the lid of a paint can using water-tight joints (D. Li et al., 2017). A following discussion was conducted by Gausden and Gunn from Bifurcated and Tubular Rivet Co. Ltd about the application of the SPR in 1976 (Sunday, 1983). When the time shifted to 1980s, the SPR started to enter the horizon of automotive industries because of the light-weighting for automobile could be accomplished by the SPR joining technique. In order to join aluminum structure component and other material components, the traditional joining techniques, such as spot welding (SW) and resistant spot welding (RSW), were hard to accomplish the joining. As a result, the SPR became to an alternative choice to join aluminum and other material parts. Nevertheless, the large-scale application and research work of the SPR technique became to an issue until the beginning of 1990s. Patrick and Sharp worked on the research of comparing the SPR with other joining techniques in joining aluminum body structure in 1992 (Patrick & Sharp, 1992). At the same time, Edwards reported that the SPR was a potential method to replace spot welding for automotive industry [6]. One year later, Doo introduced the Henrob the SPR system and reported its the application in industry (Doo, 1993). Bokhari followed by Doo was working on Henrob the SPR facility and showed the SPR application (Bokhari, 1995). The advantages of the SPR technique comparing to the traditional joining has been

summarized in the following (D. Li et al., 2017): 1. The SPR is environmental friendly, there is no restrict working condition requirement compared to welding; 2. The SPR can be used to join the similar and different materials and the adhesive can be applied during the operation; 3. Compared to traditional riveting, there is no requirement for pre-drilled holes and alignment; 4. The short cycle time, long facility life with at least 200,000 operation cycles and low energy consumption; 5. Automation and process monitoring are easy to be applied; 6. No specific treatment required for the joint materials. 7. With high static strength and long fatigue life for the SPR joints.

However, the disadvantages of the SPR in the following could limit its application: 1. Required enough space to conduct the process; 2. A joint button appears on the one side; 3. The high force facility is required for the SPR facility. 4. Not suitable for brittle materials.

CHAPTER 2. LITERATURE REVIEW

2.1 Introduction

The SPR was initially applied in automotive industry by Audi since 1993 (Abe, Kato, & Mori, 2006). Because of the all-aluminum body design in 1993 Audis A8, there were about 1100 SPR rivets used for A8 model (D. Li et al., 2017). When Audi took advantages from the SPR technique in A8 model, the following model Audi A2 started to use the SPR to replace spot welding on Audi second generation space frame. There were about 1800 SPR rivets that been used in Audi A2 (Miller et al., 2000). And Audi TT couple model used about 1600 SPR rivets (*Audi TT Coup 07-Body*, 2013). After the SPR was applied by Audi, Jaguar Land Rover (JLR) brought the SPR technique to their industry and applied it in large scale. XJ and XK model from JLR with a monocoque structure design and all-aluminum body used about 3600 SPR rivets and 2400-2600 SPR rivet, respectively (Mortimer, 2001). The new Range Rover model also used about 3800 SRP rivets. And Jaguar XE and new XF with aluminum body are using the SPR as their major joining technique. Because of the excellent fatigue life of the SPR joint, Volvo used the SPR to replace resistant spot welding (RSW) to join the high strength steels on their FH series trucks (Bonde, 1996). BMW and Daimler also applied the SPR technique as their main joining technology for their products (*Automotive*, 2013). Since the SPR technique was initially developed and applied in Europe, the European automotive industry has tested and applied for a while. Then North America industries paid attention on this technique and applied the SPR to their products. Ford has used the SPR their recent F150 pick-up truck. There were 2000-2700 SPR rivets have been used for this pick-up. And Ford produced approximately 1 million of aluminum F150 bodies in the first year production. It is a significant step forward to apply the SPR technique to a large-scale massive vehicle production (Weber, 2015). Figure 2.1 shows the main body structure of Ford F150 and Jaguar XJ joined by the SPR technique located at Henrob in New Hudson, Michigan.

Figure 2.1. Ford F150 and Jaguar XJ at Henrob

The SPR as a research topic has been explored since 1970s. Figure 2.2 shows the trend of research work focused on the SPR technique in the past several decades (D. Li et al., 2017). The research experienced an explosive increase from 2006. It could be related to the application of SPR in automotive industry since Audi use the SPR as their major joining technology. Sunday as one of the SPR research pioneers reviewed the SPR system and processing parameters (D. Li et al., 2017). He et al. did the specific processing parameters research and the SPR setting process, joint failure, static and fatigue behavior, process monitoring was covered by the research. He also developed the numerical model to analyze the SPR process (He, Gu, & Ball, 2012; He, Pearson, & Young, 2008). Andreas Chrysanthou and Xin Sun summarized the review of the SPR research works associated with different researchers and form a book (Chrysanthou A, 2013).

There are sort of the SPR techniques that have been applied in real world. For example, solid SPR (Kaščák & Spišák, 2012; Mucha, 2014, 2015), clinch riveting (*Clinch Rivet Tool*, 2015; Mucha, Kaščák, & Spišák, 2013; Mucha & Witkowski, 2013), single-side SPR (Liu et al., 2016), gun powder-driving SPR (B. Wang, Hao, Zhang, & Zhang, 2006), friction SPR (Duan et al., 2014; G. Han, Wang, Liu, & Wang, 2013; Ma, Lou, Yang, & Li, 2015), inner flange pipe rivet (Huang, Xue, Lai, Xia, & Zhan, 2014) and rivet-welding SPR (Lou, Li, Li, & Chen, 2013; Lou, Li, Wang, Wang, & Lai, 2014). However, the regular SPR is still a main technique for automotive industry. Section 2.2 of this thesis is going to introduce the general the SPR joining process and the major components of the SPR system. In addition, the essential SPR parameters will be listed and discussed in detail. And the recent research on simulation of the SPR process

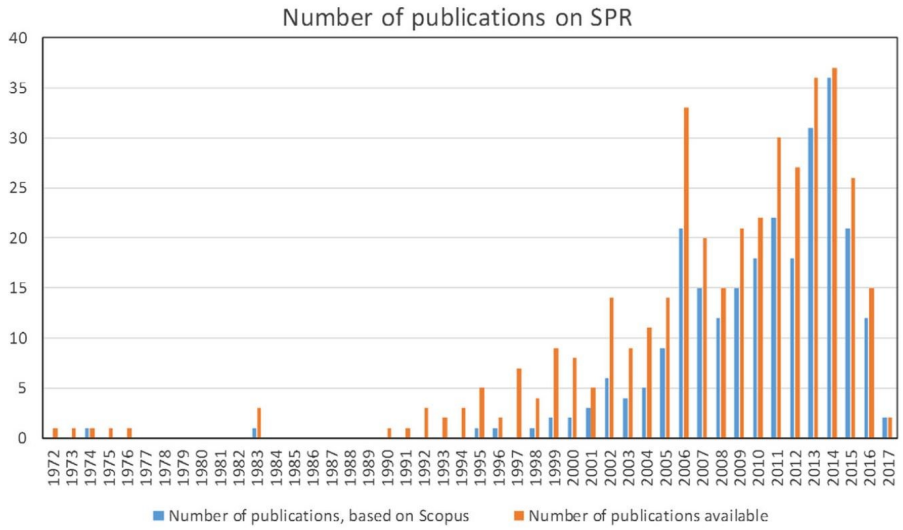

Figure 2.2. The SPR study statistics based on the publication (D. Li et al., 2017)

will be addressed. Eventually, the current dilemma and the future of SPR are discussed at end of this chapter.

2.2 The SPR system and joining process

The SPR system is composed of six major parts. Figure 2.3 shows a laboratory electric-driven the SPR system. The control unit on the bottom part of figure is responsible for adjusting the punch speed and punch force monitoring. The vertical facility on the right of figure is the main joining system. The servo-motor is located at the top part of the whole facility. It will drive the punch and provide the given speed from controller to force the rivet into the materials. C-frame play a role of the fixture. The die and other parts are built in the C-frame structure.

The SPR system usually has hydraulic and electric servo-motor driving system. And the whole riveting process can be summarized as pushing or punching process. As a simple and cheap SPR solution, hydraulic driving system can finish the SPR with a simple pushing process. During the pushing process, the rivet is pushed into the end position when the force increases. But the pushing process can lead to more local distortion comparing to punching. Instead of simple pushing, electric servo-motor driving system

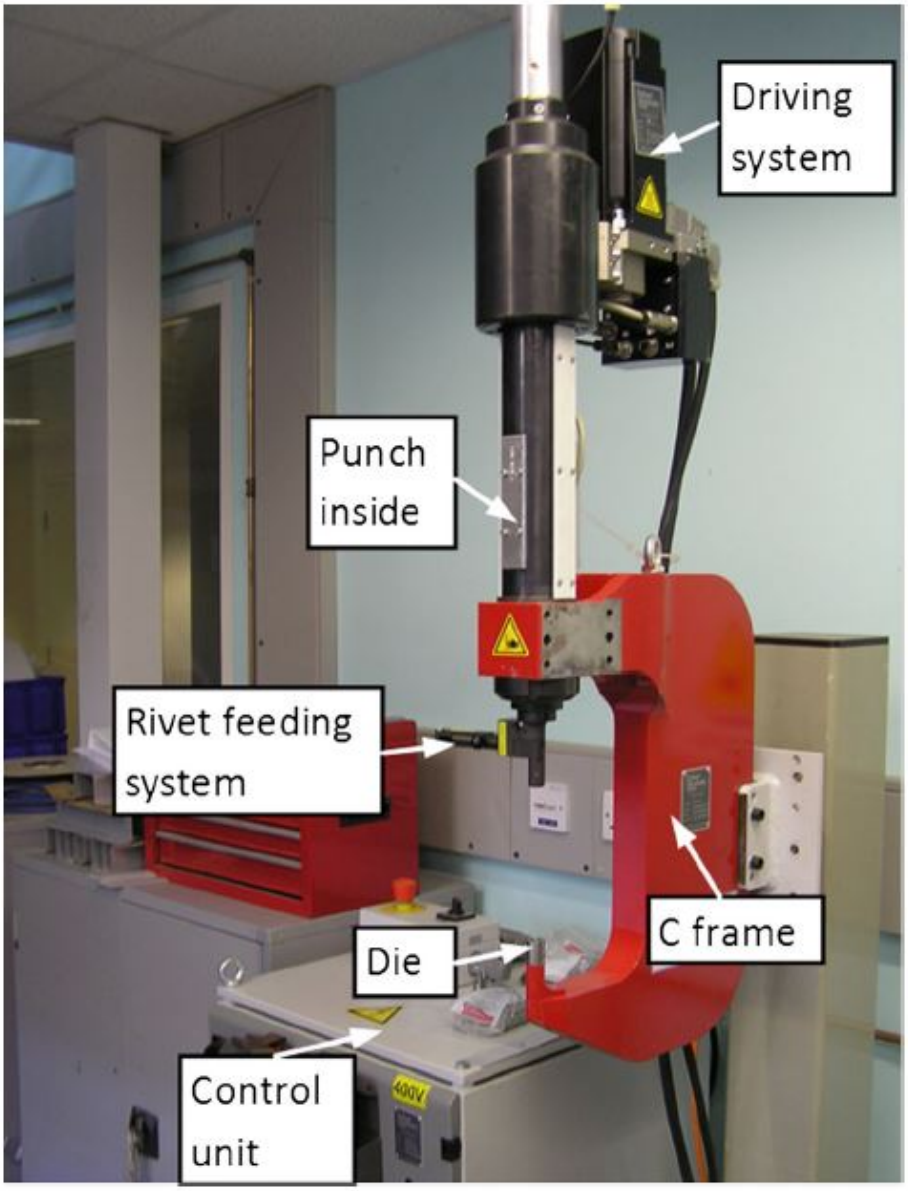

Figure 2.3. A laboratory SPR system overview (D. Li et al., 2017)

can hit the rivet at a certain speed and punched it into the materials with a powerful impact. The less local distortion will be introduced by punching process (D. Li et al., 2017). Wang et al. used gun powder driving the SPR system with the punching process that also obtained the less local distortion results (B. Wang et al., 2006). Combining with the electric SPR system, the modern SPR system can be automated and monitored. The electric system is relatively compact than hydraulic system. It is easy to combine with

robotics to achieve automated production system. The monitoring system is able to control the joint quality. The process parameters, such as alignment, setting force, and punching speed, can be detected and modified spontaneously with this system.

To better understand the SPR process, the dynamic joining process plays a significant part in the whole process. Figure 2.4 indicates the four stages of riveting process. Holding as the first stage that the nose will press the material firmly on the die and make sure the material sheets stand steady. Depending on the study from Li et al. (D. Li et al., 2017), the low holding force will allow more bottom sheet material to flow into the die cavity. It will lead to the less local work hardening effect and the cracks on the joint button can be reduced. In opposite, the large holding force can enhance the local work hardening effect because the less bottom material in the die cavity is going to be deformed. Eventually, the cracks are formed on the joint button due to the low resistance of excessive deformation.

Piercing as the second stage is mainly responsible for punching the rivet into the materials. The punch is going to press the rivet and the rivet starts to penetrate the top layer material and stopped by piercing into the bottom layer material. Depending on the mechanical properties of the materials, the harder materials are supposed to place on the top. The hardness of rivet and top layer material is about determining the possibility of rivetability. For a hard top layer, the rivet could break the top layer into a small piece and push it into the bottom layer at the end. For a softer top layer, the rivet usually pierces through the top layer and the rivet leg will flare inside of the bottom layer.

Flaring as the third stage, which is going to finish the riveting process by flaring the rivet leg in the bottom sheet material until the force or punch speed reach the determined value. When the bottom layer is squeezed into the cavity, the flaring starts to proceed at position where the bottom layer material touches the pip inside of the die or the button of the die. The pip can facilitate the rivet leg to spare out and penetrate into the bottom layer with a mechanical interlock.

Releasing is the final stage of the whole joining process. The punch and the nose part will go back to the original working position and the workpiece can be released from the die part. The next joining cycle can be followed up after this stage.

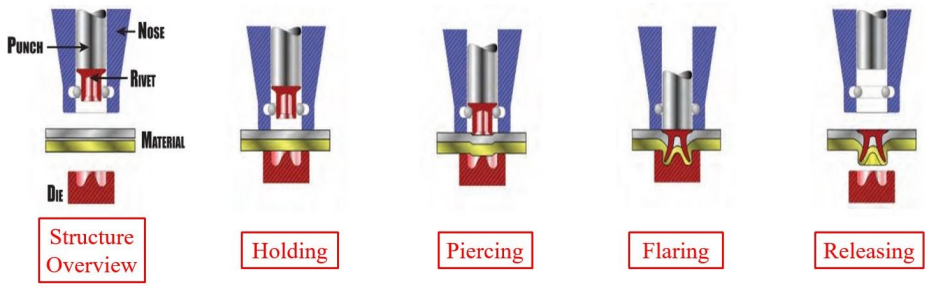

Figure 2.4. The SPR joining process

To further understand the SPR joining process, the force-displacement curve is useful to sight into the SPR dynamic process and observe the magnitude of piercing. Figure 2.5 developed by Hou et al. (Hou, Mangialardi, Hu, Wang, & Menassa, 2004) shows the rivet moving trajectory depending on the punch force and rivet displacement. There are four major stages in Figure 2.5 indicates the joining process in terms of the variation of the setting force. The first stage covers the beginning of piercing and this stage ends up with the completely penetration of top sheet. The force at this stage results in a little elevation before the rivet enters the second layer. At the second stage, the rivet starts to penetrate the bottom layer. And the rivet leg tends to flare out because the bottom layer touches the pip in the die cavity and the rivet leg starts to deform in the orientation of force. The force increases steadily with a small elevation at this stage. The third stage with a drastic force elevation starts from the closing-up of the gap between the top and bottom layer. Then the rivet leg further flares out and penetrates into the bottom layer deeper indicates third stage approaches to the end. The beginning of the fourth stage shows the rivet is approaching to the finishing position. The difference can be relatively observed is the head height of rivet becomes to smaller. Eventually, the rivet is firmly pressed into the material and the rivet leg reaches the final position at the force is about 60kN. The force-displacement curve was initially studied by the Budde et al. (Budde, Lappe, & Liebrecht, 1992) and Lappe and Budde (Lappe & Budde, 1993) in the purpose of monitoring SPR process. Then King et al. (King, OSullivan, Spurgeon, & Bentley, 1995) indicated that the relationship among force-displacement curve, process parameters,

rivet geometry, die geometry, material sheet thickness and material type in his study. In addition, the force-displacement curve was also used by Atzeni et al. (Atzeni, Ippolito, & Settineri, 2009) to validate the SPR simulation results. Haque et al. (Haque, Beynon, & Durandet, 2012) used sheet material thickness and rivet hardness as the variables to study the force-displacement curve. In a word, there are numerous parameters that will affect the profile of force-displacement curve. The strength and thickness of material sheets, the rivet length and hardness, the die geometry, and sheet stack number and the order of the materials in the stack are the key factors to determine the profile shape of force-displacement curve.

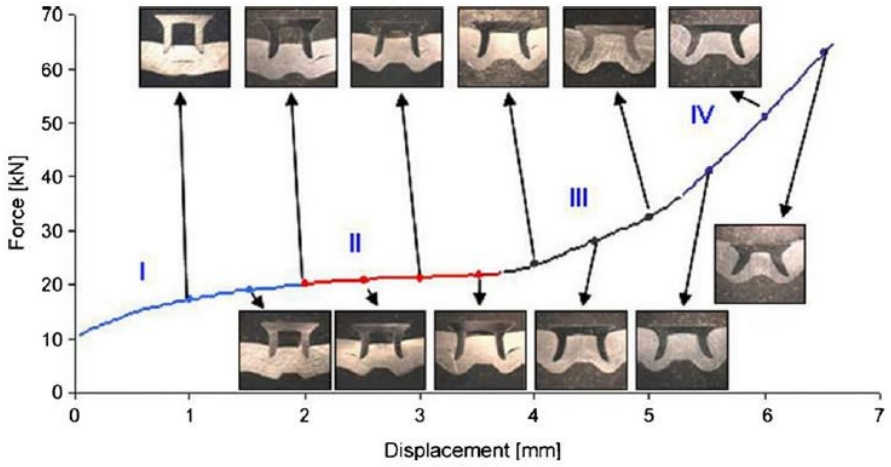

Figure 2.5. Force-displacement curve for the SPR process

2.3 The SPR process parameters

The process parameters of SPR have a close relationship with the components of SPR facility. The major components of the SPR facility including C-frame, rivet, die geometry and setting force are also the significant process parameters that can determine the joint quality. It is substantial to utilize the logical combination of the process parameters in order to obtain the best joint performance. The influence of each parameters is necessary to be explored in detail.

2.3.1 C-frame design

The typical C-frame needs to withstand the setting force in the range of 20 to 100kN. The perfect tool alignment plays an important role to successfully obtain a qualified joint. Thereby, the strong and rigid C-frame design is suggested to satisfy the system specification. Industry provided the C-frame design reference, which required that the deformation of a qualified frame should be smaller than 7 mm along the loading line and the angular deflection needed to be less than 1 degree in the meantime (Westgate et al., 2001). Instead of the alignment, the C-frame throat depth and weight are also substantial to vary the joining capability. The throat depth can determine the lateral access ability of the joining system. And the weight of C-frame will decide the automation ability and the final cost of SPR system. The combination of a deep throat depth with a light weight design will be best candidate to form the perfect SPR system. Since the servo-motor SPR system was developed in the recent years, the traditional hydraulic system has been gradually replaced. The light-weighting and simplicity of servo-motor system are the advantages to achieve the automation in system capability and cost perspectives.

2.3.2 Setting force

An appropriate setting force is essential to form a qualified joint. The setting force is related to several qualification parameters after joining. The small setting force could lead to the large rivet head height, which can cause the cosmetic and corrosion issues. Furthermore, the interlock distance will be quite small if there is no enough setting force applied during the joining process. It can result in the low joint strength in the end. In opposite, the overlarge setting force is easy to damage the top sheet material. And the too small minimum remaining bottom material thickness due to the large setting force will also reduce the joint strength.

To better understand the relationship between setting force and joint qualification, there were several researchers conducted the experiments to dig it in depth. Hill (Hill, 1994) indicated that the rivet shank diameter, the rivet shank geometry, the rivet hardness,

the die shape, the sheet material thickness and hardness, the friction between rivet and sheet materials were the variables to affect setting force. The die geometry, the material stack, the die geometry, the planar misalignment and the axial misalignment were studied by Hou et al. (Hou et al., 2004). Their research concluded that the planar misalignment was able to reduce setting force. But the axial misalignment had a little effect on setting force. Unlike the previous two research groups, Kim et al. (Kim, Xu, Li, & Blake, 2006) showed that setting force was determined by the deformation force of the rivet. The strength and hardness of the substrate was mainly related to the force required by piercing the top sheet material. Their results also pointed out the close relationship between the joining temperature and the setting force.

In terms of the SPR facilities, setting force can be set by the operators. Bollhoff hydraulic SPR system utilizes setting force as the adjustable value to obtain the SPR joints. Henrob servo-motor SPR system uses the punch speed as the variable to form the SPR joints. Setting force will be regarded as the reference number to determine the joint quality. Stanley servo-motor SPR facility uses the rivet head height as the setting value to form the SPR joints. Although setting force is a significant parameter for the SPR joints, it is not the only parameter that can determine the joint quality and performance. In order to obtain a good SPR joint, there are several parameters that will be discussed in the following.

2.3.3 Rivet

As one of the most significant parts of the SPR system, the investigation of rivet is always being conducted in the SPR development history. The SPR rivets were defined as a solid rivet that was flared inside of a fluted die with the insertion of three legs since 1970s. This type of rivet was also called Trifurcation rivets. After about ten year development, the rivets changed to the semi-tubular design with the basic tip geometry. In 1990s, the SPR rivets were further designed and developed with the compact web thickness and the better tip geometry. This improvement brought the more uniform flaring and consistent joint strength to the SPR technique. The most of current the SPR rivets have been shifted to a

semi-hollow geometry design and fabricated by a multi-blow cold formation process using metal wires (D. Li et al., 2017).

Nowadays, there are many different types of the SPR rivets that have been designed and developed for different applications. Figure 2.6 shows the various type of commercial rivets designed by Henrob. Countersunk head rivet is one of the most common rivet types that has been used by numerous industries. It can provide the flushness on the head side of the SPR joint and the good fatigue resistance. Flat head, pan head and dome head are designed for the joint for the plastics and thin sheet metals with a good peel strength. But the protruding head on the top sheet could be an issue due to the aesthetic requirements. Furthermore, there are several special design rivets that can be used for combining the riveting with additional features (*Rivet types*, 2018). As one of the SPR system development companies, Henrob did a large amount of experiments to apply the SPR for various joining situation.

Figure 2.7 shows the three layer sheets joined by two different types of the SPR rivets. A semi-tubular rivet was used in Figure 2.7 (a) for a stack. The broken material from the top and the middle sheets was squeezed into the rivet cavity and finally pushed the bottom sheet to form the joint. However, there was no enough space in the die cavity and the bottom sheet had to share the space with the broken material from the different sheets. As a result, the material was pushed away from the center to the sides and the remaining bottom material thickness was smaller than the minimum value. Instead of using the semi-tubular rivet, Henrob also designed and tested the fully tubular rivet in order to improve the process. Figure 2.7 (b) indicates the cross-section view of the joint formed by a fully tubular rivet. Compared to the semi-tubular rivet, the remaining bottom material thickness using full-tubular rivet was obviously larger because the fully tubular rivet allowed the material from the top and middle sheet to flow into the rivet cavity. This type of design is beneficial to join the less ductile or brittle bottom sheet materials. It can improve the remaining bottom material thickness and avoid the crack generation for brittle materials like the high strength aluminum alloy and the structural aluminum alloy made by die casting process.

Figure 2.6. Different types of the SPR rivets designed by Henrob

The common size of the SPR rivets are 3 mm and 5 mm in stem diameter. And the length varies from 4 mm to 14 mm depending on the stack thickness. The rivet selection is related to a series of parameters, such the joint strength, the sheet thickness and the die type etc. In order to normalize the rivet selection for automobile industry, European Aluminum Association provided the guidelines as a reference. For a rivet with 3 mm

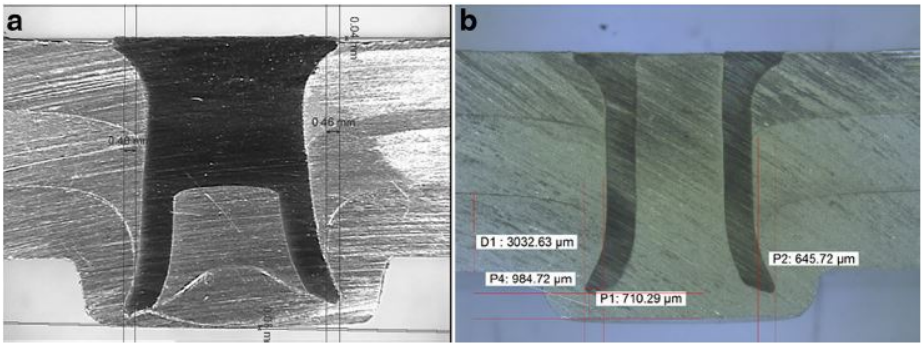

Figure 2.7. The three sheets joined by (a) a semi-tubular the SPR rivet and (b) a full-tubular the SPR rivet

diameter, the rivet length should be the sheet stack thickness + 2.5 mm; For a rivet with 5 mm diameter, the rivet length should be the sheet stack thickness + 3.5 mm (D. Li et al., 2017). Henrob Ltd. also suggested that the rivet length is supposed to 1.5-3.0 mm and 2.0-4.0 mm longer than the stack length for 3 mm and 5 mm rivets, respectively. Although the stack thickness is the main standard to determine the rivet length, the stack configuration also needs to be taken into consideration. If the top sheet is thicker than the bottom sheet, the rivet length should be larger than the stack thickness. Otherwise, the rivet length can be shorter than the stack thickness if the top sheet is thin and the bottom sheet is thick (D. Li et al., 2017).

In the early days of the SPR application history, the joint stack thickness would be the major factor to determine the rivet length. The thicker stacks needed the larger diameter rivet to form the joint (Hill, 1994). However, there are more and more factors that can influence the rivet selection in the current SPR application. For example, the joint strength, the material and stack thickness, the required joint robustness and the accessibility to the joint area will be the factors to selection the suitable rivets (*Rivet types*, 2018). Generally speaking, the rivets with smaller diameter have the lower strength for the joints. However, the small rivets have more flexibility on the facility requirements. And the access area, the nose-piece and flange size for small rivets application will be smaller than the large rivet facility. Moreover, the different size rivets in terms of the application will be used for various application in a vehicle. For instance, 3 mm rivets is generally

used for closure in automobile. But the larger diameter rivets, like 5-14 mm diameter, are selected for joining the parts with relative high strength and anti-buckling structure positions (D. Li et al., 2017).

The rivets are usually fabricated by the forging process and the general material of the rivets is steel. Steel rivet can be directly used by the SPR in as-forged state. In addition, the steel rivets also can be heat-treated to the different hardness level (250 600 HV) depending on the application requirements. The selection of the rivet can be determined by the properties of the stack materials. When the hardness of rivets is not enough, the rivets are prone to buckle during the riveting process. If the hardness of the rivets is too large, the rivets are hard to deform and the interlock distance will be smaller than the expected value. As a result, the both cases will lead to the low joint strength.

The coating after fabrication is significant to guarantee the rivet quality during and after the joining process. The coating enables to reduce the friction force during the riveting process. And it also can prevent the corrosion between the rivets and stack materials. The general coating materials used by the rivets include electroplated zinc nickel, mechanically plated zinc/tin, mechanically zinc/tin/aluminum, Kal-gard, zinc flake and epoxy. The combination of mechanical plating zinc/tin coating with e-coated has been used and tested for aluminum body automobile without the corrosion issue more than 15 years (D. Li et al., 2017).

The rivet design process has been explored by many researchers in simulation for the decades. Xu (Xu, 2006) was focused on the influence of the rivets yield strength on the setting force. He pointed out that the low yield strength could lead to the rivet buckling before the piercing. However, the rivet with high yield strength was hard to form the sufficient interlock distance due to the little deformation after piercing. Presz and Cacko (Presz & Cacko, 2010) simulated the riveting process with the small rivet diameter. Based on their simulation results, they proved that the SPR process with micro-size rivets could also obtain the qualified joints.

2.3.4 Die

Die plays an important role for the SPR process. The joining process is finished in the die cavity and the joint quality is highly related to the parameters of the die. Figure 2.8 lists the typical dies used for the SPR process and a series of dies used by Henrobs lab. Tool steel as the most common material for the dies can withstand the most of riveting situation. Furthermore, there are several different parameters of the die, such as the die cavity diameter, die cavity depth and die cavity geometry, that are significantly related to the quality of SPR joints.

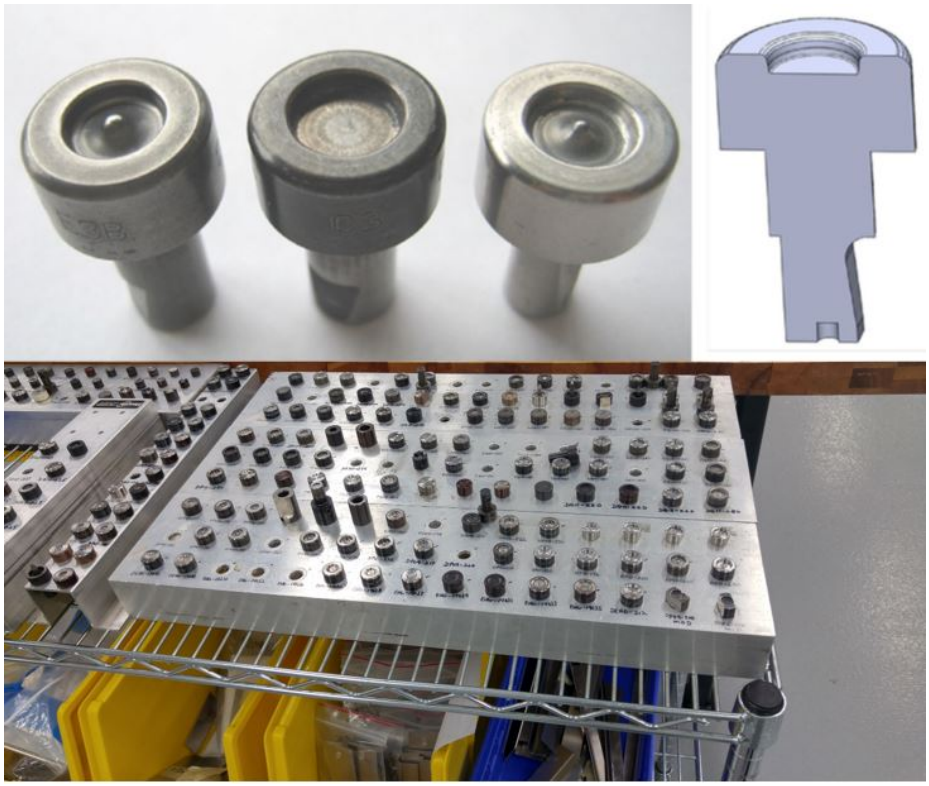

Figure 2.8. The common dies and various dies used for the SPR process

The joint in the SPR process is formed inside of the die cavity. Therefore, the various parameters of the die can essentially affect the SPR joint quality. Die cavity diameter as the one of the critical parameters can determine the magnitude of the plastic deformation during the riveting process. The die cavity diameter is supposed to be larger

than the rivet stem diameter. However, the excessive large die could lead to the small interlock distance. When the other parameters stay constant, the die with larger diameter will allow the material to flow in the radial direction. It can lead to the excessive plastic deformation formed in the die. Li et al. (D. Li et al., 2017) indicates that the rivet with 3 mm diameter should use the die with 6 or 7 mm diameter. 5 mm rivet should have a die with the diameter is less than 8 mm.

Die cavity depth is the second parameter that needs to be taken into consideration of optimizing joint strength. If the die cavity depth is too deep, the die will provide the less support on the bottom sheet. The more material on the bottom sheet will be deformed inside of cavity and the interlock distance can be smaller than the shallow depth die. In addition, the extra plastic deformation also can lead to the cracking issue on the joint button. The joint performance can be seriously affected by the cracking propagation during the routine activity. As a result, die cavity depth would be one of the significant factors to cause the cracking issue in the SPR.

In terms of the joint quality, the die with different cavity geometry can result in the different joint strength. The die with a flat bottom and the die has a pip in the middle are the two typical die geometries. The flat bottom die has less support for the bottom sheet material. The interlock distance from this type of die could be less than the die with a pip. The pip profile in die cavity can increase the rivet flaring and the plastic deformation during the riveting process. However, it may need the larger setting force and the more plastic deformation will be applied on the bottom sheet material. It is easy to form the cracks on the joint button if the bottom material is lack of ductility.

In order to obtain the best joint performance, Li et al. (D. Li, Han, Thornton, & Shergold, 2010) suggested that the die with shallow depth and tilted sidewall is suitable for the bottom sheet material has the low ductility because this type of design can avoid the excessive plastic deformation. Based on their research, they investigated that AA6008 high-strength aluminum alloy with good ductility would have the cracking issue when the die with a vertical sidewall and a 2 mm die depth. Sunday (Sunday, 1983) also showed that the die with a tilted sidewall enabled to improve the die release process. A die designed by Iguchi and Ohmi (Iguchi & Ohmi, 2003) with a spring-loaded sliding pin the

center of the die as shown in Figure 2.9 was aimed to improve the capability of the SPR process. The denting applied on the top thick sheet could be avoided and more penetration would be applied on the bottom sheet.

Instead of the physical experiments, the simulation was helpful for die design and die geometry optimization. LS-DYNA was used by Mori et al. (Mori et al., 2006) to investigate and design the optimal die geometry in joining an ultra-high-strength steel to an aluminum alloy. They indicated that the punch force can be reduced and the extra plastic deformation was prevented during the piercing by increasing the diameter of the cavity and decreasing the height of the projection. Mori et al. (Mori, Abe, & Kato, 2014) also utilized the simulation to improve the rivetability of multi-layer steel sheets.

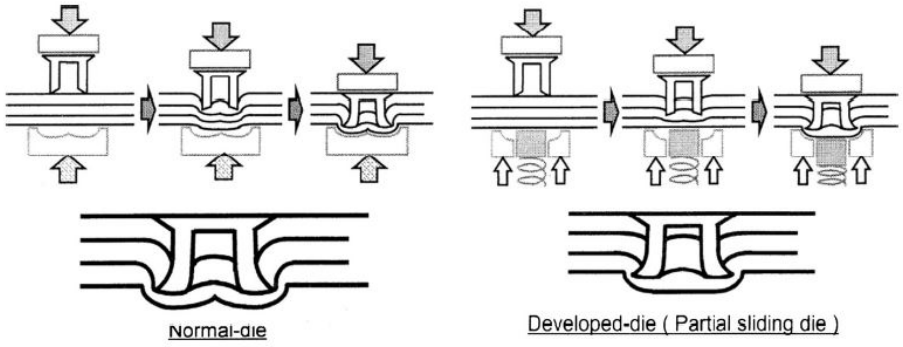

Figure 2.9. A die with a spring-loaded sliding pin design

2.4 The SPR joint qualification

The qualification of SPR joint is critical to determine and improve the quality of SPR joint. Figure 2.10 shows the cross-section view of three-layer material joint. There are several parameters in the figure that have been pointed out and these parameters are substantial to decide the quality of the joint in different perspective. Rivet head height, interlock distance, and the minimum remaining bottom material thickness (T_{min}) are important to determine the joint strength and corrosion resistance etc.

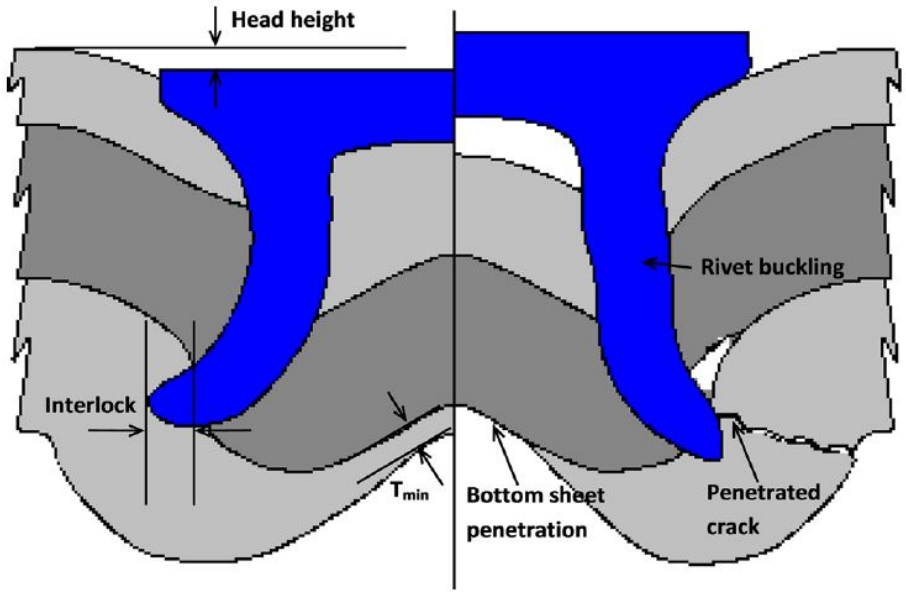

Figure 2.10. The SPR joint quality cross-section overview (D. Li et al., 2017)

Head height is not only going to affect cosmetic appearance, but also can influence the tightness and even the joining quality of the joints. The joint with a large head height, there will be a gap between the rivet and the top sheet. This gap is easy to cause the corrosion issue later in the daily use situation. Furthermore, the large head height indicates the interlock distance is small. The smaller interlock distance will finally cause the low joint strength because the appropriate interlock distance would provide the sufficient lock force to connect the material sheets. However, the excessively small head height could cause the bad quality of the joint. First of all, the over penetration would lead to the damage of top sheet material. Moreover, the over-press on the rivet could cause the remaining bottom material thickness is smaller than T_{min}. Han et al. (L. Han, Thornton, Li, & Shergold, 2010) reported that a head height of the joint should be between 0.3 and -0.5 mm. The interlock distances are supposed to reach at least 0.4 mm and 0.2 mm for the bottom sheet materials are made of aluminum alloy and steel, respectively. And T_{min} should be larger than 0.2 mm.

2.5 Influences of the SPR joint performance

The SPR joint performance is not simple to be determined by the process of piercing the rivet into the stack material. There are various factors and parameters that could influence the joint strength and quality. Many researchers made the contributions to test and explore the influence of parameters on the joint performance.

2.5.1 Contributing elements of static strength

The application of contributing elements of the static strength is useful to demonstrate the dynamic relationship between each elements during the SPR process. A research done by Hill (Hill, 1994) presented that the lap shear strength of SPR joint was compose of a frictional force and a direct shear force between the sheets. But the strength of SPR joint is unpredictable because the compression force was not high enough. The other researchers also mentioned that the frictional force between each sheets played an important role to determine the static strength of SPR joints. Han and Chrysanthou (L. Han & Chrysanthou, 2008) indicated that the static strength between rivet and sheet material could be affected by the residual compressive pressure from the rivet setting process. And Han et al. (L. Han & Chrysanthou, 2008; L. Han, Young, Hewitt, Alkahari, & Chrysanthou, 2006) also found that the sheet surface conditions could lead to the variation of the joint strength and failure modes caused by the different friction at the interface. Li et al. (D. Li, Han, Thornton, & Shergold, 2012; D. Li, Han, Thornton, Shergold, & Williams, 2014) indicated that the fraction between the top and bottom sheets had a tight relationship with static lap shear strength at site of the tip around the punched hole.

Li et al. (D. Li et al., 2017) summarized that the strength of SPR joint was mainly determined by the combination of several factors: the deformation force of top sheet at rivet head or the force required by locking the rivet tail in the bottom sheet material; the flaring force; the friction between rivet head and the top sheet material or the friction between the rivet tail and the bottom sheet material; the friction between the top and

bottom sheet at the tip area of the punched hole. However, the peel and shear strength have no significant influence by the friction.

2.5.2 Material stacks

The joint performance is highly related to the material stacks and their property. The property of material stack can affect the rivet selection and after joining strength. Generally speaking, the soft stack materials do not require the high hardness rivet to join them. But the hard stack materials do need the rivets with high hardness and toughness. Nevertheless, the hard rivets may face the less flaring issue after the joining also due to its property. Furthermore, the thickness of the material stacks is another significant parameter that can influence the joint performance. Thereby, this section is going to discuss the influence of the parameters about the material stacks.

Nowadays, the SPR technique is going to be used for joining the identical and different material sheets. The SPR process of joining same material sheets was investigated by Madasamy et al. (Madasamy, Faruque, Tyan, & Thomas, 2001) by using some of aluminum alloy as the material sheets with 1, 2 and 3 mm in thickness. They indicated that the joint strength was related to the thickness of top sheet. Madasamy et al. (Madasamy, Faruque, & Tyan, 2002) in the following research investigated the crash performance of the SPR joints using the aluminum alloy rails and steel rails. The results showed that the thickness of aluminum alloy sheet was the primary factor to affect the joint performance. However, the multiple parameters, such as the sheet thickness, the impact speed and the temperature, had significant influence on impact performance for steel rails. Hill (Hill, 1994) and Taylor (Taylor, 1997) both showed that the lap shear and cross-tension strength of both steel and aluminum alloy SPR joints could be improved by increasing the stack thickness. Porcaro et al. (Porcaro et al., 2006a) did the systematic experiments with using aluminum extrusion AA6060 material stack. Figure 2.11 shows the shear results under different conditions. They showed that the joint strength can be increased by increasing the sheet material thickness at the same heat treatment condition. But this was no direct relationship between the joint strength with the width of the plate.

Furthermore, the T6 heat treatment can improve the joint strength comparing to T4 heat treatment by using 2 mm plates. Li and Fatemi (B. Li & Fatemi, 2006) investigated aluminum alloy joints with T-peel configuration. They pointed out that the static T-peel strength can be enhanced by increasing the stack thickness. However, 3 + 3 mm combination joints performed the low joint strength than 2 + 2 and 2 + 3 mm stacks. Based on the outliners results they indicated that the higher stiffness against plate bending and the low friction and high shear force could be the reason to cause the low strength of 3 + 3 mm combination. Khanna et al. (Khanna, Long, Krishnamoorthy, & Agrawal, 2006) did the similar experiment to investigate the mechanical performance of the SPR joints by using AA6111 aluminum alloy in multiple thickness. The results showed that the static and fatigue strength were improved by increasing the stack thickness when the top and bottom material sheets had the same thickness. Once the thickness of the top and bottom sheets is unequal, the joint strength was mainly determined by the property of the thinner sheet. Moreover, when the total stack thickness is identical, the combination of unequal thickness stack has lower joint strength than the equal thickness stack.

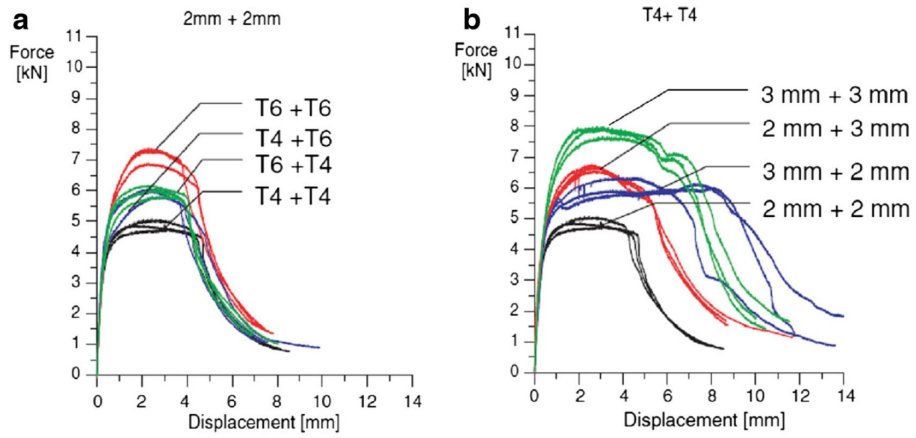

Figure 2.11. The force-displacement shear results with various heat treatment and thickness condition (Porcaro et al., 2006a)

In terms of the sheet material types, the combination of different top and bottom material sheets results in more complex performance in joint strength. Li et al. (D. Li et al., 2010) investigated the joint quality performance of a high-strength aluminum alloy

SPR joints. The static lap shear and T-peel strength could be largely improved by increasing the top sheet materials (AA5754) thickness. But the thickness of bottom sheet, which is made by AA6008, only had a slight effect on the joint strength. This result could be ascribed to the cracking issue on the bottom sheet when the top sheet was too thin.

Instead of altering the material thickness and material types of stack, the joint performance also can be improved by the treatment of material sheet. In general, many of the structural components for automobile need to be stamped. The strength of these components is enhanced by the introduction of strain into the materials. Han et al.(L. Han, Young, Chrysanthou, & Osullivan, 2006) used 2 mm AA5754 to investigate the influence of the pre-straining effect on the mechanical performance for the SPR joints. Figure 2.12 indicates the comparison of pre-straining level in static and fatigue shear strength. The top and bottom material sheets were identical and the magnitude of pre-straining were 3%, 5% and 10%, respectively. The curves in the figure clearly indicate that the both types of shear strength is enhanced by increasing the percentage of pre-straining. Furthermore, the artificial aging could have the same strengthening effect on joint strength.

The last but not the least, the SPR joint performance also can be varied by combining a various stack orientation. Madasamy et al. (Madasamy et al., 2001) studied the influence of stack orientation by using aluminum alloy sheets with 1, 2 and 3 mm in thickness. The results showed that the SPR joint could have the high strength and high energy absorption when the rivet was pierced from the thinner sheet to the thick sheet. Porcaro et al. (Porcaro et al., 2006a) also investigated the influence of stack orientation on the SPR joint performance. It showed the similar results as Madasamys study. Furthermore, the influence of stack orientation for the mixed aluminum and steel stacks was investigated by Sun (Sun, 2014) and Stephens (Stephens, 2014). Aluminum alloy AA5182 in 2 mm thickness and high-strength low-alloy steel (HSLA) in 1 mm thickness were used to test the influence of the stack orientation. Figure 2.13 indicates the cross-section view of the joints in the different orientation. The lap shear and T-peel results showed that the joint with steel sheet on the top layer had better performance in strength and energy absorption than the steel sheet in the bottom layer. Li et al. (D. Li et al., 2017) summarized that the SPR joint with the thicker sheet on the bottom was easy to

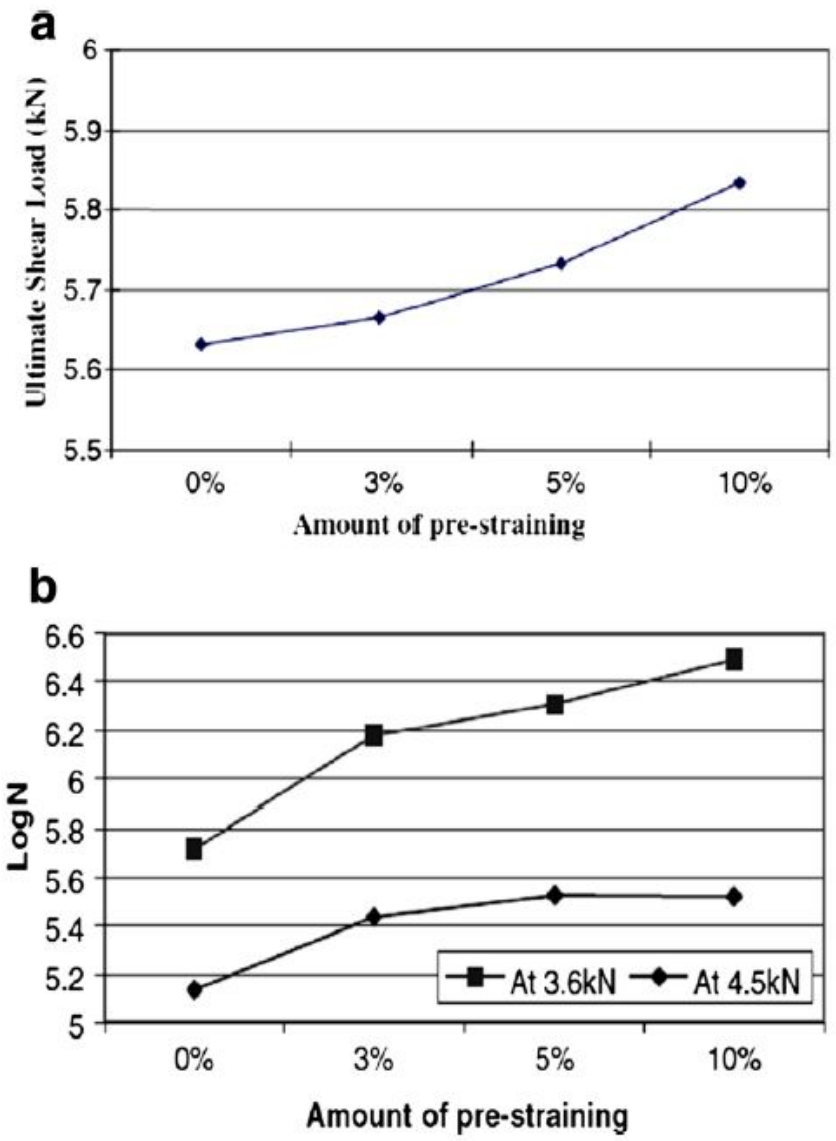

Figure 2.12. The static and fatigue shear strength comparison under the different amount of pre-straining condition (L. Han, Young, Chrysanthou, & Osullivan, 2006)

obtain the large interlock distance to guarantee the high joint strength. Lou et al. (Lou et al., 2014) also improved the shear strength of the SPR joint in 12% larger than the resistance spot welding by this approach.

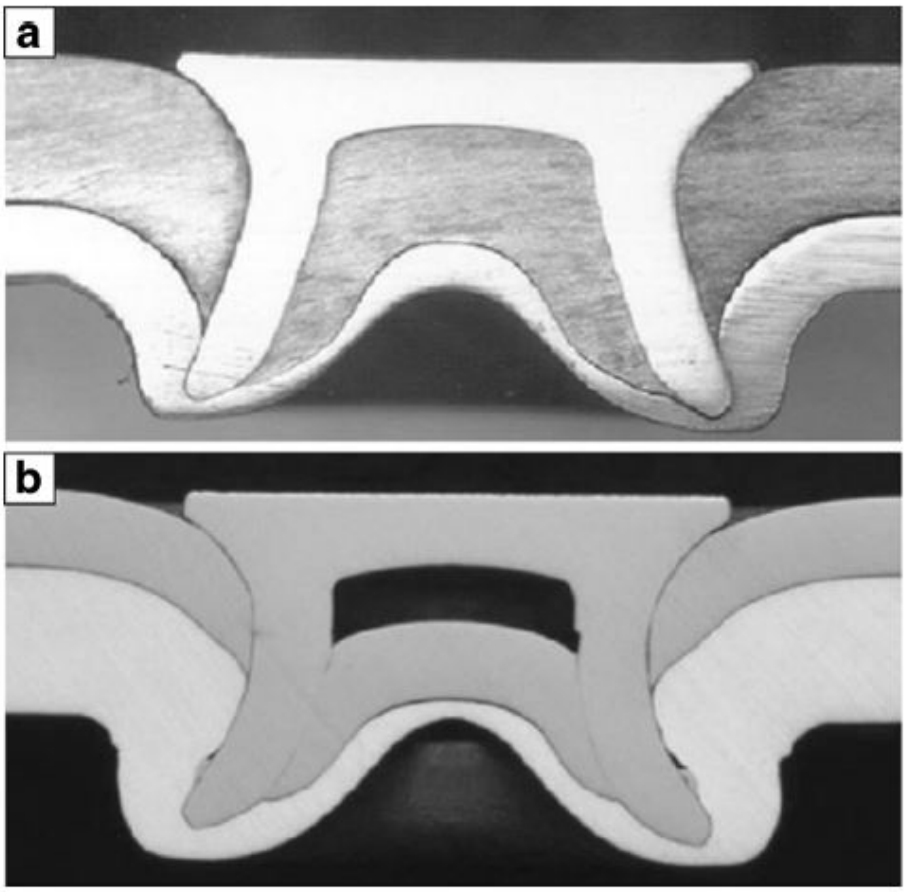

Figure 2.13. The cross-section view of joint by using 1 mm HSLA 350 steel sheet and 2 mm AA5182 aluminum alloy sheet, a AA5182 + HSLA 350 and b HSLA 350 + AA5182 (Stephens, 2014; Sun, 2014)

2.5.3 Selection of rivet and die for the SPR

The selection of rivet and die is significant to improve the SPR joint performance and ensure the joint quality. The die and rivet selection should be based on the properties of material sheets and the specification required by the joint. If we need the joint with high strength, the large diameter rivet can be the first option for picking rivet. In order to obtain the high joint strength, the SPR joint with a larger interlock distance is supposed to be obtained. Thereby, the die with a pip in the middle can be selected to create more interlock distance because of the excessive flaring. However, the special joining stack and

lacking of ductility on bottom sheet material can result in the low interlock distance and severe cracking issue on joint button.Therefore, the SPR joint performance still needs to be studied and investigated with the development of automotive industry.

Nowadays, body-in-white concept in automobile industry is quite popular. The manufacturers start to join the components made by the different materials together to further reduce the weight of vehicle. the SPR technique has the more advantages than the welding to joint aluminum alloy structural components with high-strength steel and other parts. But some of the issue, such as cracking, could lead to bad joint quality. Li et al. (Stephens, 2014) initiated the studying of the influence of the die cavity profile on the joint button quality using high-strength aluminum alloy joints. Their results indicated that the severe cracks appeared on the joint button (high-strength aluminum alloy AA6008 T61 as the bottom sheet) when the die with deep cavity or the die with vertical sidewall (the sharp corners) was equipped for the SPR process. The cracks are mainly caused by the large bending and tension deformation inside of the die cavity. Once the bottom sheet is thinner, it tends to have less cracks on the button because of the lower bending stress. The profile of the joints is shown in Figure 2.14. This results also pointed out that the appearance of cracks on the joint button could reduce the static and fatigue lap shear strength, but there was no obvious influence on the static and fatigue T-peel strength.

Penetration of rivet on the bottom material is another common issue due to the rivet and die selection. The overlong rivet, the wrong die selected and too high setting force could lead to the penetration issue. Han et al. (D. Z. Li et al., 2012) investigated the penetration problem, which used 2 mm AA5754 aluminum alloy and 1 mm HSLA as the joint materials. Their results concluded that the penetration on the bottom sheet had major effect on the peel strength. There was only minor influence on the shear strength. However, the failure modes during the shear test were quite different because of the penetration. The joint with the rivet penetration failed by tearing the bottom sheet; the joint without penetration failed by pulling out the rivet from the bottom sheet. The failure modes of both cases during the peel tests were pulling out the rivet from the bottom sheet. These results indicated that the rivet penetration on the bottom sheet had higher resistance to against the pull-out force due the larger interlock distance. But the penetration didnt

have sufficient resistance to against the tearing force. The results also showed that the penetration had a few influence on the joint fatigue life. But the corrosion resistance of the joint was reduced by the penetration.

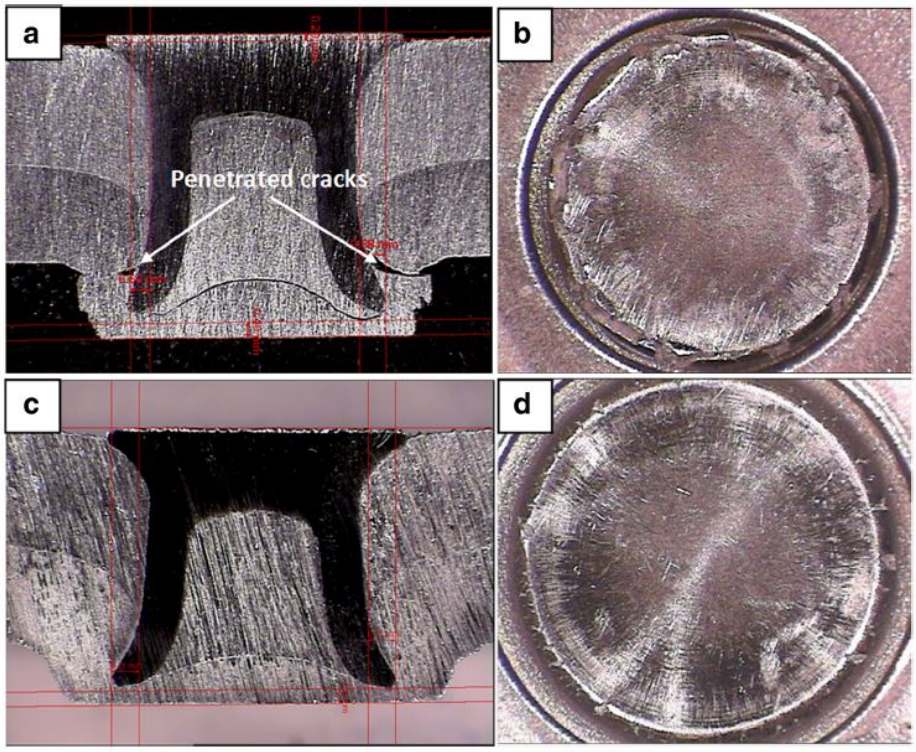

Figure 2.14. Cross-section view of joints, 3.0 mm AA5754 + 2.5 mm AA6008 T61. a, b the die with deep cavity and c,d the die with shallow cavity and tilted sidewall (D. Z. Li et al., 2012)

2.5.4 Selection of setting force

The setting process is essential to determine the joint performance during the SPR process. Based on the properties of the rivets, material stacks and required joint strength, the setting force need to be appropriately selected to ensure the joint performance. Amount of researches have been investigated to the influence of setting force on the SPR joint performance.

The SPR joints were formed by using 2 mm AA5754 has been tested by Li et al. (D. Li, Han, Chrysanthou, et al., 2014) to investigate the influence of setting force (setting velocity). When the setting force was low, the rivet head height was too high and there was a gap between rivet head and top sheet. In opposite, the over-high setting force was easy to over-press the rivet into the material sheet. It could result a dent on the top sheet and the top sheet could experience the corrosion issue because of the top sheet damage. During the lap shear and T-peel tests, all the shear test specimens were failed by pulling out the rivets from the bottom sheets and all the peel test specimens were failed by pulling out the rivets from the top sheets. Based on these results they summarized that the static shear strength was mainly determined by the interlock distance, and the static peel strength was related to the rivet head height. Their results also indicated that the high setting force could have the joint with a large interlock distance, but the damage of top sheet was the side effect. And the damage on top sheet would eventually lead to the low peel strength. In order to obtain the best performance of the joints, their study was shifted to investigate the variation of the joints mechanical performance at a specific setting force range as shown in Figure 2.15. The joint fatigue performance was also investigated by this group. They pointed out that the setting force did not have too much influence on the lap shear fatigue strength. But the T-peel fatigue strength increased by raising the setting force to a specific value.

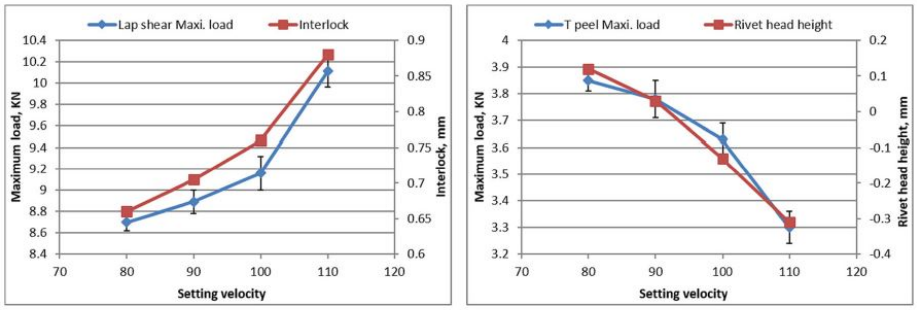

Figure 2.15. The joint performance at different setting velocities, a lap shear strength and interlock distance and b T-peel strength and rivet head height (D. Li, Han, Chrysanthou, et al., 2014)

Han et al. (L. Han, Young, Hewitt, et al., 2006) studied the similar process to investigate the influence of setting force/velocity on the joint performance using the aluminum alloy and steel sheets. Their results elicited that the remaining material thickness decreased by increasing the setting force. Meanwhile, the increased interlock distance led to a higher lap shear strength but a lower T-peel strength. Fu and Mallick (Fu & Mallick, 2003) exerted the rivet setting pressure to investigate the influence on the mechanical property of SPR joints. Their results showed that a higher setting pressure would have a higher lap strength before the pressure reached 95 bar. But there was no obvious effect on the fatigue strength of the joints.

2.5.5 Comparison of joints between the SPR and other joining techniques

As a young joining technique, the SPR only has a relative short history than some other joining techniques. Resistance spot welding (RSW) as the first choice has been well developed and utilized by the automotive industry for years. And RSW enables to provide a feasible and reliable solution to join the body components made by steel. For light-weighting purpose, more aluminum alloy components have been used for replacing the some of the steel components and the aluminum components as a strong candidate have been proved by the researchers and automotive industry enable to compete with steel components in strength. For joining the dissimilar components, RSW has a inborn weakness to join the different materials or aluminum alloys due to its joining principle. Thereby, the SPR was rapidly growing up in the recent years and became to the first option to achieve body-in-white structure with different types of materials.

In order to further investigate the difference between two techniques, a series of experiments were conducted by the researchers. Sunday (Sunday, 1983) compared the joint performance on aluminum alloy by using the SPR and RSW. The steel rivet with 4.76 mm diameter had been used for the SPR, and the RSW nugget diameter of the joints was from 4.67-5.67 times of the square root of the thinner sheet thickness. The results indicated that the SPR joints had a fluctuant lap shear strength than the RSW joints, and the tension strength of SPR joints were lower than the RSW joints. With a double layer

2.16 mm AA5182 material stack, the SPR joints had a lower lap shear strength. But the fatigue strength of the SPR joints was outstanding. Patrick and Sharp (Patrick & Sharp, 1992) also proved the excellent fatigue strength of SPR joints in their study. And Khanna et al. (Khanna et al., 2006) and Blacket (Blacket, 1995) indicated the similar results using AA6111 and AlMg3W19 joints. Riches et al. (Riches, Westgate, Nicholas, & Powell, 1995) used 1.6 mm AA5182 as the joined material to investigate the static peel and shear strength of SPR, RSW and cliched joints. Their results showed that the SPR joints had the highest strength, and the cliched joints had the lowest strength. Doo (Doo, 1993) investigated the static joint strength of SPR and spot-welded with 5000 series aluminum alloy in different stack thickness. The results showed that the lap shear strength of SPR joints was higher than RSW by using 2 mm and 3.2 mm aluminum alloy sheets. Once the sheet thickness increased to 4.3 mm, spot-welded joints took the lead. Additionally, the peel strength of SPR joints was always higher than the spot-welded joints at each thickness. And the strength comparison between SPR and spot-welded joints is shown in Figure 2.16. Krause and Chernenkoff (Krause & Chernenkoff, 1995) compared the mechanical strength of joints made by spot-welded and SPR using 2 mm AA5754 as the material stacks. The static lap shear strength of SPR joints with steel rivets was much smaller than the spot-welded joints. But the SPR joints showed the superior lap shear fatigue strength. Mizukoshi and Okada (Mizukoshi & Okada, 1997) indicated the similar results, which pointed out that the SPR joints had the higher static shear strength and outstanding shear fatigue strength.

Instead of RSW and spot-welded techniques, Briskham et al. (Briskham et al., 2006) conducted the joint performance comparison between the SPR and spot friction-welded technique. The static strength of SPR joints showed the equivalent or superior lap shear and peel performance than welded joints. Few years later, Han et al. (L. Han, Thornton, & Shergold, 2010) prove than the strength of SPR and RSW joints was related to the process parameters, such as material stack etc. The static strength of SPR joints can be altered by using different material stacks compared to RSW. But SPR joints always have superior peel strength and RSW shows the leading position in shear strength. Furthermore, the comparison of steel and mixed material joints was conducted

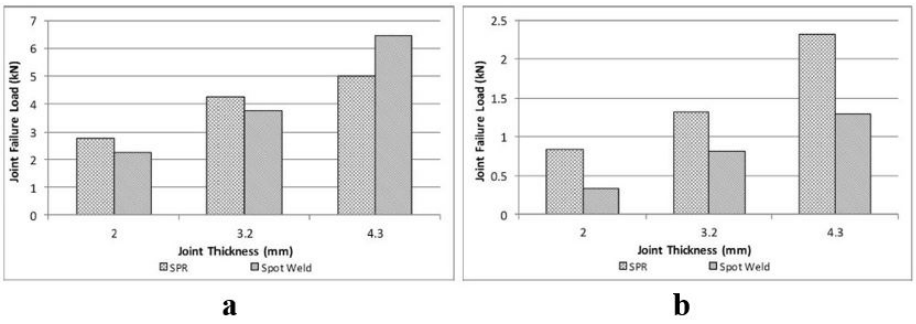

Figure 2.16. Comparison of the joint performance between the SPR and spot-welded, a the static shear strength comparison and b the static peel strength comparison (Doo, 1993)

by Booth et al. (Booth, Olivier, Westgate, Liebrecht, & Braunling, 2000). The steel rivets with 5 mm diameter and the nugget diameter was about five times of the square root of the thinner sheet thickness had been compared to investigate the difference. Their results also showed the similar trend in shear and fatigue strength as previous researchers.

A series researches were conducted to investigate the influence of SPR and RSW joints performance by utilizing different materials. Bonde and Grange-Jasson (Bonde, 1996) showed that the static shear strength of SPR joints was slightly lower than RSW joints with 1.5 mm RP220 and 1.2 mm IFHS180 material sheets. But the SPR joint still had a better performance in fatigue strength than RSW and relative welded joints. Galtier and Gacel (Galtier & Gacel, 2002) used high-strength steel sheets as the main variable to investigate the fatigue strength difference between SPR and RSW. Their results indicated that the fatigue strength of SPR was increased by elevating the strength of steel. And the joint strength was improved dramatically by increasing the substrate strength. But there was no obvious changes for the RSW joints. They also indicated that the SPR joints had a superior fatigue strength than the RSW joints when the high-strength steel had a yield strength higher than 300 MPa. And the results from Li et al. (D. Li et al., 2017) indicated that the strength of the high-strength steel didnt have much influence on the joint strength when RSW was applied. Dannbauer et al. (Dannbauer, Gaier, Dutzler, & Halaszi, 2006) stated that the SPR joints had better joint performance than the RSW joints for high-strength steel stacks. And Svensson and Lrsson (Svensson & Larsson, 2002)

conducted a series high-strength steel stacks experiment. They demonstrated that the SPR technique was able to provide a better joint performance than the RSW technique for joining high-strength steels.

In order to further investigate the feasibility of mechanical joining techniques, Li et al. (D. Li et al., 2017) studied the joint performance by using various material sheets, such as steels, aluminum alloys and aluminum/polypropylene/aluminum sandwich structure. Their results indicated that the joint strength was highly related to the material types. And the RSW joints showed better strength in some cases. Razmjoo and Westgate (Razmjoo & Westgate, 1999) used 1.2 mm AA5754 and 1.2 mm low carbon steel coated by iron/zinc alloy to investigate the joint strength difference. Moreover, the results showed that the fatigue strength of SPR joints was higher than the spot-welded joints. Mori et al. (Mori, Abe, & Kato, 2012) investigated the mechanisms behind the outstanding fatigue strength of mechanical clinching and the SPR techniques. They pointed that the high fatigue strength of SPR and clinching joints were caused by the stress relaxation at joint interface and work hardening on the substrate material sheet. The fatigue strength of RSW joint could be reduced by the heat-affected zone around the nugget. Blundell et al. (Blundell, Han, Hewitt, et al., 2005) made a comparison between the SPR joints and the spot friction-joined joints. Their results pointed out that the SPR joints owned a higher joint strength. And it was caused by the ductile failure mode during the shear and peel tests.

2.5.6 Selection of joined materials

The SPR was designated to join the similar and dissimilar materials. And the joined materials should have the sufficient ductility to withstand the plastic deformation during the riveting process. Nowadays, body-in-white concept is popular in automotive industry. The manufactures try to join the different types of materials to reduce the weight of vehicles. These materials includes steel, aluminum alloy, magnesium alloy, plastics, composites etc. However, some of the materials dont have enough ductility to be joined with other materials, such as carbon fibers and cast alloys. Thereby, the rivetablity of materials needs to be taken into consideration. As one of the most popular candidates,

aluminum alloys with the lightweight and relative high strength become to the first option for automotive manufacturers. The wrought aluminum alloys, such as 5xxx and 6xxx series, have an excellent rivetability and superior mechanical properties to fulfill the specification. Furthermore, the steels, including mild, high-strength and advanced high-strength steel, also can be joined by the SPR.

Rivetability is the first essential requirement to select the materials because the materials should have enough ductility to experience severe plastic deformation in die cavity and avoid forming the cracks on the joint button. Moreover, the hardness of materials should be lower than the rivets. Otherwise, rivets unable to pierce the material sheets and provide the sufficient interlock distance. Meanwhile, the rivets could be over-compressed and buckled during the joining process. In addition, the thickness of materials also can influence the rivetability. In general, a good SPR joint is composed by a thinner top sheet and a thicker bottom sheet. Therefore, the rivet is easy to pierce the thinner top sheet and there is enough material on the thicker bottom sheet that can be deformed inside of die cavity to maximize the interlock distance.

In terms of the various applications of SPR, more and more investigations about the rivetability of potential light-weighting materials have been conducted. Abe et al. (Abe et al., 2006) studied the feasibility of joining aluminum alloy to mild steel. Their results showed that the top sheet should be thinner than the bottom sheet if the aluminum alloy was on the top sheet material. Once the order of materials was reversed, the joint was easier to be formed based on their results. The fatigue performance of SPR joint by joining 1.5 mm AA5051 aluminum alloy to 1.5 mm cold rolled mild steel was investigated by Chung and Kim [89]. They pointed out that the SPR joints had a better static shear strength by using steel as the top sheet. And the SPR joints had a better fatigue performance when the steel was regarded as the bottom sheet. Joining ultra-high strength steel to aluminum alloy by the SPR was also been studied by Mori et al (Mori et al., 2006). They indicated that if the hardness of rivets was too low, the rivets could experience compression, fracture and bending (buckling). And Figure 2.17 shows a series failure modes on rivets. Because the ultra-high strength steel SPFC 980 with 980MPa yield strength is hard to be pierced by the normal steel rivet, the rivets should be

heat-treated to further improved the mechanical properties. The similar rivets failure was also caught by Hoang et al. (Hoang, Porcaro, Langseth, & Hanssen, 2010) in joining aluminum alloy with aluminum rivets.

Instead of the aluminum alloys, magnesium alloy is another strong candidate for light-weighting consideration. However, the low ductility of magnesium alloys at room temperature could be the shortcoming to apply SPR. Hahn and Horstmann (Hahn & Horstmann, 2007) studied the joining of magnesium alloy AZ31 by local heating technique. Since the ductility of magnesium alloy can be improved by raising up the material temperature, AZ31 was heated to 280°C by induction heating facility to alter its rivetability. Their results showed that it was a feasible solution to join AZ31 as the top or bottom sheet by SPR and mechanical clinching. Durandet et al. (Durandet, Deam, Beer, Song, & Blacket, 2010) used the laser-assisted SPR facility to join the strips made by wrought AZ31B-H24 magnesium alloy. When the material was heated up to 200°C, the strips could be joined by SPR without any cracks on the joint button. Furthermore, Henrob also patented an ultrasonic assisted SPR process to join the magnesium alloys to avoid crack generation on joint button (D. Li et al., 2017).

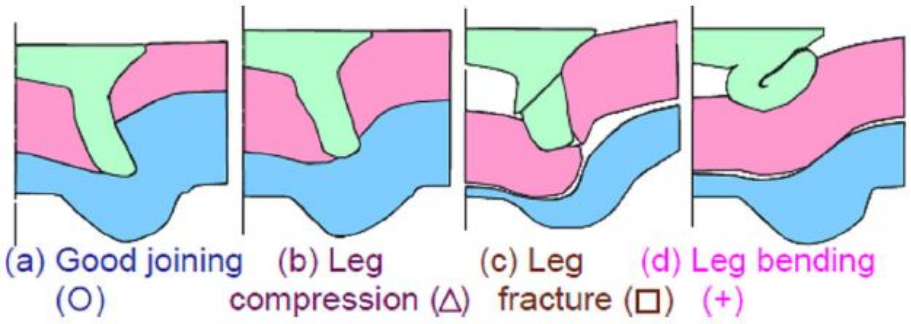

Figure 2.17. The failure modes of rivets to join ultra-high strength steel to aluminum alloy (Mori et al., 2006)

In order to further investigate the rivetability of magnesium alloys, Sjstrm (Sjöström, 2006) conducted the experiment of joining cast magnesium alloy, AM60B, and ultra-high-strength steel, DP800, with SPR. Without any heating, AM60B showed the bad rivetability. The cracks appeared on both magnesium alloy sheet and joint button area.

Once the local heating was applied, the cracks could be effectively reduced and the interlock distance was also increased. Luo et al. (Luo et al., 2011) tried to join magnesium alloys with aluminum alloys. Their results indicated that the joints could be formed by using the cast magnesium alloy AM50 as the top sheet and the extruded aluminum alloy AA6063 as the bottom sheet. However, the severe cracks that appeared on the joints button when the bottom sheet was AM50. The cross-section view of both joints is showed in Figure 2.18. Wang et al. (J. Wang et al., 2011) studied the influence of local heating on magnesium alloy joint strength and the corresponding failure modes of joint quality test. They used 2 mm thick AZ31 magnesium alloy to observe the cracks. They pointed out that the severe cracks would appear on the joint button at room temperature condition. Once the AZ31 was pre-heated to 180°C and above, the cracks were suppressed. During the lap shear test, the failure modes transformed from the pull-out rivet to the tearing bottom sheet when the pre-heating was applied. This tranformation indicated that the ductility of magnesium alloy was improved and the interlock distance was also increased by the pre-heating. And the larger interlock distance provided the higher joint strength and the lap shear failure mode was also changed.

Due to the popularity of SPR, this technique was also utilized by joining different metal sheets. Because of the good ductility of copper, the researchers successfully joined the copper stacks by SPR (J. Wang et al., 2011) and the aluminum to copper SPR joining was also successfully conducted (He, Zhao, et al., 2015). Even the titanium alloys could be successfully joined by SPR when the material was heated above 700°C (He, Wang, et al., 2015; X. Zhang et al., 2016).

The SPR is also capable for joining the composite materials to the metals. Fratini and Ruisi (Fratini & Ruisi, 2009) investigated to join glass fiber composite to aluminum alloy. They also indicated that the composite could be joined to the aluminum alloy when the composite was settled as the top sheet. Because the composite is brittle, it is hardly to create an effective interlock distance if the bottom sheet is composite. Di Franco et al. (Di Franco, Fratini, Pasta, & Ruisi, 2010) further proved the possibility of joining composite to metals. The SPR joint formed by joining a carbon fiber reinforced polymer composite to an aluminum alloy could have a qualified joint strength by using this type of

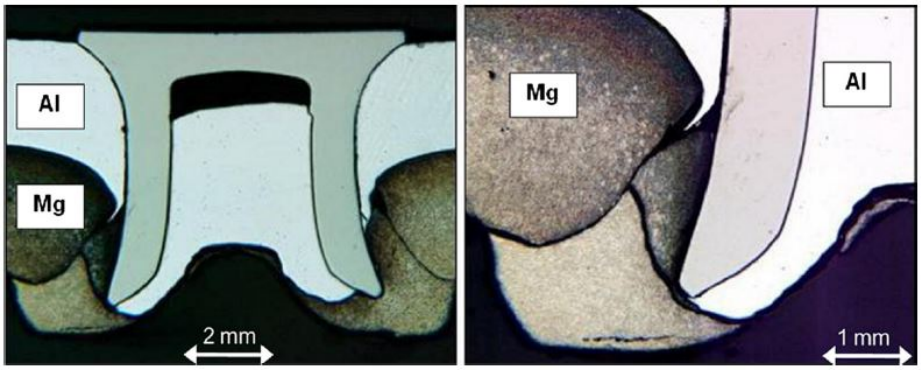

Figure 2.18. The cross-section view of the joint from joining aluminum alloy(AA6063) to magnesium alloys (AM50) (Luo et al., 2011)

stack-up. Settineri et al. (Settineri, Atzeni, & Ippolito, 2010) exerted that joining polymer and relative composites to aluminum alloys by SPR had a great potential in the market. However, the results of joining a various thermal plastic polymer PA6-based materials to aluminum alloy AA5754 from Zhang and Yang (J. Zhang & Yang, 2015) were opposite to previous researchers. They pointed out that the severe cracking was going to occur when the composites were used as the bottom materials. And the carbon fiber reinforced thermal plastic as the top sheet experienced the fracture during the riveting process. In order to additionally improve the joint strength of composite-metal joints, Di Franco et al. (Di Franco, Fratini, & Pasta, 2013) used adhesive bonding to successfully enhance the SPR joint performance, such as the joint strength, stiffness and energy-absorption. Fiore et al. (Fiore, Alagna, Di Bella, & Valenza, 2013) tried to join a Basalt fiber-reinforced polymer to the aluminum alloy AA6086. They pointed out that the adhesive bonding joints had a high joint strength than the normal SPR joints. Gay et al. (Gay et al., 2015, 2016) investigated the fatigue performance of joining glass fiber-reinforced composites to aluminum alloy. Their results indicated that the domed rivets would provide the high fatigue strength than the counter-sunk rivets. Moreover, Pickin et al. (Pickin, Young, & Tuersley, 2007) even tried to join a sandwich material, which was compose of 0.2 mm steel, 1.6 mm polymer and 0.2 mm steel, to a 2 mm aluminum alloy. They asserted that it was possible to form this type of joints by the SPR.

Since the SPR was designed for joining the materials with sufficient ductility, the researchers tried to modify the SPR process in order to accommodate the brittle materials like composites and plastics. Henrob Ltd. (D. Li et al., 2017) designed a process, which used a pre-drilled washer and a non-drilled washer to modify the joining process. The rivet will initially go through the pre-drilled washer, which was placed between the rivet head and the top sheet. Then the rivet can further pierce through the bottom sheet and it will eventually flare inside of the non-drilled washer to form the joint. Ueda et al. (Ueda, Miyake, Hasegawa, & Hirano, 2012) also developed a modified SPR process to join the brittle materials. There were two pre-drilled washers that would be placed at the similar location as the Henrob did. They also successfully joined the composite stacks with a reliable joint strength.

2.6 Modelling of the SPR process by finite element method

The SPR as a complex mechanical cold forming process has multiple parameters, which are able to influence the joint performance. In order to avoid a large amount of physical experiments to obtain the ideal process parameters, modeling will be the best tool to achieve this goal. Since the SPR process is mainly going to introduce the severe plastic deformation into simulation, the analysis will concentrate on the stress and strain distribution at deformation areas. Based on the SPR analysis specifications, there are several computer software packages can be used for SPR simulation, such as ANAYS, LS-DYNA, DEFORM 2D etc. And Casalino et al. (Casalino, Rotondo, & Ludovico, 2008) studied the mathematical equations about building the finite element model of SPR process. In addition, many of the parameters are significant to affect the simulation results, including mechanical properties of the materials, friction at the joint interfaces, fracture consideration and joint strength simulation.

The mechanical properties of SPR rivets and material sheets are essential to determine the deformation process during the riveting. The mechanical properties of material sheets can be easily obtained by test tensile test bars, which are fabricated from material sheets by CNC. However, the rivets with irregular profile are hard to be fabricated

to the tensile test specimens. Depending on this issue, Xu (Xu, 2006) came up with a method to determine the strength of rivets. He used the hardness and strength relationship of rivets material to calculate the strength once the hardness was obtained. Khezri et al. (Khezri, Sjöström, & Melander, 2000) used the compression tester to press the rivet along the longitudinal direction. The mechanical properties of rivets was able to obtain by the compression test. Porcaro et al. (Porcaro, Hanssen, Langseth, & Aalberg, 2006b) used the similar compression test to obtain the mechanical properties of rivets by pressing the rivet tube in radial direction.

The friction can be found at the multiple locations between rivet and material sheets during the riveting process. It is hard to be measured by in situ method due to the variation from several different perspectives, such as surface condition, setting pressure, the type of movement and setting speed etc. Based on the understanding of SPR riveting process, the different researchers used various friction coefficients in their simulation. Xu (Xu, 2006) used 0.1 as the friction coefficient in his simulation. A value of 0.15 was applied on the simulation by Khezri et al. (Khezri et al., 2000). Kato et al. (Kato, Abe, & Mori, 2007) and Abe et al. (Abe, Kato, & Mori, 2009) both used 0.2 as the friction coefficient in their simulation for all the surfaces. Krishnappa (Krishnappa, 2008) started to apply 0.15 and 0.3 as the friction coefficients on different surfaces. Atzeni et al. (Atzeni, Ippolito, & Settineri, 2007) used 0.2 as the friction coefficient to the interface of punch and rivets and the interface of rivets and material sheets. A value of 0.15 was applied to the interface of top and bottom sheets. And the friction coefficient between the bottom sheet and die was 0.1. Carandente et al. (Carandente, Dashwood, Masters, & Han, 2016) used the values of 0.15, 0.09, 0.15 as the friction coefficients at the same interfaces as Atzeni (Atzeni et al., 2007).

Mucha (Mucha, 2011) studied the influence of friction coefficient on displacement-force curve. The results indicated there was a little influence on the middle part of curve and no any variation for the rest of curve when the friction coefficient varied from 0.05 to 0.25. Hoang et al. (Hoang et al., 2013) used LS-DYNA to simulate the SPR process in order to find out the fracture mechanisms. Figure 2.19 showed that the variation of friction caused the different strain distribution during the riveting. With a value of 0,

there was no much strain that distributed at the contact field between rivet and top sheet. Once the value changed from 0.2 to 0.5, there was more strain that started to generate along a specific direction. The strain concentration became more and more obvious when the friction coefficients were 0.6 and 0.8. Westerberg (Westerberg, 2002) simulated the SPR process by ABAQUS to join 1.15 mm DP600 stacks. The results indicated that high friction coefficients could result in the high maximum load. And a high energy absorption and a large displacement were needed to form a joint.

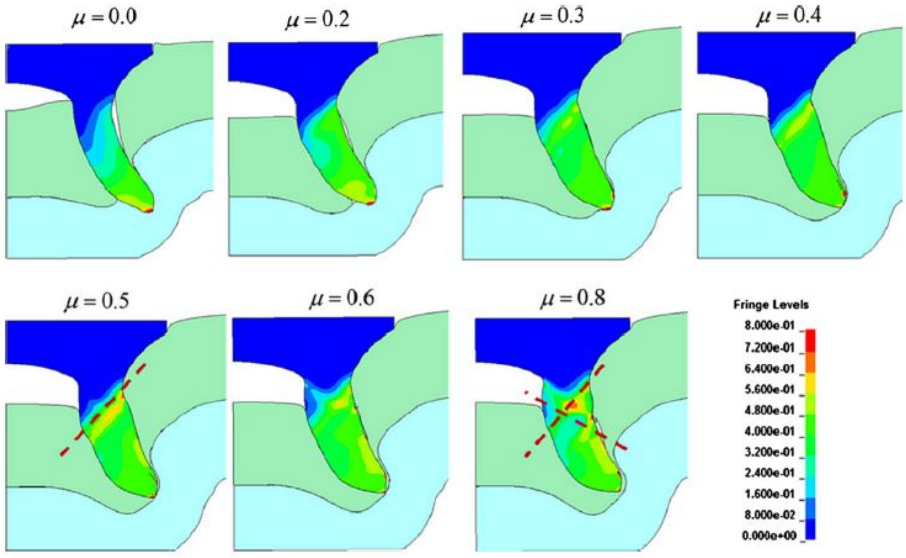

Figure 2.19. The strain fields under different values of the friction coefficient (Hoang et al., 2013)

The SPR as a cold forming process, the deformation of the bottom sheet in die cavity will introduce the severe plastic deformation. The fracture can happen on the joint button due to lacking of ductility for bottom materials. In the simulation of SPR process, the fracture had been studied by several researchers. Kato et al. (Kato et al., 2007) considered the fracture into simulation and used the fracture criteria to simulate the fracture at specific areas. When the height to width ratio of a single element was less than 0.1, this element would be removed to represent the fracture. Khezri et al. (Khezri et al., 2000) used Cockroft and Latham fracture model to define the fracture during the simulation. And equation 1 represents the fracture criteria by mathematic expression.

$$D_c = \int \sigma_{max}/\sigma_e d\varepsilon_e \tag{2.1}$$

Where D_C, σ_{max}, σ_e and ε_e represent the critical fracture value, the maximum principle stress, the effective stress and the effective strain, respectively. They used 0.5 as the criterial value to define occurrence of fracture. Furthermore, Atzeni et al. (Atzeni et al., 2009) used Gurson-Tvergaard model to define the fracture during the simulation. And Bouchard et al. (Bouchard, Laurent, & Tollier, 2008) used Lemaitre-coupled damage model as the criteria to remove the elements during simulation. Equation 2 shows the mathematic expression of Lemaitre-coupled model.

$$\sigma_e = \frac{\sigma}{1-D} \tag{2.2}$$

Where D is the internal damage variable and σ is the stress. D also can be defined as the void surface area (S_D) to the whole surface area (S) ratio. When the internal damage variable reached the limit, the element will be removed by setting zero of mechanical contribution to the stiffness matrix. Casalino et al. (Casalino et al., 2008) used a finer mesh and a higher effective plastic strain to reduce the volume loss from elements removal.

The simulation of SPR process has been used by many researchers. Di Franco et al. (Franco, Fratini, & Pasta, 2012) used DEFORM 2D to simulate the SPR process of joining carbon fiber reinforced polymer composites to aluminum alloys. And they summarized the failure mechanism of riveting process (Di Franco, Fratini, Pasta, & Ruisi, 2013) based on the compatible results between physical experiments and simulation results. Bouchard et al. (Bouchard et al., 2008) simulated the SPR process and listed the comparison between the physical experiments and simulation results in Figure 2.20.

The SPR technique has been studied comprehensively by many researchers. But there were still have some issues and topics that didnt solve and explore. The rapid development of body-in-white concept stimulates the further investigation on application of SPR for the die casting materials. The research is going to investigate the application of SPR for die casting aluminum alloys.

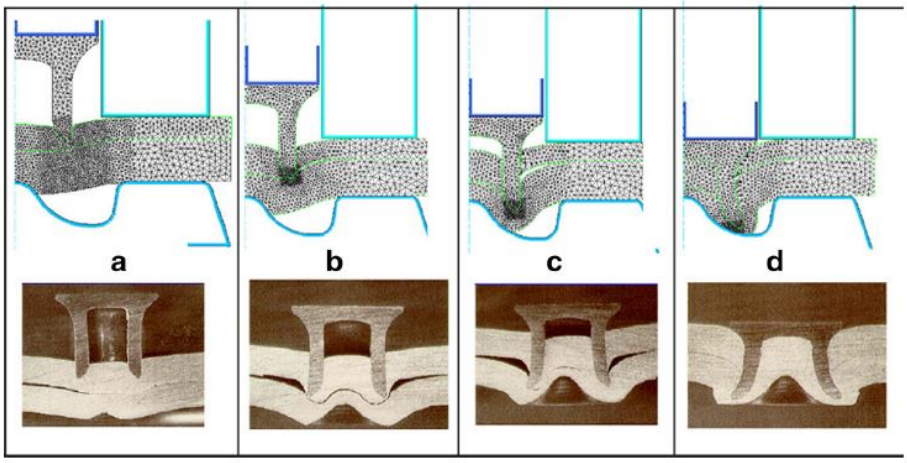

Figure 2.20. The comparison between the simulations and physical experiments of the SPR process in four stages

The main purpose of this research is going to improve the rivetability of die casting aluminum alloys. Because of the discrepancy in composition and microstructure, the die casting aluminum alloys trend to form the cracks on the joint button compared to wrought aluminum alloys. This research concentrated on disclosure of the cracking mechanism for casting aluminum alloys. Furthermore, the feasible solutions to suppress the cracks initiation and propagation was also provided in this study.

Instead of the crack mechanism analysis, the joint performance qualification has been introduced and discussed in detail because the joint strength is highly related to the cracking issue and the joint performance is substantial to reflect the influence of cracks. Furthermore, the study of SPR process parameters was also covered by this research because the process parameters played a significant role to determine the joint performance and joint quality. Eventually, the SPR simulation was introduced and studied in this thesis article because it was significant to further investigate the cracking mechanism. Moreover, it was useful to optimize the process parameters in order to improve the rivetability for die casting aluminum alloys.

CHAPTER 3. METHODOLOGY

The SPR was initially designed for joining the ductile materials because the localized severe plastic deformation would be introduced during the riveting. And the wrought aluminum alloys, such as 5xxx and 6xxx aluminum series, with sufficient ductility are capable to accommodate the riveting. Unlike the wrought aluminum alloys, the ductility of die casting aluminum alloys is not enough to accommodate too much plastic deformation. It becomes to the obstacle to apply SPR on die casting aluminum alloys. In order to improve the rivetability of die casting aluminum alloys, the influence of material composition, the microstructure evolution under heat treatment, the influence of riveting process parameter and simulation of riveting process are going to be introduced and investigated in this research.

3.1 Influence of composition on ribetability

There are three types of commercial aluminum alloys, A380, Ryobi alloys (W3), A6061, which have been used for experiment to study the SPR process. A380 as a common casting alloy has been widely used for die casting industry to fabricate high pressure die casting products. W3 alloy was developed by Ryobi Die Casting to produce the casting parts with a specific customer requirements. A6061 is an popular wrought aluminum alloy, which is used by many industries for their structural components and other parts. The composition of these three aluminum alloys has been listed in Table 3.1.

Table 3.1. The SPR experiment specimens composition (unit: wt%)

	Si	Fe	Cu	MN	Mg	Zn	Ti	Sr
A380	7.5-9.5	1.3	3.0-4.0	0.5	0.1	3.0	N/A	N/A
W3	7.5-8.5	0.1	0.1	0.5	0.2-0.3	N/A	N/A	0.02
A6061	0.4-0.8	0.7	0.15-0.4	0.15	0.8-1.2	0.25	0.15	N/A

In terms of the present understanding of rivetability, the ductility of aluminum alloy has a tight connection with the rivetability of material. Silicon (Si) as one of the high content elements in die casting aluminum alloys plays an important role to determine the ductility of casting alloys due to the brittleness of eutectic silicon phase. Moreover, the eutectic silicon structure is displayed as the plate-like morphology. The plate-like morphology under the loading condition would be the main reason to cause the crack initiation and propagation. In terms of the study on strontium addition to refine eutectic silicon for casting aluminum alloy, the influence of strontium (Sr) on eutectic silicon morphology will also be investigated to improve the rivetability of die casting aluminum alloy.

To make a comprehensive compare and contrast, A6061 as a typical wrought aluminum alloy with the low silicon content and good ductility has been used for SPR. In order to prove the influence of silicon content on rivetability of casting aluminum alloy, A6061 with 0.4-0.8 wt% of silicon has been used for forming a SPR joints. Without the obvious eutectic silicon phase in aluminum matrix, A6061 is an appropriate control group to investigate the effect of Si and Sr.

3.2 Applying heat treatment on die casting aluminum alloys

The influence of microstructure evolution on cracking initiation and propagation achieved by heat treatment has been conducted in this study. Based on the current knowledge of casting aluminum alloys, the eutectic silicon phase as a brittle phase could be the main reason to cause the cracks during the riveting process. Heat treatment would be the best choice to modify the silicon morphology in order to investigate the influence of silicon phase variation on the rivetability of die casting aluminum alloy.

W3 alloy as the major material has been used for heat treatment with the temperature varies from 200°C to 400°C with 50°C interval. And the heat treatment duration changed from 1 hour to 3 hours with 1 hour interval. Air cooling was applied until the specimens reach the room temperature after the heat treatment in order to imitate real production heat treatment. The heat treatment plan is shown in Table 2.2 in detail.

Table 3.2. Heat treatment plan for W3 alloy

Material	HT Temperature	HT Duration
Ryobi W3 Alloy	200°C	1hr, 2hrs, 3hrs
	250°C	1hr, 2hrs, 3hrs
	300°C	1hr, 2hrs, 3hrs
	350°C	1hr, 2hrs, 3hrs
	400°C	1hr, 2hrs, 3hrs

The heat treatment furnace made by Thermo Scientific is shown in Figure 3.1. The microstructure of alloys was characterized by optical microscope and SEM to analyze the microstructure evolution after heat treatment. And the SEM specimens were deeply etched by 0.5 %wt HF acid with 2 hours duration to observe three dimensional the silicon morphology.

According to the hypothesis on the discrepancy in composition and microstructure for aluminum alloys, the microstructures of three different alloys have been observed and characterized by optical microscope and Nova Scanning Electron Microscope (SEM). The optical microscope and SEM are made by Leica and FEI, respectively.

3.3 Shear Test of the SPR joints

Shear and peel tests were used for measuring the strength of the joints in the form of force verse displacement curve. The shear test specimen is made by a joint formed by joining two or multiple one times four inches sheets. The rivet is supposed to place in the middle of one inch overlap area. The peel test is going to use the same dimension sheets, and the overlap area needs to be bent with a 90 angle. However, the die casting aluminum alloys with the limited ductility are not able to be bent with a large angle. Thereby, shear test becomes to the only option to measure the joint strength. The SPR specimens were tested by the universe INSTRON tensile tester and the joint strength was recorded and expressed by the preload program in force verse displacement curve. The shear and peel test configurations and the shear test results are shown in Figure 3.2. In particular, there is

Figure 3.1. Heat treatment furnace for aluminum alloy specimens

a 30% F*max* line that appears in the force verse displacement curve. In order to avoid the data from the sliding at the early stage of shear test, the initial 30% of force is exclusive from the effective joining. The total energy, which will be absorbed by the joint, is calculated by computing the shaded area below the curve and above 30% F*max* line.

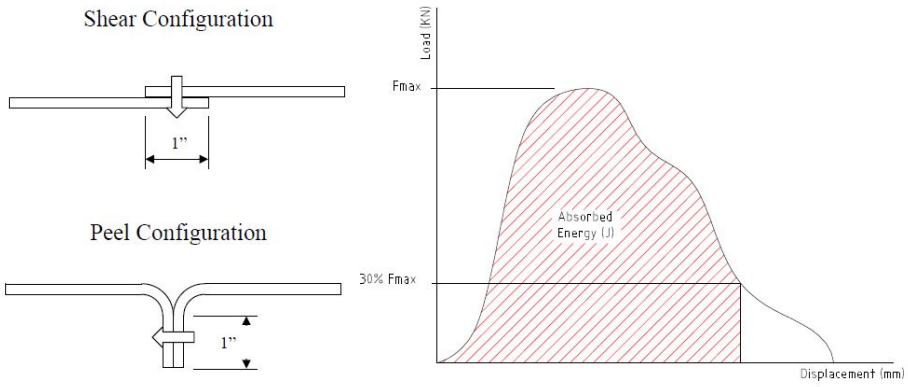

Figure 3.2. The shear and peel test specimens configuration

In order to investigate the influence of heat treatment on rivetability, shear test is an effective method to reflect the variation of joint strength. Heat treatment enables to modify the microstructure of casting aluminum alloy. The mechanical property and the rivetability of casting material can be altered by the microstructure evolution. The joint strength from shear test can quantify the magnitude of the improvement on rivetability and also can investigate the influence of material property on the joint performance.

3.4 Influence of die depth on joint performance

The two or three layers material sheets are joined by the rivet shank flaring for the SPR process. The joint strength is mainly determined by the interlock distance after riveting. There are several process parameters that can affect the interlock distance. Die depth as an effective and simple process parameter that can be adjusted in experiment and manufacturing to adjust internlock distance.

In theory, the deeper die enable to obtain the larger interlock distance due to introduction of more plastic deformation during the riveting. However, the high plastic deformation could result the severe cracks on the joint button if the bottom material is lacking of ductility. The joint strength can be reduced by the appearance of those cracks and there are some of unknown side effects that could affect the joint performance, such

as corrosion. In order to understand the influence of die depth on joint performance, the dies with 1.8 mm, 2.0 mm and 2.2 mm in depth and 8 mm in diameter as shown in figure 3.3 were about to use for this study. The material sheets with different heat treatment conditions were tested by using three different dies and the joined specimens were also examined by shear test to obtain the joint strength.

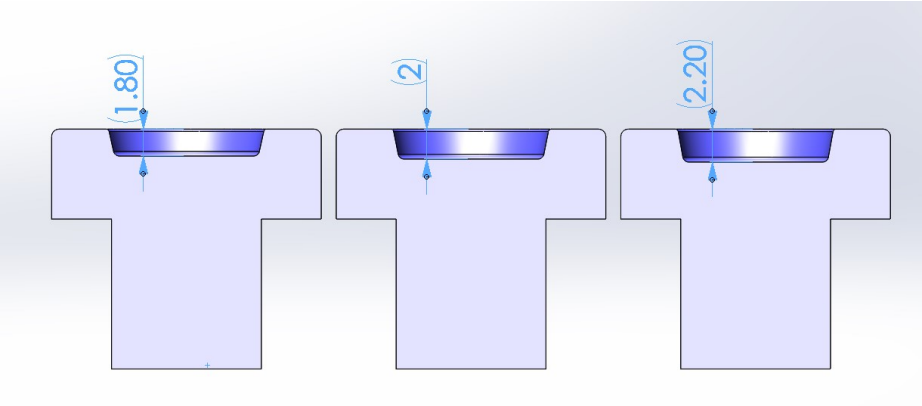

Figure 3.3. The die with three different depths

The shear test specimens were made and joined by the SPR facilities at Ryobi and Henrob. The facilities are shown in figure 3.4. the SPR system at Ryobi is equipped with hydraulic driving system. The SPR facility at Henrob has servo-motor driving system with adjustable punching speed. The high strength steel plates (DP600) with 1.4 mm thickness were joined to the aluminum alloy plates. And the rivets with 5 mm in diameter were used for the experiment.

3.5 Influence of cracks on joint performance

To better understand the relationship between the cracks and joint strength, a novel cracks statistical method was created and utilized by this study. There are two types of cracks that can be observed on the joint button. The small cracks look like an irregular lines, which are usually distributed on the joint button area in radial direction. The large cracks with a certain amount of opening can lead to the further failure of the joint. Figure 3.5 shows the schematic of the two types of cracks in detail.

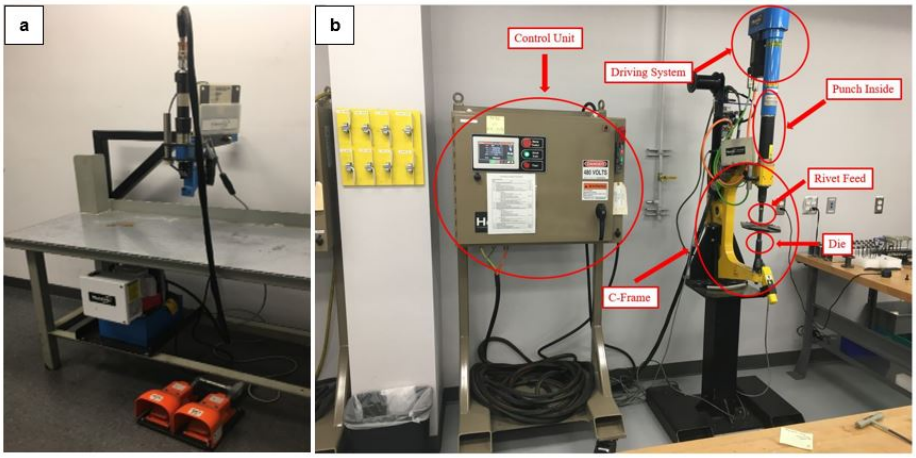

Figure 3.4. The SPR system at (a) Ryobi Die Casting (b) Henrob Corporation

In order to understand the connection between cracks and joint performance in a scientific way, both types of cracks were calculated and summarized in this study. ImageJ as a powerful image processing software was used for counting the quantity of the small cracks in higher magnification pictures and measuring the large cracks opening length. The profile of the joint button looks like a compressed cylinder and all the cracks appear on the top circle area. Because the small cracks look like a line and the large cracks are shown as the discontinuous opening spaces on the button field, the small cracks were counted in number and the total length of large cracks were counted and calculated by ImageJ. If the top circle is opened up and expanded to perimeter line, the two types of cracks will be laid on the perimeter line. Eventually, the fraction of small cracks in number over top circle perimeter and the total length of large cracks over top circle perimeter were calculated and summarized in order to compare the cracking conditions by normalization for the joined materials with a various processing conditions.

Based on the results from crack counting and the joint strength from shear test, it is clear to build the relationship between the two types of results and conclude the relationship between each other by combining all the data.

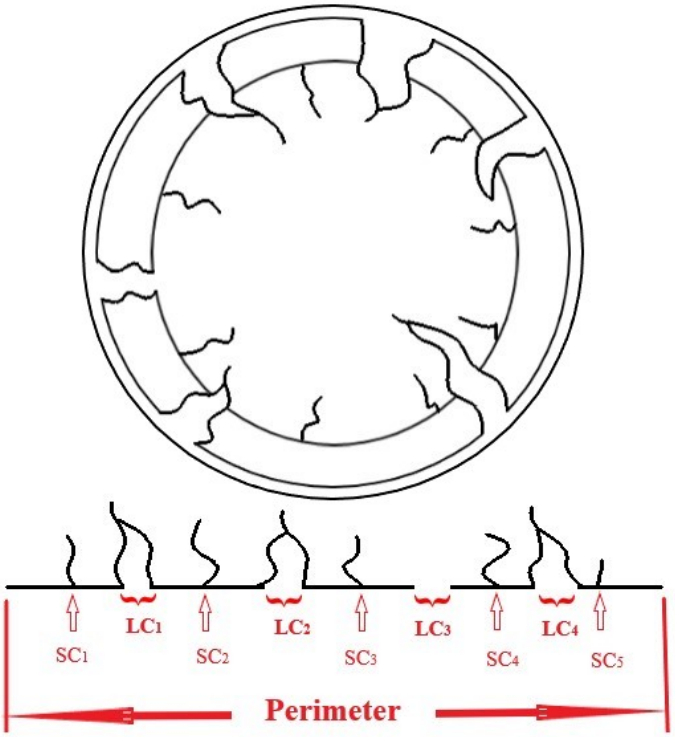

Figure 3.5. The schematic of crack calculation method

3.6 Simulation of the SPR process

Finite Element Analysis (FEA) achieved by the commercial simulation software is a powerful and an effective tool to provide the assistance in virtual. The SPR also can take advantages from simulation to optimize the whole process without the physical experiments.

The SPR simulation in this study was proposed and conducted by FORGE, which is developed by Transvalor to analyze the cold metal forming process. The simulation models, such as rivets and dies, were built according to the real dimensions of commercial the rivets and dies from Henrob. And the specifications the materials were set based on database and references from the other researchers. The model design of SPR process is shown in figure 3.6. The models used in the study is a 2D symmetric design. It is helpful to reduce the calculation load instead of using the whole piece design.

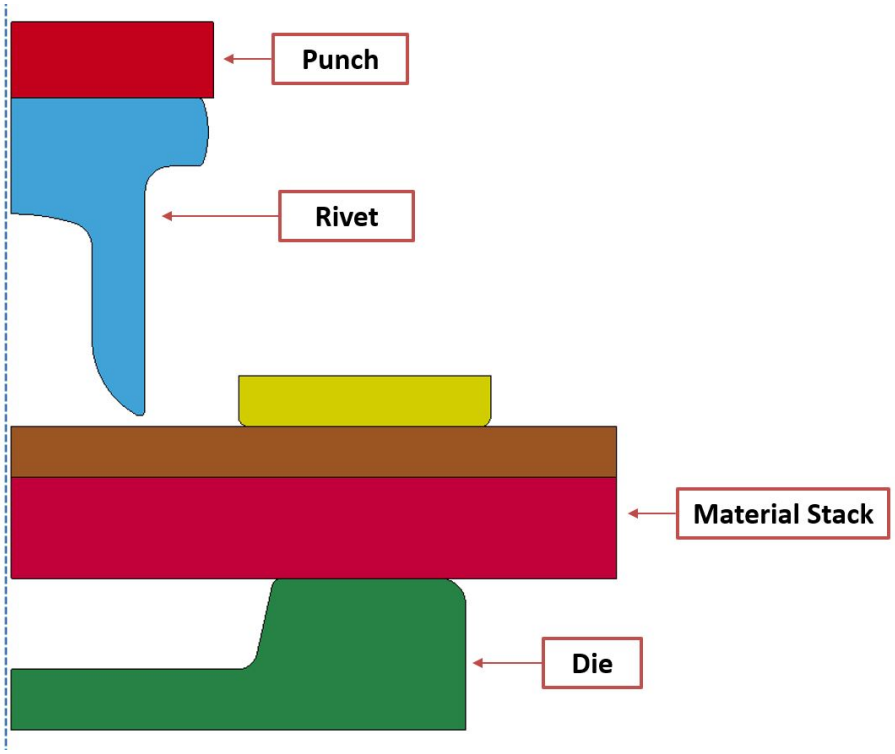

Figure 3.6. The model design of the SPR simulation

The general outputs of simulation will be the strength and strain distribution on each components. Because of the severe plastic deformation during the riveting, the fracture conditions have been analyzed according to Normalized Cockcroft & Latham criterion for cracks prediction. Because of the simplicity of simulation, the die with different cavity geometries were also simulated to improve the rivetability of the die casting aluminum alloys.

CHAPTER 4. RESULTS AND DISCUSSION

4.1 The influence of composition variation on crack formation

Three different types of material have been used for the SPR test. The feature of joint button shows in Figure 4.1. This figure indicates that A380 and W3 alloy turn out the severer cracks on the button site. The cracks on A380 joint button are worse than W3 alloy because these cracks have started to connect with each other. The crack connection could lead to the joint button peel off and destructive failure under loading condition. Unlike A380, the cracks on joint button with W3 alloy have smaller opening distance and each cracks are relatively independent. However, appearance of cracks on the button still could lead to the catastrophic failure under intense driving situation and severe corrosion condition. In comparison, A6061 is much better than both casting alloy to resist crack generation. With the same riveting condition, there is no obvious crack that exists on the joint button. Because of the good ductility of A6061, the wrought aluminum alloys have the better reivetability rather than the die casting alloys.

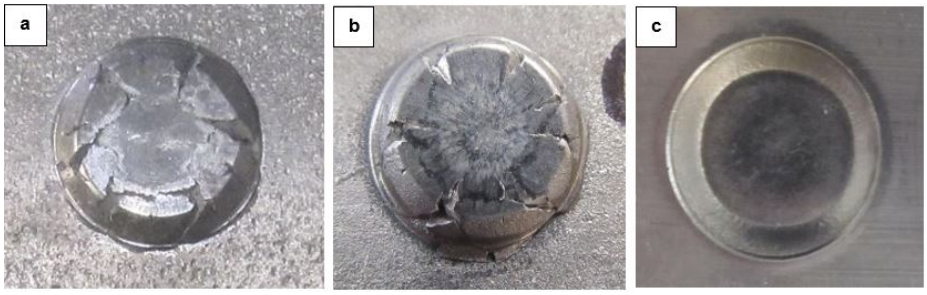

Figure 4.1. The feature of the SPR joint button, (a) A380 (b) W3 alloy (c) A6061

Table 3.1 shows the composition difference among each materials. The major difference between the casting alloys (A380 and W3) and wrought alloy (A6061) will be the silicon content. The silicon in the A380 and W3 is at least seven folds larger than A6061. The high silicon content in casting alloys can guarantee the castability during the casting process. Especially the high pressure die casting process requires the excellent

mobility of molten aluminum because the liquid aluminum should be squeezed into the complex structure die cavity in a second. The microstructure of silicon in casting alloys performs as a brittle silicon network comparing to the wrought aluminum alloys. And figure 4.2 shows the microstructure comparison between W3 alloys and A6061 alloy. The main difference between the two alloys is the existence of eutectic silicon phase. The corral-like eutectic silicon phase fills the large amount space in the aluminum matrix. But there is no obvious the silicon phase that can be found in A6061 alloy. Furthermore, the silicon phase performs as the brittle phase in casting aluminum alloys. Generally speaking, the ductility or elongation of the casting alloys is lower than the wrought alloys. Actually, the brittle silicon phase is main reason to cause the brittleness of casting aluminum alloy. Because the silicon phase will firstly start to break when the alloys under the loading condition. And the fracture of silicon phase will occur at the multiple locations in the eutectic silicon network. The fracture initiation and propagation at multiple sites on the silicon network will eventually lead to the visible cracks of the material. Compared to the casting alloy, there is no visible brittle phase that can be found in A6061 alloy. Lacking of the brittle phase is also the main factor to cause the better elongation of wrought alloy.

In terms of the silicon content difference and the brittleness of eutectic silicon phase in the casting alloys, the appearance of cracks on the joint button is supposed to have a tight relationship with the silicon content and phase. However, the several elements in the three alloys may have the influence on cracking. The significance of these elements needs to be investigated and discussed.

Iron (Fe) as a common element usually can be found in many alloys. Nowadays, most of the aluminum products are made by the secondary alloys. The content of iron is hard to control at the ideal range. A380 as a one of the most common casting alloys has been used for industry for years. The high iron level could be caused by large-scale utilization. W3 alloy from Ryobi is made by the primary alloy, the iron content can be perfectly controlled by the melting and casting process. Iron is usually used for die soldering control purpose. The high iron level can avoid the soldering during the casting. Manganese (Mn) has the same function as iron. It can keep the die stay away from the soldering. Mn has been used by die casting industry to compensate the iron. Because iron

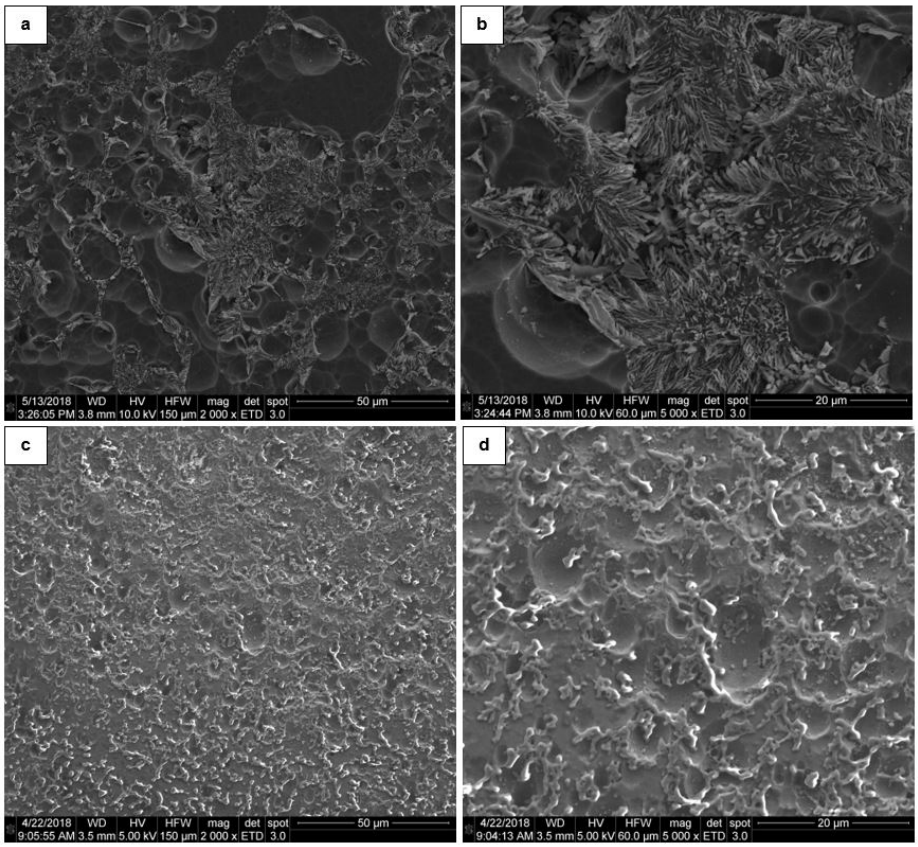

Figure 4.2. The microstructures characterized by SEM (a) W3 alloy in 2000X (b) W3 alloy in 5000X (c) A6061 in 2000X (d) A6061 in 5000X

tends to form the brittle second phase during the cooling, the addition iron needs to be replaced by manganese. Meanwhile, the alloys still have the function to avoid the die soldering. Copper (Cu) and Zinc (Zn) at specific range do not have much influence on the mechanical property of these aluminum alloys. However, the 3 4 wt% Cu in A380 can provide the strengthening phase during the aging process. Meanwhile, Cu and Zn can provide the good corrosion resistance to the alloys. Magnesium (Mg) plays an important role in aluminum alloys because the content of Mg is highly related to the mechanical property of the alloys after heat treatment.

Generally speaking, Mg will be used for strengthening the aluminum alloys by the precipitation hardening process via natural aging process and heat treatment. Natural aging process is a relative slow hardening process. The saturated Mg will gradually

precipitates in aluminum matrix as Mg_2Si phase. But the whole process needs to take several days and even several months to make the materials reach the ideal strength. The typical heat treatment method, such as T6, will initially dissolve more Mg into the aluminum solid solution. Then the artificial aging is exerted to accelerate the aging process. The more Mg_2Si as the hardening phase can be precipitated in aluminum matrix in several hours. The strengthening mechanism of Mg_2Si particles is called pinning effect as shown in Figure 4.3 (Gladman, 1999). The uniformly distributed Mg_2Si solid particles can pin the dislocation in aluminum matrix under loading condition, and the materials under the pinning effect can obtain the higher ultimate and yield strength. Although the precipitation hardening can elevate the mechanical property of material, it could lead to the cracking issue during the riveting due to the scarification of ductility. A380 and W3 alloys have limited amount of Mg, the precipitation hardening wont be the primary reason to cause the cracks. A6061 alloy has sufficient Mg in the material, the cracking issue has been observed during the riveting process once A6061 alloy experienced T6 heat treatment.

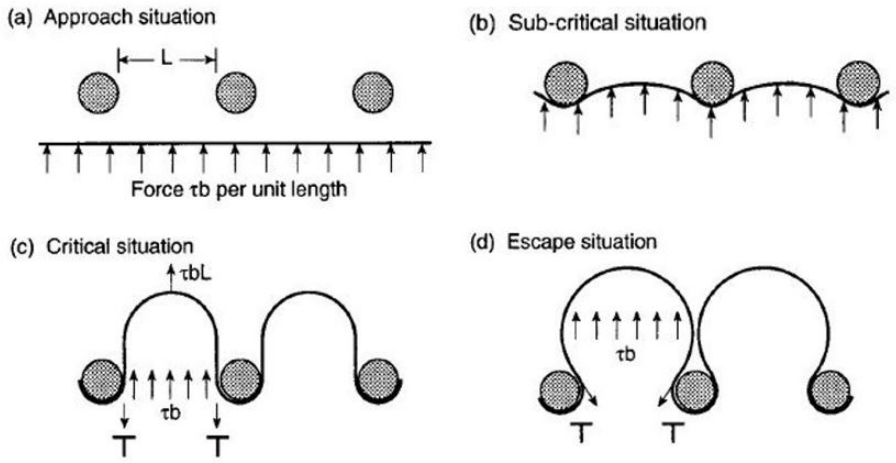

Figure 4.3. Pinning effect of precipitation hardening (Gladman, 1999)

There is another element called Strontium (Sr) that only existed in W3 alloy. However, this element is the key to determine the morphology of eutectic silicon for the die casting aluminum alloy. Wang and Shivkuar (L. Wang & Shivkumar, 1995) studied

the influence of strontium on the eutectic silicon morphology. Figure 4.4 shows the evolution of eutectic silicon morphology with different amount of Sr addition. It is clear to see that the eutectic silicon changed from the plate-like and needle-like morphology to the corral-like form. The silicon phase was gradually refined when the amount of Sr increased to 0.015%. Hedge and Prabhu (Hegde & Prabhu, 2008) indicated that the eutectic silicon with a large plates or needles morphology would turn out the low ductility and tensile strength. Once the alloy is modified by Sr, the ductility of material will be undoubtedly improved by refinement of eutectic silicon phase. In consideration of cracking issue, Sr indeed provided the help to control the crack. Figure 4.1 shows the joint button features with three different alloys. A380 without Sr modification showed the severe cracks on the joint button. The material on the button could break into pieces because some of the cracks have connected with each other. The eutectic silicon phase in W3 alloy with 0.02 wt% Sr addition has been refined to the corral-like morphology as shown in Figure 4.2. The cracks initiated from the edge of the joint button and started to propagated in radial direction. But there was no converge of cracks that occurred on the joint button. Although the magnitude of cracking is linked to the morphology of eutectic silicon, the further study of the relationship between cracking and eutectic silicon morphology needs to be conducted and proved.

Combining with the previous results, the cracks can be reduced in quality and magnitude when the silicon content goes lower and the eutectic silicon phase transforms from plate or needle-like morphology to corral-like morphology. A6061 with the lowest silicon turns out the best rivetability among three alloys. Once the silicon content goes higher, it will introduce more brittle eutectic silicon phase in the aluminum matrix. The eutectic silicon phase under the server plastic deformation situation is easy to break. The massive silicon phase breakage in aluminum matrix results the crack generation and those cracks are going to propagate along the silicon network. There is no big difference between A380 and W3 in silicon content. Nevertheless, the addition of strontium in W3 alloy modifies the silicon morphology. The silicon phase will transform from the coarse plate-like morphology to the fine corral-like morphology under the effect of strontium. It leads to W3 alloy with the corral-like silicon morphology has the better rivetability than

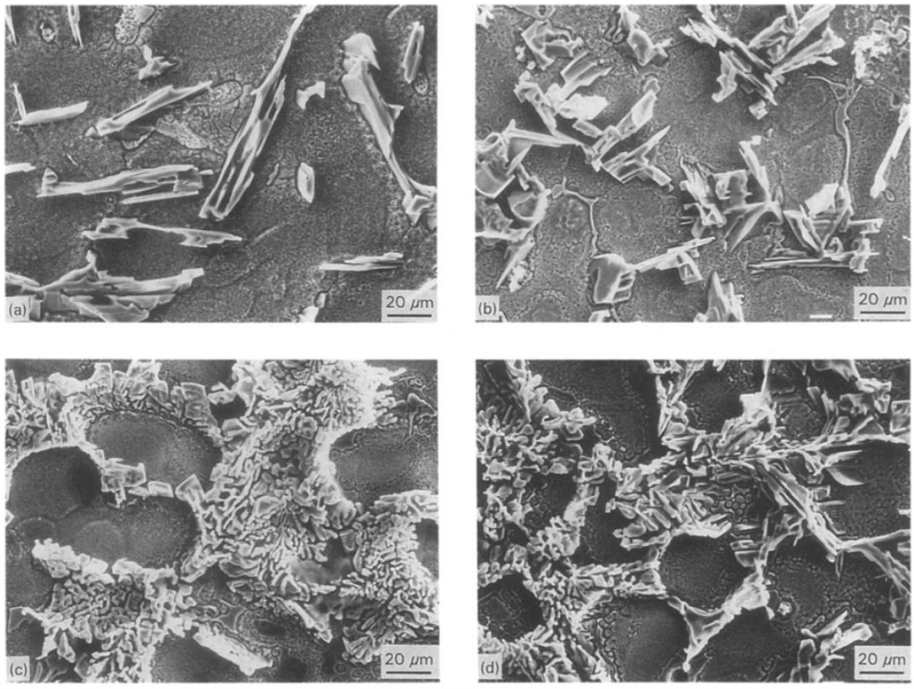

Figure 4.4. The eutectic silicon morphology evolution with different amount of strontium, (a) 0.0004% (b) 0.011% (c) 0.015% (d) 0.025% (L. Wang & Shivkumar, 1995)

A380 alloy. Thereby, the silicon content and the morphology of silicon phase for casting alloy dominates the cracking issue on joint button.

4.2 Cracking mechanism analysis

To further understand how the crack generate and propagate on the joint button, the crack mechanism needs to be explored and studied. In macro-perspective, the bottom aluminum alloy sheet at the joint spot will be compressed into the die cavity in a short time period. The aluminum sheet at the joint button site will experience a severe plastic deformation during the SPR process. Partial materials are going to deform under the compression, and some of them are about to deform under the tension.

Figure 4.5 shows the effective strain and fracture distribution at the joint button area in cross-section view from the SPR simulation. In term of the effective strain field distribution, the most of deformation fields have at least 0.15 effective strain, which can be

measured by the scale bar on the left hand side. The highest strain fields concentrated around the rivet shank because the material around it have the largest deformation when the rivet penetrates the both sheets. Then the secondary high strain fields are mainly located at the area under the rivet shank and the areas at the interface of the bottom sheet and die cavity. Depending on the strain field calculated by the simulation, the materials inside of the die cavity will almost experience the fracture due to the effective strain in these areas is much larger than the material can withstand. However, the real case is the cracks will generate at the edge of the joint button and propagate in radial direction as shown in Figure 4.1.

In fact, the distribution of strain field around joint button area is determined by two types of deformations. The material deformation in die cavity is caused by tension and compression. The material inside of the yellow oval as shown in Figure 4.5 (a) is being compressed when the rivet shank is flaring. And the materials in two red ovals is being pulled by the tensile force to deform. The elongation or strain of the materials is usually measured by the tensile test. Therefore, only the effective strain of materials at tension area can be used to determine the fracture by the strain comparison. In order to observe the fracture field distribution, the Normalized Cockcroft & Latham criterion is introduced to analyze the fracture situation. Figure 4.5 (b) indicates that the main fracture fields concentrated at the right-hand side of rivet shank and the field of interface between the bottom material and die cavity. Combining with the analysis of tension and compression and the cracks positions on joint button as shown in Figure 4.1, the cracks prefer to initiate on the edge of joint button and then the cracks will propagate along a specific direction.

From the micro-perspective to understand how the crack initiate and propagate, Figure 4.6 (a) and (b) show the microstructure of W3 alloy at crack site is a good start. Figure 4.6 (a) shows that the crack starts at the edge of joint button and propagates in radial direction during the SPR process. In terms of the previous analysis from simulation, the cracks are easy to form at the high tension areas, such as the edge of joint button. Since the material can not withstand the high tensile force, it will start to break from the tension field. Then the cracks will keep propagating a certain direction under the tension.

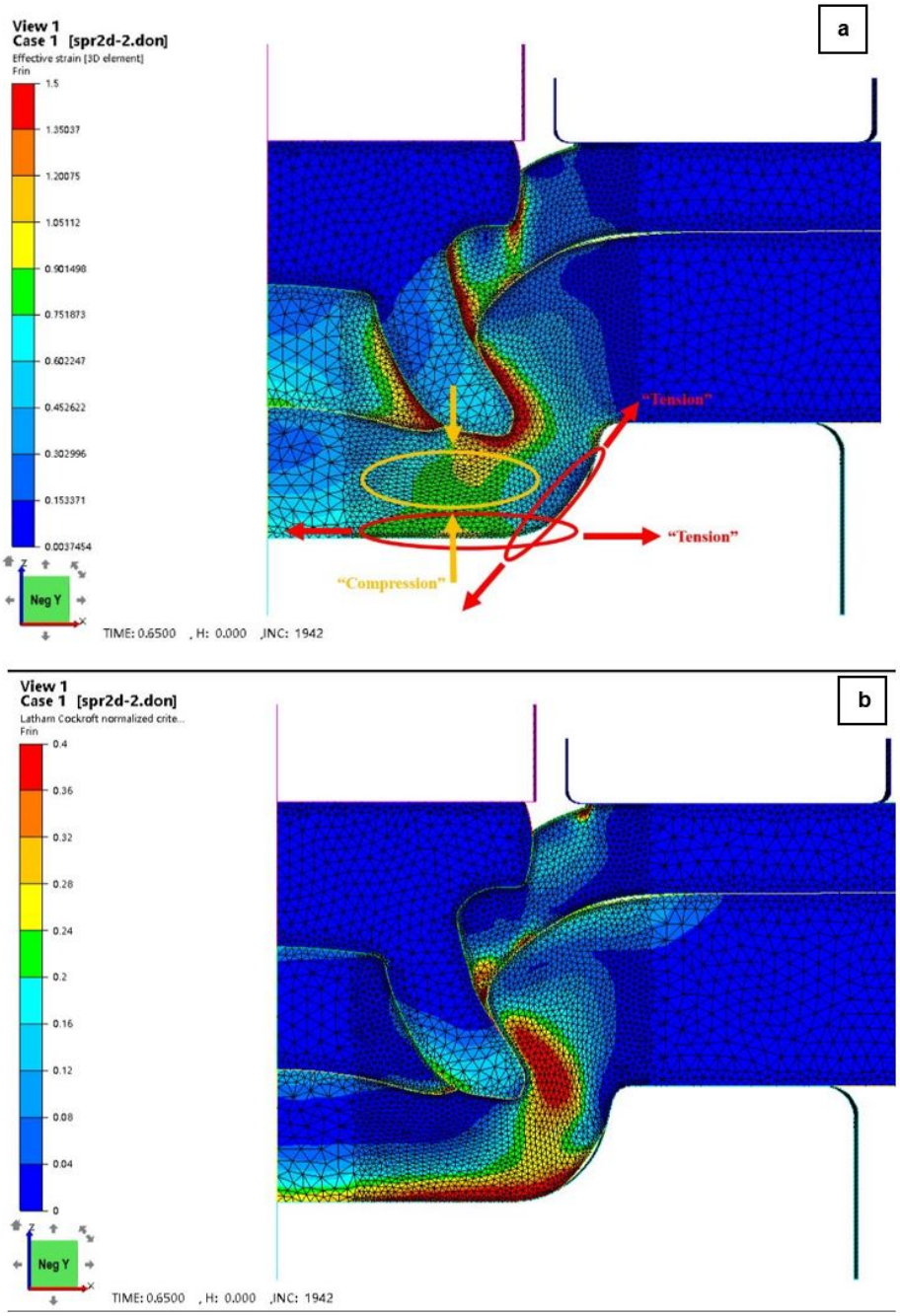

Figure 4.5. The SPR simulation with (a) effective strain field distribution (b) fracture field distribution

In order to find the cracking path after breakage, the higher magnification of crack propagation site image as shown in Figure 4.6 (b) needs to be discussed. The figure indicates that the crack initiates from larger opening crack site and propagates along the

eutectic silicon spots. Based on the understanding of eutectic silicon phase, the crack propagation path is mainly caused by the brittleness of eutectic silicon phase. Generally speaking, material failure is caused by the applied stress or strain is over the threshold that the material can sustain. The threshold or mechanical property of the die casting aluminum alloy is tightly related to the eutectic silicon content and morphology. Because of the brittleness of eutectic phase, the cracks will start to generate at the eutectic silicon sites and further propagate along the brittle silicon network.

The morphology of the eutectic silicon phase is another main reason to cause the cracking initiation. Figure 4.6 (c) shows that the silicon phase is presented as the corral-like network morphology. Because the silicon phase under high loading situation is easier to cause the stress concentration on the sharp-tip sites, the crack will initiate at the sharp-tip and keep propagating along its network. Eventually, the convergence of multiple site cracks will finally lead to the visually large opening cracks on the joint button. Therefore, the morphology of eutectic silicon plays an important role to control the crack generation and propagation.

In terms of the analysis from macro- and micro-perspectives of cracking issue on the joint button, the content and morphology of eutectic silicon phase play an important role to influence the rivetability of die casting aluminum alloys. Because the certain amount of silicon content is crucial to determine the castability of the aluminum alloys, the modification of silicon morphology become to the most feasible solution to improve the rivetability of the die casting aluminum alloys.

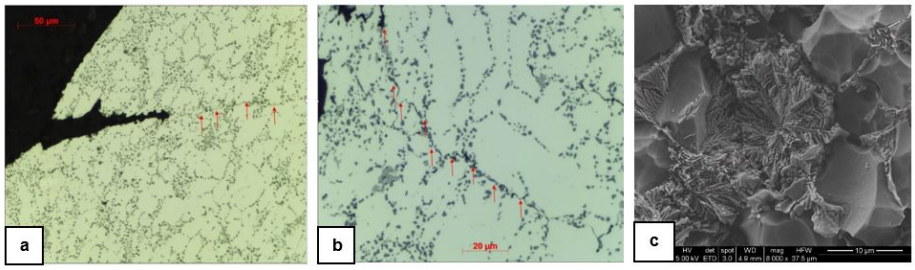

Figure 4.6. The microstructure at crack site, (a) low magnification (b) high magnification (c) SEM picture of as-cast bulk material

4.3 Rivetability improvement by heat treatment

In order to change the morphology of eutectic silicon in die casting aluminum alloy, heat treatment will be the first and foremost option. Because the most of the die casting parts need to be heat-treated for strengthening and thermal stress release purpose, there is no additional work that needs to be conducted and the rivetability can be improved by simply setting and adjusting the heat treatment plan.

4.3.1 Microstructure evolution of eutectic silicon phase

Heat treatment is a feasible solution to manipulate eutectic silicon morphology. Silicon phase in as cast W3 alloy performs as the corral-like morphology. But eutectic silicon can change its morphology under the certain heat treatment condition and the elongation of the material also could be improved.

Figure 4.7 and 4.8 shows the joint button profile associated with the corresponding bulk material microstructure at each heat treatment temperature condition. The rivets were used for joining with 5 mm in diameter and the die cavity depth was 1.8 mm. Without heat treatment, as cast alloy performs a corral-like silicon morphology, and the joint button exhibits the severe cracking condition after SPR. Once the heat treatment was applied, the silicon phase started to change its morphology.

There was no obvious change when the temperature went up to 200°C. The silicon phase was similar to the as cast condition and the joint button showed the minimum difference in cracking profile. However, when the temperature reached 250°C, the silicon phase began to break and the silicon dendrite arms were not protruded like as cast condition. By increasing the temperature up to 300°C, the dendrite arms were additionally broken and the thickness of the dendrite arms were reduced dramatically. And there was no such big corral-like dendrite existed in the aluminum matrix. In addition, the cracks on the button were further suppressed and the large opening cracks were gradually closed and turned into the smaller size. Nevertheless, the most obvious transformation of silicon

phase occurred when the temperature raised up to 350°C. There was no corral-like silicon phase in the aluminum matrix and the most of dendrites had been broken into pieces.

Corresponding to the joint button profile, the large opening cracks were completely wiped out at this temperature and there were only several small cracks shown on the button area. To further change the silicon morphology, the heat treatment temperature was increased to 400°C. The silicon particles had been spherodized in aluminum matrix. And there was no large opening cracks that appeared on the button.

4.3.2 The influence from the eutectic silicon morphology variation

The eutectic silicon morphology of die casting aluminum alloy can be modified by the heat treatment, the rivetability of the casting alloy also would be improved by this phase modification. Because the silicon phase with the spherical-like morphology comparing to corral-like structure is relatively difficult to cause stress concentration during the riveting. Although some of the micro-cracks enable to form at the silicon sites, these cracks are hard to propagate and further cause destructive material failure by taking advantage of the broken silicon network. As a result, heat treatment can be regarded as a feasible solution to improve the rivetability for die casting aluminum alloy by the modification of silicon morphology.

The heat treatment not only improved the rivetability of the aluminum alloys, but also caused the variation of mechanical property of the material. Figure 4.9 shows the overall tendency of mechanical property for W3 alloy under various heat treatment conditions. The elongation was inclining with the heat treatment temperature. Eventually, the broken silicon network and the spherical eutectic silicon particles improved the elongation of die casting aluminum alloys. In opposite, ultimate tensile strength (UTS), yielding strength (YS) and hardness were reduced by the heat treatment. Although the silicon phase shows its brittleness in aluminum alloy, it also can reserve the hardness and rigidity of material under the loading condition. Once the silicon network was broken and most of the silicon phases become to spherical-like morphology, the strength and hardness of aluminum alloy were further decreased.

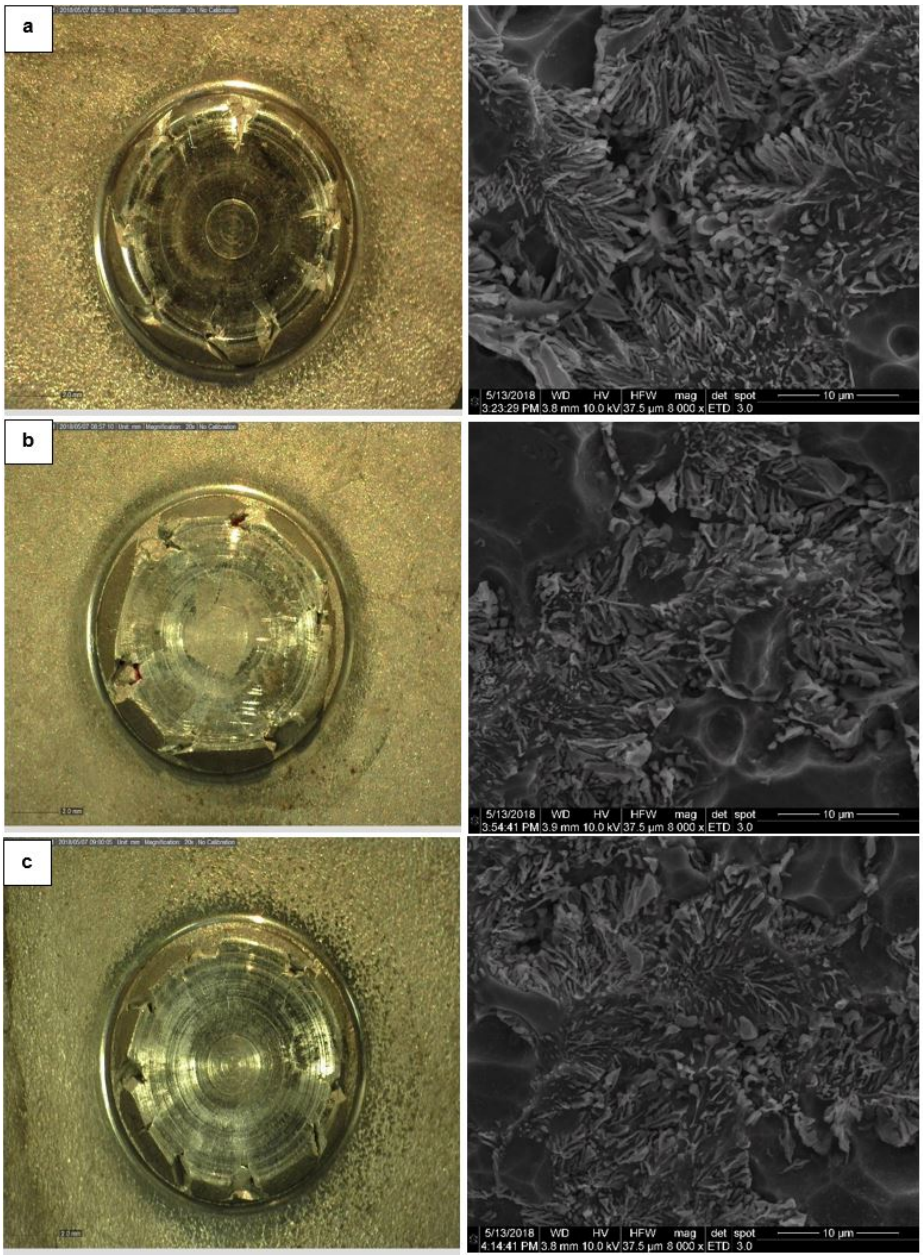

Figure 4.7. The joint button profile and bulk material microstructure evolution under different heat treatment condition, (a) As Cast (b) 200C (c) 250C

In fact, the silicon phase is not only hardening phase in aluminum alloy. The magnesium particles dissolved in aluminum matrix is going to precipitate into the matrix in Mg_2Si form. The precipitation hardening by aging process would be the most important hardening method used by industry. The strength of W3 alloy was also enhanced by the

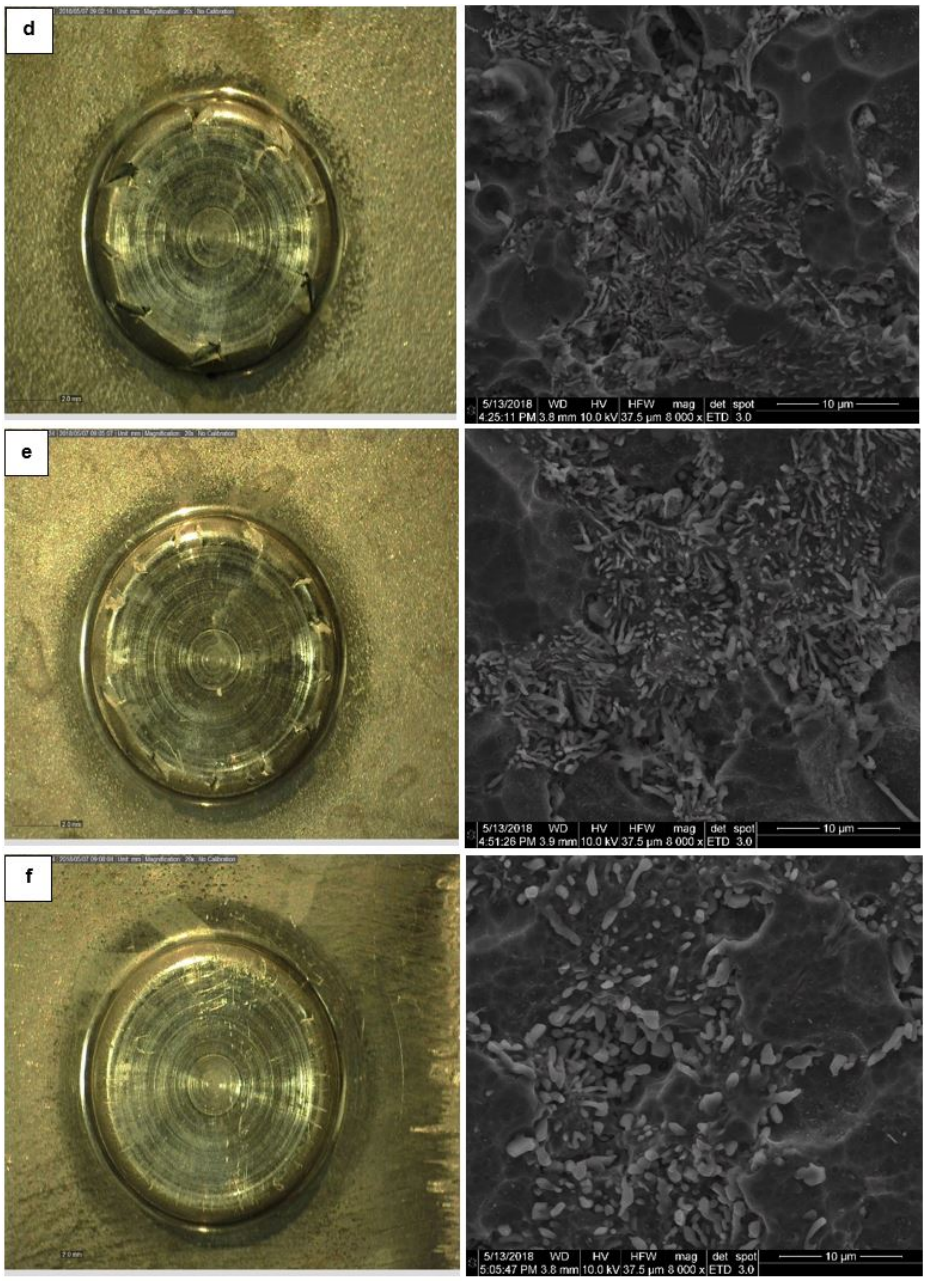

Figure 4.8. The joint button profile and bulk material microstructure evolution under different heat treatment condition, (d) 300C (e) 350C (f) 400C

precipitation hardening process as shown in Figure 4.9. When the alloy was heat-treated at 200°C for 3 hours, the strength of the material was slightly increased. However, the strength of the alloy started to decline when the temperature increased to 250°C. In terms

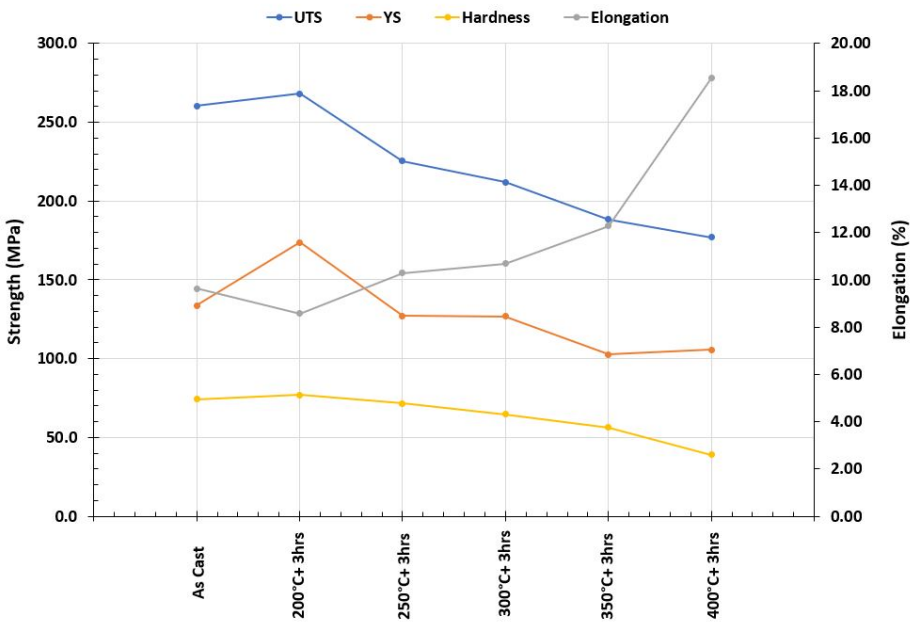

Figure 4.9. The mechanical property variation of W3 alloys under different heat treatment conditions

of the silicon morphology evolution and precipitation hardening mechanism, the strength was reduced by both eutectic silicon phase spherization and the confined solubility of magnesium in aluminum matrix. In general, the die casting aluminum alloys strengthening by heat treatment includes two steps. The first step called solutionization, which is going to dissolve more magnesium into the aluminum matrix and form the oversaturated solid solution. Then the second step is going to precipitate the magnesium into the matrix in Mg_2Si form. Because of lacking solutionization process for W3 alloy, the magnitude of hardening by Mg_2Si precipitation was smaller than the magnitude of softening by eutectic silicon network breakage. The combination of two effects finally resulted in the strength decline of the material.

Although the rivetability of die casting aluminum alloy would be improved by the heat treatment, the mechanical property of material was sacrificed in the meantime. The heat treatment in 400°C can result the best rivetability, but W3 alloy with only 177 MPa in UTS and about 106 MPa in YS was unqualified for most the products specification. The

other methods need to be studied for rivetability improvement of die casting aluminum alloy.

4.4 Rivetability improvement by adjusting process parameter

The process parameters of SPR process are essential to determine the quality of SPR joint because the joining process is highly related to these parameters. Even by simply changing a SPR process parameter, the SPR joint performance can be affect in a large scale. Because of the multiple variables in SPR process, the several parameters need to be constant, such as the rivet, sheet material thickness, die cavity geometry and punch speed etc. Die cavity depth as one of the SPR process parameters is substantial to determine the joint quality in terms of controlling the volume of material filling. In general, the deep die can create larger interlock distance, and the joint strength also can be improved. However, the deep die needs more material to flow into the die cavity and the high ductility is required by the bottom layer material. Otherwise, the bottom material tends to cause the cracks on the joint button and the joint strength could be reduced due to this defects. Once the cracks are formed on the joint button, it could lead to more quality issue, such as corrosion and low fatigue strength. In order to further learn the influence of die depth on joint quality and improve the rivetability of die casting alloy, the die depth is the best candidate to be used and investigated.

The various die with different depths have been used in this study. The joints were formed by joining a 1.4 mm DP600 steel to a 3 mm W3 die casting aluminum alloy. And the die with 1.8 mm, 2.0 mm and 2.2 mm depth were selected for the SPR joining process. In order to check the joint quality, the shear tests were also conducted on Instron tensile tester at Henrob and the results were presented as the displacement verse force curve. Due to the low ductility of die casting alloy, the cracks were formed on the joint button. A novel crack statistical method was introduced in the following to systemically calculate the number of cracks appeared on the joint button. Eventually, a method to combine the crack observation results and shear test results were introduced and discussed in this study.

4.4.1 The influence of heat treatment and die depth on the joint strength

As the most important parameter of SPR joint, the joint strength can be measured by the shear test. In fact, shear test and peel test are the typical tests to evaluate the SPR joint strength. But the peel test is required the materials have a good ductility to bend the testing plates with 90 angle. Because of this limitation, the shear test becomes to the first option for die casting components. Shear test is going to show how much energy that SPR joint can absorb during the shear loading situation, and the result is presented as the force verse displacement curve. In theory, the joint is formed by the deeper die depth can turn out higher joint strength because the deep die depth will create the larger interlock distance. However, the severe cracks will appear on the joint button if the bottom layer material doesnt have enough ductility. The cracks on the joint button could lead to destructive failure, which is coming from the crack propagation on the joint button. In order to comprehensively check the joint quality, the joint strength from shear test and the cracks statistics both need to be taken into consideration.

Figure 4.10 shows the shear test report exported by the preload program of Instron tensile tester at Henrob. The joint strength was represented as the load verse the total displacement curve from the beginning to the joint failure. The area under the curve was calculated and presented as the total energy that absorbed by the joint. The effective total energy should be calculated to get rid of the area below 30% of load because the energy within the 30% load area could be caused by the specimen sliding at initial testing period and null joining at the end the test. In addition, the die with 1.8 mm, 2.0 mm and 2.2 mm depth has been tested to investigate the influence of die depth on the joint strength. Based on those results, the analysis of joint strength under different joining and material conditions will be discussed in the following.

Figure 4.11 shows the SPR joint strength comparison by using 1.8 mm die when W3 alloys was heat-treated under various temperature conditions for 2 hours. The values of joint strength don’t vary too much and the heat treatment doesn’t have too much effects on joint strength improvement. Although the UTS and YS of W3 alloy have a obvious

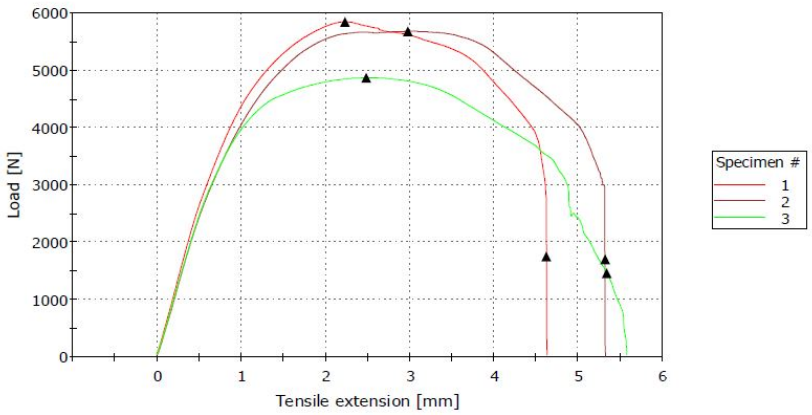

	Specimen No.	Head Height [mm]	Peak Load [N]	Energy to Peak [N-mm]	Total Energy (30% Break) [N-mm]	Elongation at Peak [mm]	Failure Mode
1	180	0.26	5840	8983	21296	2.25	Tail Pullout
2	200	0.34	5673	12701	24202	2.99	Tail Pullout
3	220	0.29	4864	9109	20320	2.50	Tail Pullout
Mean		0.30	5459	10264	21939	2.58	
Min		0.26	4864	8983	20320	2.25	
Max		0.34	5840	12701	24202	2.99	
Std Dev		0.04	522	2111	2019	0.38	
Mean -3 SD		0.18	3893	3930	15882	1.44	
Mean +3 SD		0.42	7025	16598	27997	3.72	

Figure 4.10. Shear test results exported at Henrob

decline when the heat treatment temperature goes up, the SPR joint strength can still keep the constant level at high temperature condition.

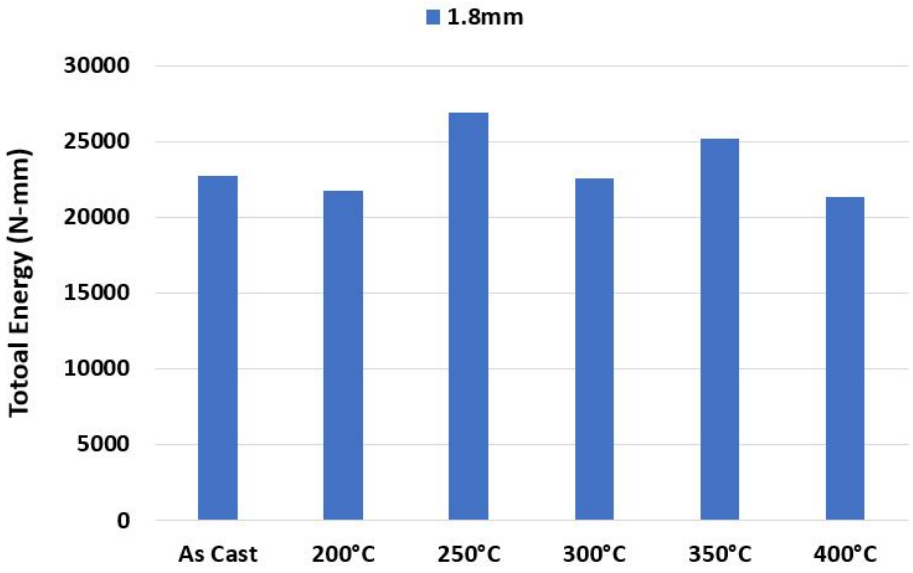

Figure 4.11. Joint strength comparison with 1.8mm die

Figure 4.12 summarized the SPR joint strength variation when the die depth increased to 2.0 mm. Unlike the die with 1.8 mm, the SPR joint strength with 2.0 mm die has a inclining tendency. Although the joint with 250°C heat treatment is a outliner, the overall trend still shows the positive effect of heat treatment on joint strength.

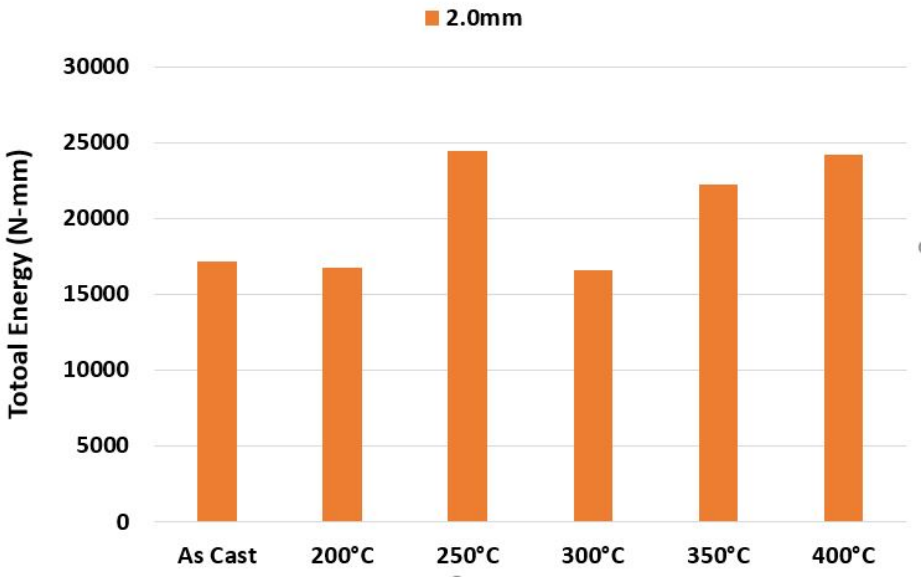

Figure 4.12. Joint strength comparison with 2.0mm die

By further increasing the die depth to 2.2 mm as shown in figure 4.13, the joint strength improvement by heat treatment become more effective and obvious. The SPR joint strength shows a near perfect tendency by raising the heat treatment temperature to 400°C. In terms of previous results, it can be concluded that heat treatment has a larger effect on the SPR joint strength when the deeper die is used.

In order to comprehensively compare the effect of heat treatment on the SPR joint strength with different dies, figure 4.14 shows the joint strength comparison under different heat-treated conditions by using three different dies. The joint strength decreases when the deeper die is applied at as-cast condition. This similar trend keeps constant until the heat treatment temperature goes up to 300°C. The difference of joint strength among each die starts to be reduced. Particularly, 1.8 mm die with 400°C heat-treated temperature has even less joint strength compared to the deeper dies. This type of differences in joint strength is mainly caused by the microstructure evolution under different heat treatment

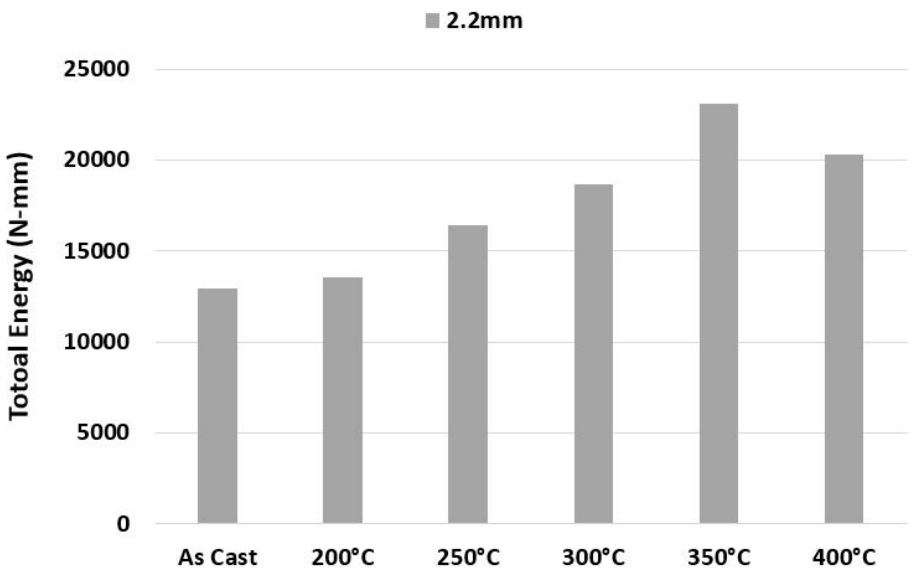

Figure 4.13. Joint strength comparison with 2.2mm die

conditions. In order to better understand the variation of joint strength, the microstructure evolution of alloy and cracking condition on joint button need to be analyzed.

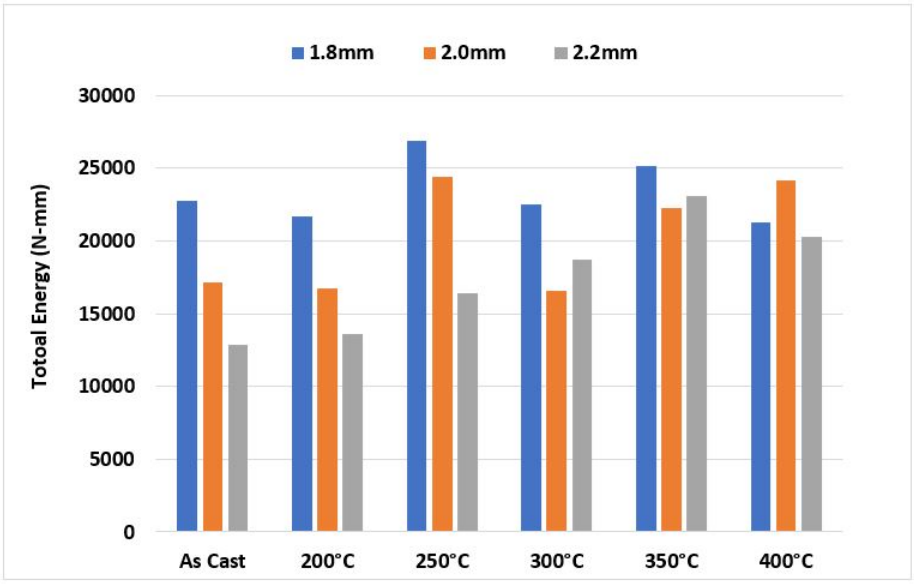

Figure 4.14. The overall SPR joint strength comparison under different heat-treated conditions

The purpose of heat treatment on the W3 alloy is going to break the eutectic silicon network and reduce the cracks on the joint button. The previous results showed that the broken silicon network and spherical-like silicon morphology would reduce the cracks in number and magnitude. However, the UTS and YS of W3 alloy after heat treatment was diminished as the trade-off. The joint strength had a certain amount of the promotion when the heat treatment temperature was gradually increased. When the die depth was 1.8 mm, the joint strength under different heat treatment conditions did not have too much difference. Once the die depth increased to 2.0 mm, the joint strength showed a stably increasing tendency with the increase of the heat treatment temperature. The similar tendency also occurred with 2.2 mm die depth case. However, the joint strength had a decline when the die depth was increased from 1.8 mm to 2.2 mm under the same heat treatment condition except 400°C specimen. In fact, the joint strength with three different die depths started to show a minimum discrepancy from 350°C.

The joint strength is supposed to be enhanced by increasing the die depth because the deeper die can create the larger interlock distance. However, the joint strength corresponding to the deeper die always showed the lower value from the as cast condition to the W3 alloy with 350°C heat treatment. We believed that this type of phenomenon was caused by the appearance of cracks on the joint button. When the die depth became deeper, the more plastic deformation will be introduced during the riveting process. Without the heat treatment or the low temperature heat treatments, the W3 alloy will be easier to form the cracks on the joint button site because of the corral-like eutectic silicon morphology. In particular, the cracks tended to propagate along the silicon network along with more plastic deformation introduced by the utilization of deeper die. With increasing the heat treatment temperature, the discrepancy of the joint strength for different die depths became smaller. W3 alloy with 350°C heat treatment showed the most similar joint strength with different die depth. It is mainly due to the eutectic silicon morphology evolution caused by the heat treatment. At 350°C, most of the silicon phase started to break into pieces and the cracks on joint button were additionally suppressed comparing to lower temperature cases as shown in Figure 4.7. The similar phenomenon also happened at 400°C heat treatment condition. In terms of these results, we can conclude

that the heat treatments from 350°C to 400°C are able to eliminate the cracks on the joint button and the discrepancy of joint strength by using different die depth is related to the eutectic silicon morphology evolution.

To better understand the influence of the heat treatment on joint strength with different die depth, Figure 4.15 shows a comprehensive joint strength comparison in terms of various heat treatment and die depth conditions. With increasing the die depth, the overall tendency of joint strength was going down. After taking the average of the joint strength at the different heat treatment conditions for three die depth, the line in the figure shows an apparent decline of the average joint strengths. In theory, the larger interlock distance will be formed by using deeper die. However, the appearance of cracks on the joint button for die casting aluminum alloy could be the issue to reduce the joint strength. In terms of qualification issues showed in Figure 2.10, the penetrated cracks would seriously affect the quality of the joints under the tension. The cracks on the joint button could lead to the interlock failure and joint button site material peel off under the loading condition.

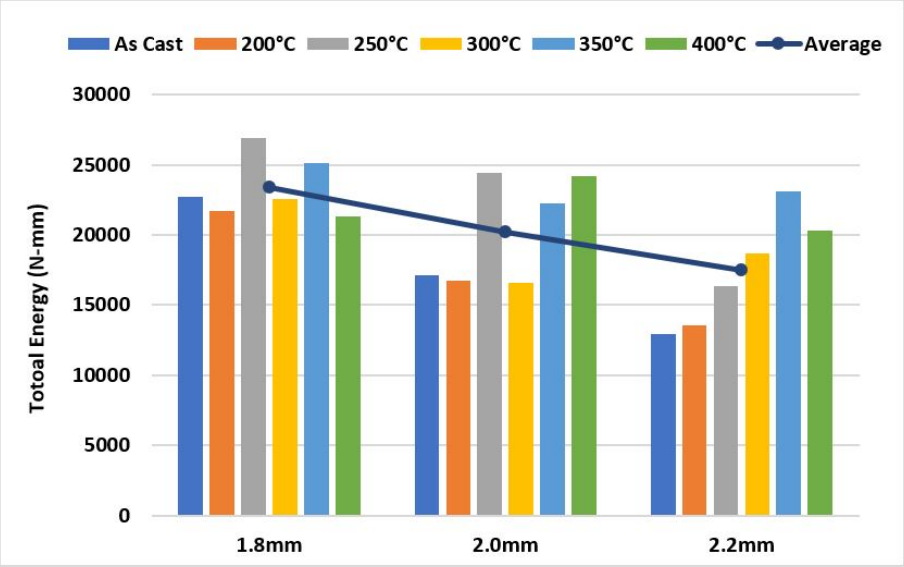

Figure 4.15. Total energy comparison of the joint at different heat treatment conditions with various die depth

With 1.8 mm die depth, the heat treatment had little influence on the joint strength. When the die depth increased to 2.0 mm, the joint strength started to show some differences among each heat treatment condition. An obvious influence of heat treatment on joint strength showed an incline tendency with 2.2 mm die depth. Corresponding to the relationship among the joint strength, the influence of heat treatment and the influence of cracks, the results can be explained by the understanding of the combination of plastic deformation during the riveting and microstructure evolution under heat treatment. Because of the shallow die depth, the joint formed in 1.8 mm die had a relative smaller plastic deformation on the joint button area. Since the plastic deformation was small, the crack quantity on the joint button was less than the other two deeper dies and the cracks were not able to take much effect on the joint strength. Once the die depth became larger, the magnitude and quantity of cracks are increased by the introduction of more plastic deformation. The overall strength of the joint with 2.0 mm was reduced by this effect as shown in Figure 4.15. At this condition, the cracks took effects on the joint strength and the heat treatment also showed the influence on the joint strength when the eutectic silicon network in aluminum alloy had an obvious phase transformation at 350°C and 400°C. When 2.2 mm die was used, an apparent increasing tendency of joint strength was shown in the figure. The cracks under this condition totally took over the authority to determine the joint strength. And the heat treatment also under this circumstance had the largest effect on joint strength.

4.4.2 The influence of cracks on joint strength based on crack statistical analysis

Because of the close relationship between cracks and joint strength, the cracks on the joint button is necessary to be calculated and analyzed to study the influence of cracks on the joint performance. In terms of the method as shown in Figure 3.5 in methodology section to calculated the both types of cracks by ImageJ, equation 3 and 4 can summarized the calculation results in expression of crack fraction:

$$\frac{S}{P} = \frac{Sum of Small Cracks in Number}{Top Circle Perimeter on Joint Button} = \frac{\sum_1^N SC}{P} \tag{4.1}$$

$$\frac{S}{P} = \frac{Sum\,of\,Large\,Cracks\,in\,Length}{Top\,Circle\,Perimeter\,on\,Joint\,Button} = \frac{\sum_1^N LC}{P} \tag{4.2}$$

According to the crack calculation method, the small cracks in number and large cracks in length with various die depth and different heat treatment conditions have been counted and calculated. Figure 4.16 shows that the cracks calculation result in terms of different die depth. When the SPR joint is formed by using deeper die, there are more large cracks that are going to form on the joint button. Because of the low ductility of W3 alloy, the deeper die are prone to cause larger deformation on the joint button during the riveting. Without any heat treatment, the material on the joint button area is too fragile to resist a large amount plastic deformation. As a result, the increasing number of cracks are going to form on the joint button when the die depth increases.

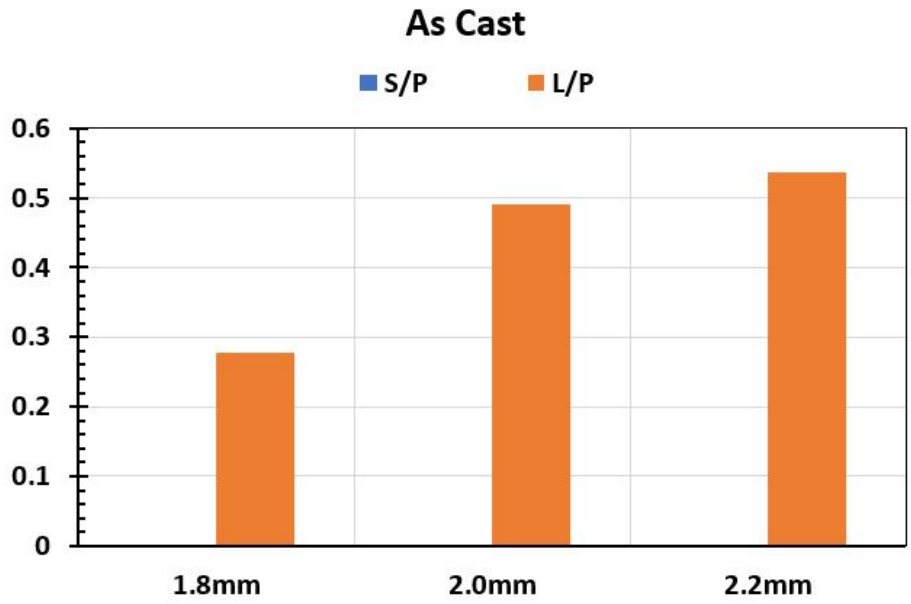

Figure 4.16. The cracks fraction calculation on the joint button at as cast condition

Although most of the high pressure die casting part needs to be heat-treated after casting, the normal heat treatment temperature in purpose of releasing thermal stress inside of parts is not good enough to resist the such high deformation from riveting process. Figure 4.17 shows the cracks calculation results when the parts was heat-treated

at 200°C for 2 hours. In terms of the profile of joint button as shown in figure 4.7 (b), the heat treatment at 200°C doesn't modify the silicon morphology sufficiently. The silicon phase is still shown as corral-like morphology with the protrude or sharp-edge structure. The material with this type of silicon morphology under the loading condition are still easy to form cracks on the joint button.

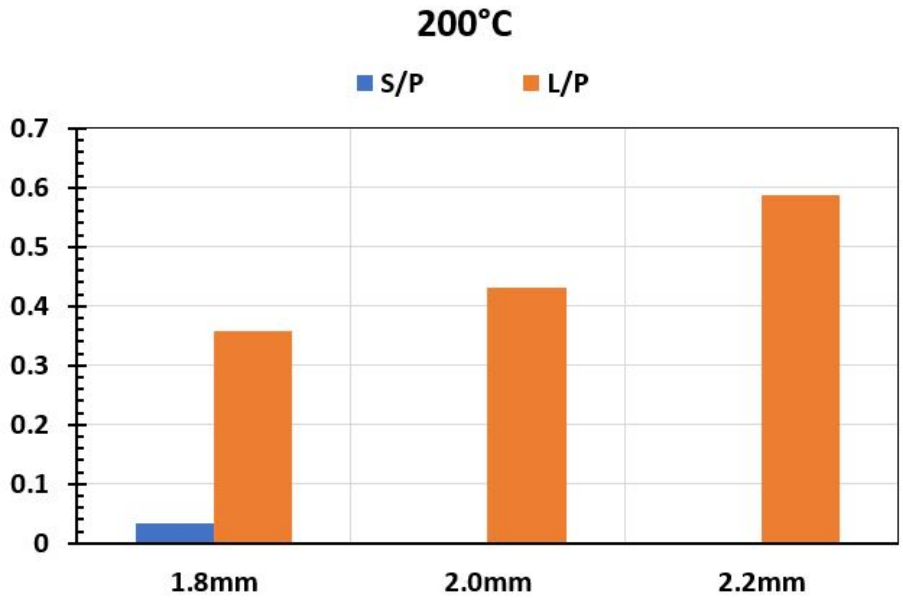

Figure 4.17. The cracks fraction calculation on the joint button with 200°C heat treatment

In order to suppress the formation of cracks on the joint button area, the key is silicon morphology modification. Once the heat treatment temperature goes up to 350°C, the large cracks fraction has a apparent drop and there are more small cracks appear on the joint button. Figure 4.18 shows the cracks calculation for W3 alloy was heat-treated at 350°C. The large cracks fraction drops from about 0.35 to 0.17 and the small cracks fraction increases from 0.04 to 0.16 for 1.8 mm die. For 2.0 mm and 2.2 mm dies, the large cracks fraction has about 0.1 decline. The decline on large cracks fraction and the incline on small cracks fraction indicates that the heat treatment takes effect on the cracks control.

To further investigate the effect of heat treatment on cracks suppression, 400°C heat treatment shows the ultimate goal of cracks control. Figure 4.19 shows that more and more small cracks have taken the place of large cracks to appear on the joint button.

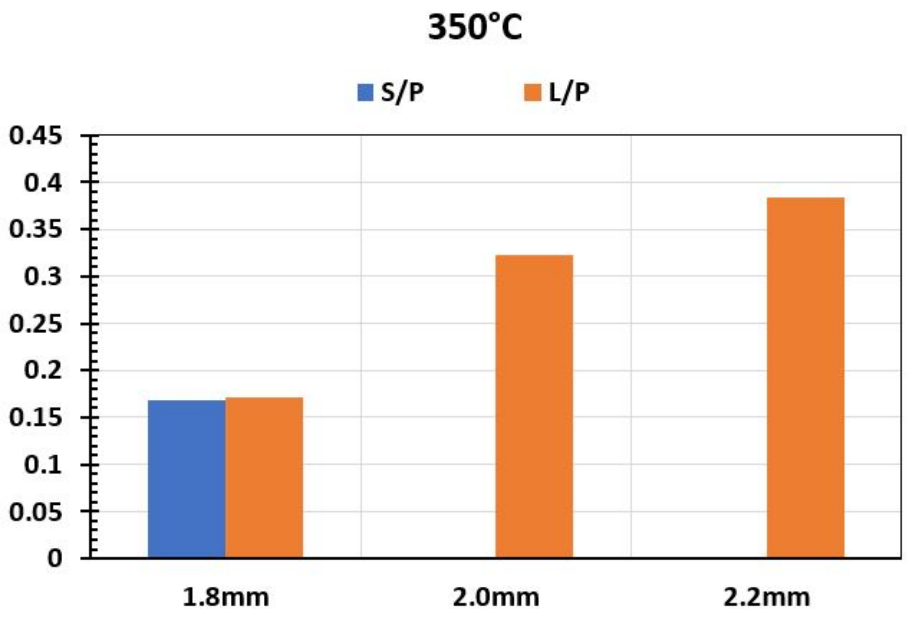

Figure 4.18. The cracks fraction calculation on the joint button with 350°C heat treatment

Taking consideration of the silicon morphology evolution as shown in figure 4.8 (f), the spherdized silicon phase dramatically reduces the possibility of cracks forming at silicon-rich sites. Even the micro-cracks form on the silicon phase, the broken silicon network are hardly to make the cracks propagate along the non-existed network. Eventually, W3 alloy with 400°C heat treatment turns out the best joint quality by using SPR.

In order to understand how the heat treatment can affect the cracks for different dies, figure 4.20 shows the variation of small and large cracks in quantity and the right side column of the figure shows the crack fraction. The figure indicates that the heat treatment had an effect on the cracks suppression. The heat treatment did not have too much effect on the cracks when the heat treatment temperature was lower than 300°C with 1.8 mm die depth. Once the temperature went up to 350°C, the number of large cracks had an obvious drop. The die with 2.0 mm die depth showed the perfect decline trend in large crack number when the temperature went higher. And there was no small cracks at all before the temperature increased to 400°C. Once the die depth changed to 2.2 mm, the

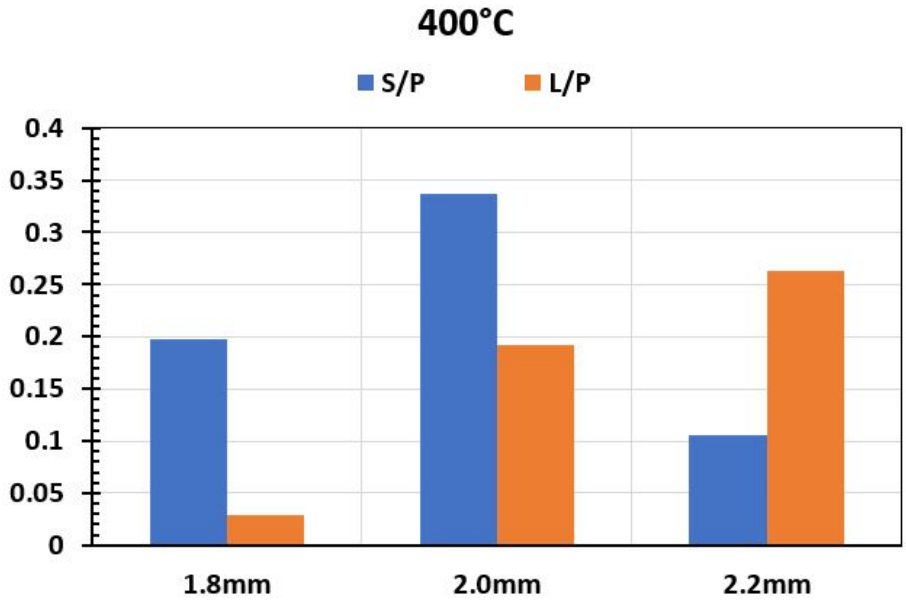

Figure 4.19. The cracks fraction calculation on the joint button with 400°C heat treatment

figure showed a similar tendency in calculation of large cracks as 1.8 mm die depth before the temperature went up to 250°C. And when the temperature was higher than 300°C, the magnitude of large cracks were dramatically suppressed. But the fraction of large cracks did not have a change until the temperature reached 400°C. Furthermore, the small cracks started to appear until the temperature raised up to 400°C.

The microstructure evolution under heat treatment and the variation of plastic deformation from the different die depth are the major factors that cause the discrepancy of cracking behavior under different riveting conditions. In consideration of the microstructure evolution perspective, the eutectic silicon morphology plays an important role to control the crack generation and propagation. When the die depth was 1.8 mm, the eutectic silicon morphology started to break and the extruded silicon dendrite arms were rounded without the sharp tips at 300°C. And the crack statistical results also indicated that the large cracks length had a decline at 300°C. Once the temperature went higher, the effect of cracking suppression was further enhanced. Especially when the temperature went up to 400°C, the obvious crack inhibition occurred due to the spherization of eutectic silicon phase. When the die depth increased to 2.0 mm, the decline of the large cracks

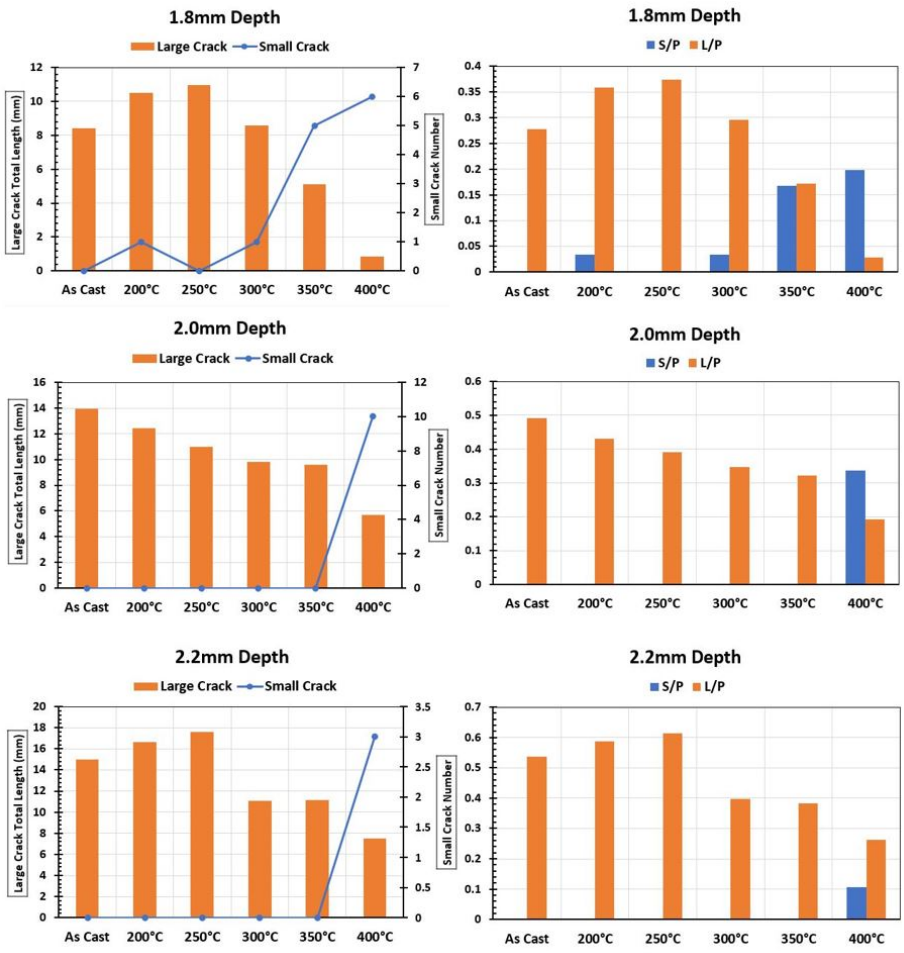

Figure 4.20. The statistical results of small and large cracks in quantity and fraction

length was corresponding to the elevation of heat treatment temperature. Once the die depth further increased to 2.2 mm, the heat treatment still showed the effect on cracking suppression. However, the heat treatment did not showed the dominated influence on cracking suppression compared to the die with 1.8 mm depth. Because the difference of large cracks in length was gradually reduced when the temperature went above 300°C.

During the riveting process, some of the micro-cracks are going to initiate at the eutectic silicon sites with the local small deformation. When the deformation further goes larger, the micro-cracks will be expanded and enlarged. Eventually, the multiple sites micro-cracks will converge and form the visual small cracks and large cracks. When the die with 1.8 mm depth, the small and large cracks were going to form on the joint button

at as cast condition. Once the heat treatment was applied, the large cracks gradually suppressed and the micro-cracks finally only turned to the small cracks. But this type of cracking mechanism was changed by increasing the plastic deformation in using deeper dies. When the die with 2.0 mm and 2.2 mm depth, the larger cracking suppression effect at 400°C were not obvious and the small cracks only appeared under 400°C heat treatment. Because the deeper die had more space to allow more volume of material to be squeezed into the die cavity, the larger plastic deformation would be introduced on the materials at joint button site and the materials was not able to withstand such large deformation during the riveting process. At this circumstance, the crack initiation and propagation were not only determined by the eutectic silicon morphology, but also the ductility of the aluminum matrix took effect on the rivetability.

Because the rivetability is composed of the joint performance and joint qualification, the joint strength and cracks statistical results both need to be taken into consideration to summarize the comprehensive the SPR joint performance. Figure 4.14 shows the comprehensive the SPR joint performance in combining with the large cracks fraction at different heat treatment conditions using three different die depths. Without any heat treatment, the total energy of the joints was decreasing with increasing the die depth. A perfect decline was shown at this condition and most of other heat treatment conditions also showed the similar decline tendency. Based on the current observation, we can conclude that the joint performance is highly related to the die depth at each heat treatment condition. When the heat treatment started to be applied, the mechanical property of the die casting aluminum alloy was reduced by the thermal strength releasing effect in alloy. Furthermore, the cracking issue still existed due to the minimal change of eutectic silicon morphology evolution when the heat treatment temperature was below 300°C. The occurrence of both type of issues caused the low comprehensive joint performance as shown in the figure. And it also proved that the joint performance was related to the mechanical property of the alloys.

With increasing the heat treatment temperature to 350°C and 400°C, the comprehensive joint performance was essentially improved. At 350°C, the joint performance with 1.8 mm die depth had approximate one times larger than the as cast

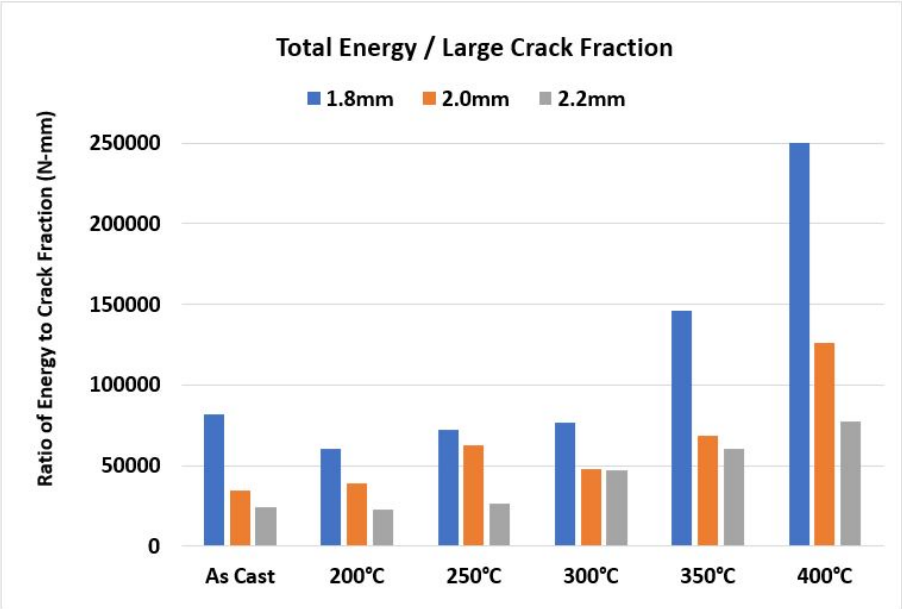

Figure 4.21. The comprehensive joint performance in terms of the joint strength and cracking statistical results

condition. In addition, the difference of joint performance between 1.8 mm die and other two die depths became larger. Although the joint with 2.0 mm and 2.2 mm die depth had lower strength than the joint with 1.8 mm die, the joint performance under this heat treatment condition was still higher than the other conditions except the 400°C heat treatment case. Combining the ideas of eutectic silicon morphology evolution and plastic deformation variation with different die depth, the comprehensive joint performance was enhanced by the effects, which were from the hindering the cracks initiation and propagation with the broken silicon network and forming the larger effective interlock distance by withstanding more plastic deformation.

The similar effects were substantially proved at 400°C condition. The comprehensive joint performance with 1.8 mm die was about 2.5 folds larger than 2.0 mm die based on the raw data calculation. In terms of the data, it also proved that the large cracks on the joint button could seriously reduce the joint strength because the cracks were easier to propagate under the shear loading condition. In addition, heat treatment enabled to improve the joint strength because the ductility of the aluminum plates was

improved by the breakage and spherization of silicon phase under the high temperature conditions. Thus, the joint could absorb more energy during the shear loading situation. The last but not the least, the smaller die depth could obtain the better comprehensive joint performance. Although the deeper die enabled to create the larger interlock distance, there were more cracks that would appear on the joint button. Then the comprehensive joint performance would be affected by those cracks. In a word, the rivetability of die casting aluminum alloy is determined by taking into consideration of the comprehensive joint performance in terms of the joint strength and cracks both perspectives.

4.5 Summary

In terms of the influences on joint strength by using different process parameters, the combination of heat treatment and die depth were analyzed and discussed. When the die with a shallow die depth, the results indicated that the heat treatment did not have too much effect on the joint strength. However, when the die depth was increased, the more plastic deformation was introduced during the riveting process. Then the broken silicon network achieved by the heat treatment turned over the responsibility to suppress the crack initiation and propagation. And the joint strength was also improved by this effect from the heat treatment. The influence from crack statistical results was focus on the quantity of the cracks under various conditions. From the analysis we concluded that the magnitude of large cracks was gradually reduced by raising the heat treatment temperature. Furthermore, the crack initiation and propagation under high plastic deformation situation was not only determined by the eutectic silicon morphology, but also the ductility of the material needed to be taken into consideration. Based on the analysis from joint strength and crack statistical results, the rivetability of die casting aluminum alloy was expressed by the comprehensive joint performance. The comprehensive joint performance was determined by the ratio of total energy absorbed by joint to the large crack fraction. The result showed that the joint performance was mainly determined by mechanical property of the material because the minimal eutectic silicon morphology evolution under low heat treatment condition. When the heat treatment

temperature increased above 350°C, the broken eutectic silicon network was able to hinder the crack initiation and propagation. According to the study from the comprehensive joint performance, the shallow die combined with high temperature heat treatment was suggested to maximize the rivetability of die casting aluminum alloy.

CHAPTER 5. SELF-PIERCE RIVETING SIMULATION STUDY

Simulation study for the SPR process is substantial to analyze the dynamic process and understand the corresponding physical phenomenon, such as cracks on the joint button. Moreover, it also can provide the assistance to find out the flaws of die design and optimize the riveting process parameters. The SPR process in this study was conducted on the symmetric two dimensional design by FORGE because 2D calculation in Finite Element Analysis (FEA) is able to drastically reduce the calculation time and the cross-section view of model can be analyzed for the riveting process under 2D view.

5.1 Simulation preparation and process parameters determination

Figure 5.1 shows the model with the mesh and the main deformation areas with the refined mesh were used to analyze the stress and strain variation in detail. And the riveting process also can be found in this figure. D value in the figure indicates the movement magnitude of punch. The whole riveting process was divided into four stages, which was associated with the value of D. The rivet was going to penetrate the upper sheet metal and the metal sheet began to deform when the force was increasing. When D reached a specific value, the rivet broke the top sheet and was further squeezed into the bottom sheet inside of the die cavity. Once the bottom sheet material started to contact with the bottom of the die, the interlock was going to form at the localized plastic deformation area. Eventually, the higher punching force was required to keep pushing the rivet into the cavity because the elevated resistance would be generated from the contact areas between the bottom material and the die.

The dynamic contact between sheet metals is defined as the combination of elastic and plastic deformation during the whole simulation process. Punch, binder and die were defined as the rigid body and the frictional contact condition among each other using Coulomb criterion shown as in Equation 5.1:

$$\tau_f = \mu \sigma_n \tag{5.1}$$

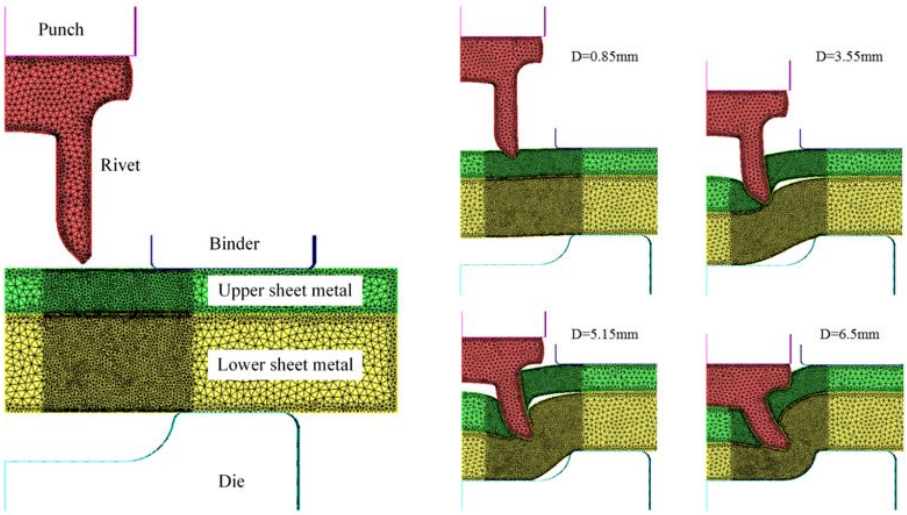

Figure 5.1. The FEA calculation model and simulation process

where τ_f is frictional shear stress; σ_n is flow stress; is coefficient of friction. The coefficient of friction in this simulation was set up as 0.1. And some other value of coefficients are shown in Table 5.1. The upper layer metal is defined as DP580 steel with 1.4mm in thickness. The lower layer metal is defined as the casting aluminum alloy A383 with 3 mm in thickness. The rivet material is special steel with relative high hardness and stress. The other material coefficients in simulation are shown in Table 5.2.

Table 5.1. The SPR simulation coefficients

Item	Value or Property
Rivet and Sheet Metal	Elastic-Plastic
Punch, Binder and Die	Rigid
Punch Speed	10mm/s
Upper Sheet Thickness	1.4 mm
Lower Sheet Thickness	3.0 mm
Rivet Length and Diameter	6.3 mm and 5.3 mm
Friction Coefficient	0.1

The fracture criterion during the SPR simulation is substantial to apply fracture on the upper metal sheet and determine the fracture condition on lower metal sheet. The upper metal sheet was penetrated by the rivet and the lower metal sheet experienced the

Table 5.2. Materials coefficients in simulation

Item	Material	Youngs Modulus (GPa)	Poisson Ratio	YS (MPa)
Upper Sheet Metal	DP580	210	0.3	440
Lower Sheet Metal	A383	70	0.3	190
Rivet	Special Steel	210	0.3	1200

deformation in die cavity. Normalized Cockcroft & Latham criterion is applied in the simulation to determine fracture. The mathematical expression as Equation 5.2:

$$\int_0^{\bar{\varepsilon}_f} \frac{\sigma_1}{\bar{\sigma}} d\bar{\varepsilon} = C \tag{5.2}$$

where $\bar{\varepsilon}_f$ is the equivalent plastic strain when the material has fracture; $\bar{\varepsilon}$ is the equivalent strain; σ_1 is the maximum principle stress;$\bar{\sigma}$ is equivalent stress; C is the critical fracture threshold of material. This simulation uses 0.35 as the fracture threshold of DP580 steel and there is no consideration of fracture for A383 alloy.

5.2 Simulation results analysis

The die cavity depth as the only variable choosing from the process parameters is essential to observe and analyze the lower sheet material deformation condition. It is also significant to obtain the fracture condition in the die cavity and the relationship between the crack and deformation area can be described by this simulation result. Figure 5.2 shows the effective strain distribution with 1.8 mm, 2.0 mm, and 2.2 mm die depth. The strain concentration area is located around the rivet tip because the sharp rivet tip can shear the both sheet materials during the riveting process. The green field on the bottom indicates that the contact area between bottom sheet and the die has relative lower strain concentration. And the high strain field with the red color was mainly distributed around the rivet shank tip.

In terms of the strain distribution associated with different depth, there were no too much difference that was able to distinguish the effect on the bottom material sheet by the

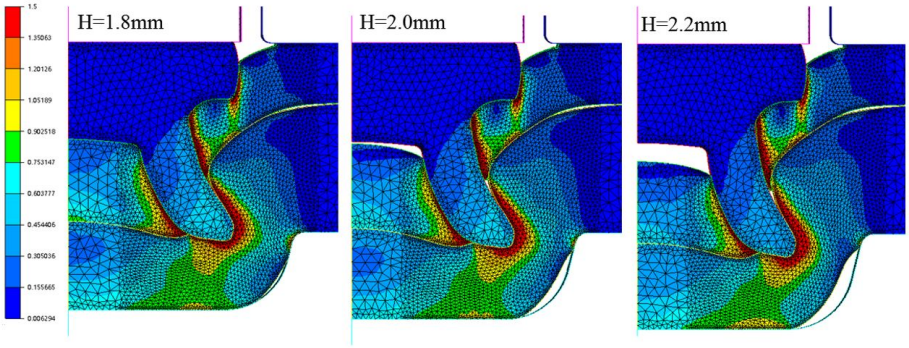

Figure 5.2. The strain distribution with different die depth

variation of effective stain distribution. Furthermore, the effective strain could be treated as one of the significant criteria to determine the fracture or damage of material corresponding to the value in the high strain field. In theory, the cracks were usually generated on the joint button because the plastic deformation would be concentrated on those areas. The high strain distribution areas shows the excessive large strain, which can cause the destructive cracks in those area. However, most of the cracks were showed on the joint button areas instead of the high strain field. In terms of the previous analysis from cracking mechanism section, the sheet materials were going to experience the tension and compression during the riveting process. Sheet materials under the compression showed the different behavior comparing to the tension and the material would have the fracture when it was compressed during the riveting process. Instead, the material under in the compression area would be compressed and hardened.

The compression played a role as the work hardening to enhance the fracture resistance of the bottom material. But the material away from the main compression field encountered the tension and it was stretched and pulled over away from the central field. As a result, the material under tension would likely to form the cracks if the strain was over the elongation of material. Nevertheless, FEA does not simply consider and calculate the single element behavior. The multiple elements will be introduced and calculated comprehensively to achieve the macro-behavior of the material. Also, the effective strain distribution was calculated in terms of the properties of material from tensile test. The

properties of material under compression were not introduced and taken into consideration to participate the calculation. Therefore, the other criteria need to be considered to determine the fracture of material during the riveting process.

In order to consider the cracking issue, the fracture analysis is necessary to be introduced and used to define the fracture. The fracture distributions using the die with 1.8 mm depth is shown in Figure 5.3, and the fracture results were calculated in terms of the Normalized Cockcroft & Latham criterion as shown in Equation 4. The figure shows that the areas around rivet tip and the contact areas between the bottom sheet and the die have the relative high fracture distribution areas.There are three major areas that need to be discussed and analyzed to investigate the fracture forming mechanism. The red circle on the picture points out the area around rivet tip has high fracture distribution. It is mainly caused by the tension from the penetration of rivet tip into bottom material sheet. The green circle on the picture indicates that the second high fracture area. This high fracture distribution is caused by the tension from the high plastic deformation on the bottom sheet during the riveting. And this simulation result also matches the real fracture field position. Finally, the yellow circle shows the filling condition of top sheet inside of rivet cavity. The tight filling represents a good die volume filling and the rivet leg can be sufficiently flared under this condition.

Figure 5.4 shows the fracture distribution when the die with 2.0 mm depth is applied. The positions of high fracture fields keep same, but the areas of high fracture fields become larger and those fields with a converge tendency start to connect with each other to form a larger fracture field. It may cause the cracks not only appear on the joint button, the cracks also could penetrate into the material sheet and form a destructive crack. In addition, there is more unfilled area that shows in the die cavity and the gap inside of rivet become larger.

The worst fracture condition is shown as figure 5.5. When the die depth further increases, the high fracture fields have formed a completed large high fracture field. The unfilled die volume and the gap inside of rivet become much larger than 1.8 mm and 2.0 mm dies. In terms of the real joining case, figure 5.6 shows the SPR joint button comparison by using three different dies. The figure shows that the cracks on joint button

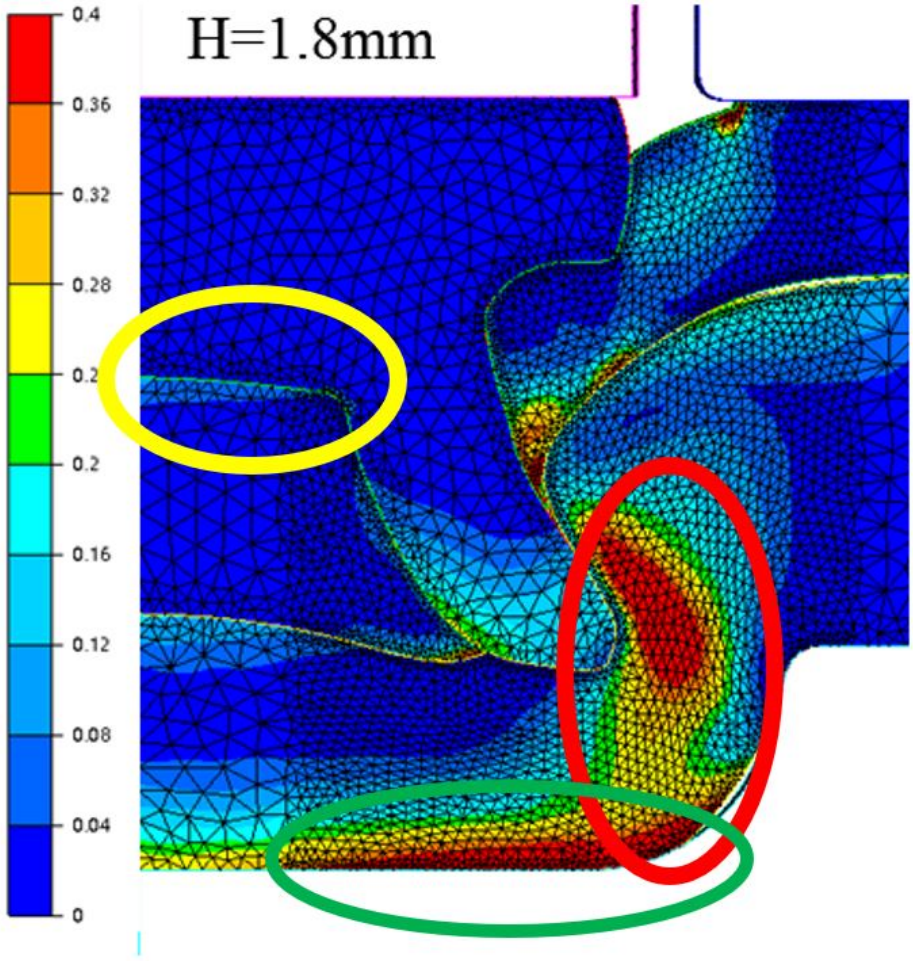

Figure 5.3. The fracture distribution using the die with 1.8 mm

with 1.8 mm die is severe. When the die depth increases to 2.0 and 2.2 mm, the adjacent cracks start to connect with each other and some materials on the joint button eventually peeled off.

In order to better understand the fracture conditions with different dies systematically, figure 5.6 shows the fracture comparison with different dies. In terms of the relationship between die depth and fracture fields distribution, 1.8 mm die can be regarded as the control group to determine the fracture field positions and the material filling conditions. When the die depth increased to 2.0 mm, the two high fracture fields started to build a connection between each other. In particular, when the die depth increased to 2.2 mm, a conjoint high fracture field was formed as shown in the figure. In

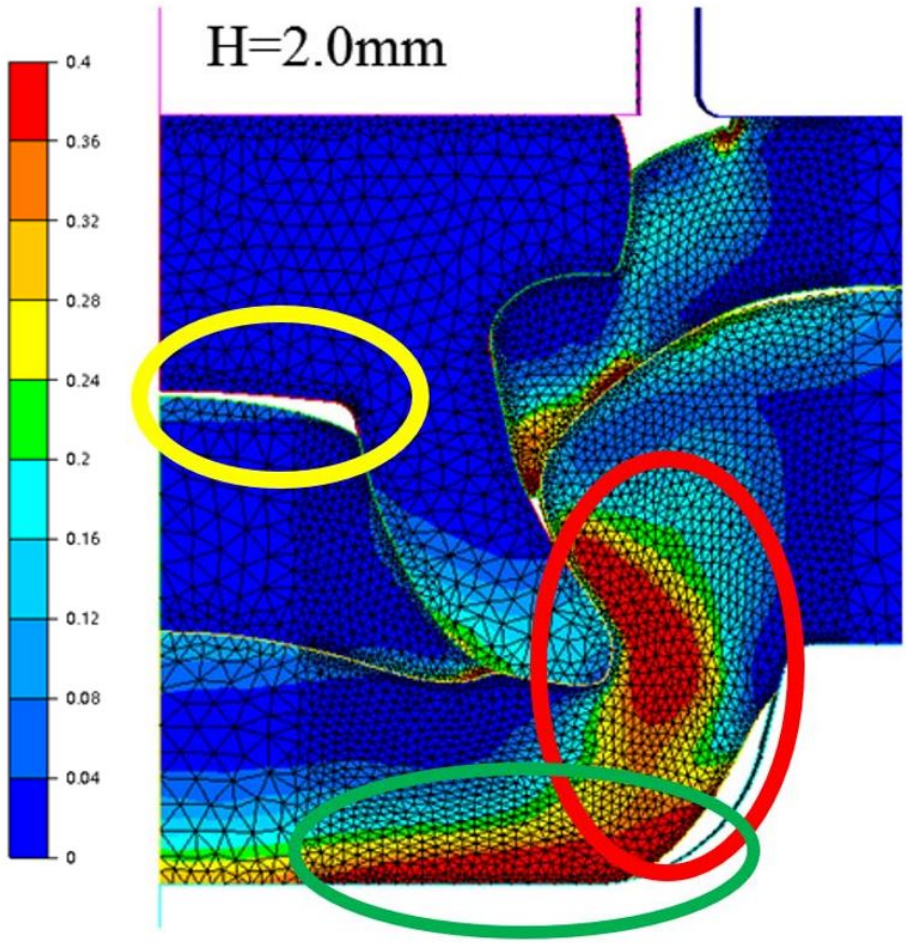

Figure 5.4. The fracture distribution using the die with 2.0 mm

the real case, the fracture not only shows on the joint button surface, it will also penetrate the lower sheet material. In terms of the fracture distribution results, the areas around rivet tip and the contact area between bottom sheet and die are likely to have cracking issues.

The three major differences are circled out by different colors as shown in Figure 5.7. The simulation was going to end when the top level of the rivet was in the same level of the top sheet, which also indicated that head height was equal to zero. The zero head height is the ideal for a SPR joint because the flat top sheet can satisfy aesthetic requirement and there will be no extra damage on the top sheet. However, the yellow circles indicated that there were the gaps left over for 2.0 mm and 2.2 mm dies. It was caused by the more space that were introduced by the deeper dies. If the punch is going to

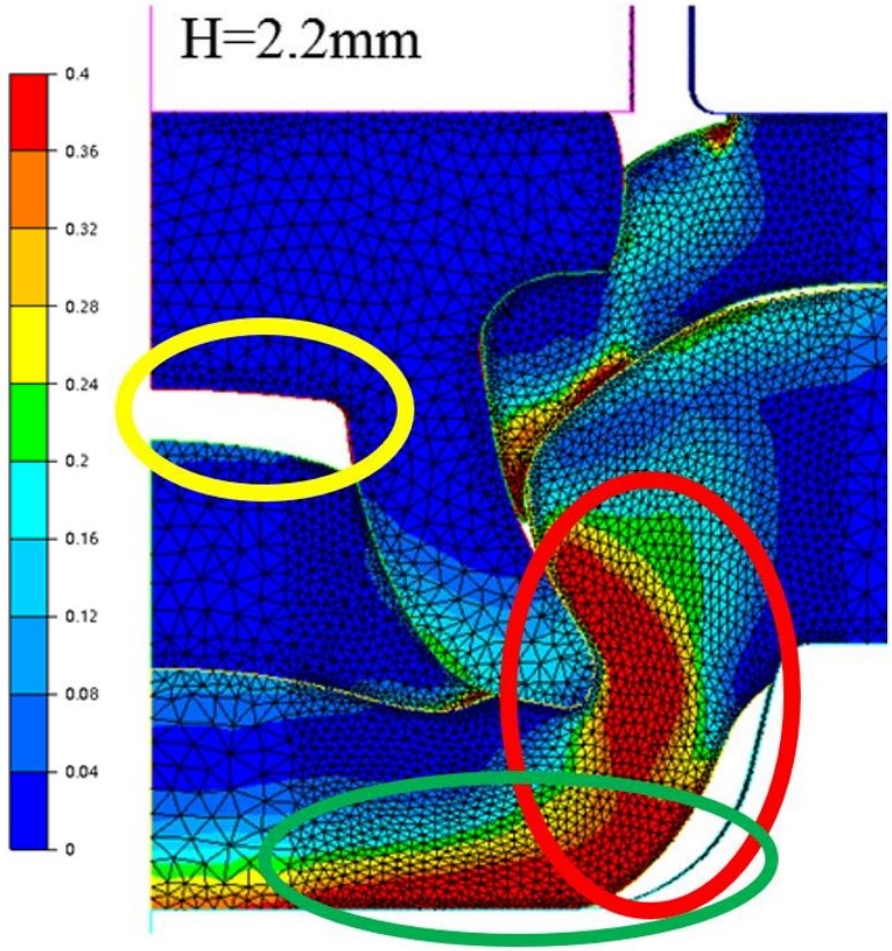

Figure 5.5. The fracture distribution using the die with 2.2 mm

Figure 5.6. The SPR joint button comparison for three different dies using as cast W3 alloys

press a little bit deeper, the top sheet is possible to be broken. Because of the extra space for the deeper dies, there were more plastic deformation that would be applied on the

bottom sheet. Red circles pointed out the fracture distribution around rivet shank and the green circles pointed out the fracture distribution on the joint button site. With increasing the die depth, the high level fracture fields was also increasing at the both locations. In particular, the high fracture fields at the both locations started to connect with each other when the die depth increased to 2.0 mm. In the riveting situation, the cracks could generate at both locations and finally merge into a catastrophic cracks to penetrate the both sheet.

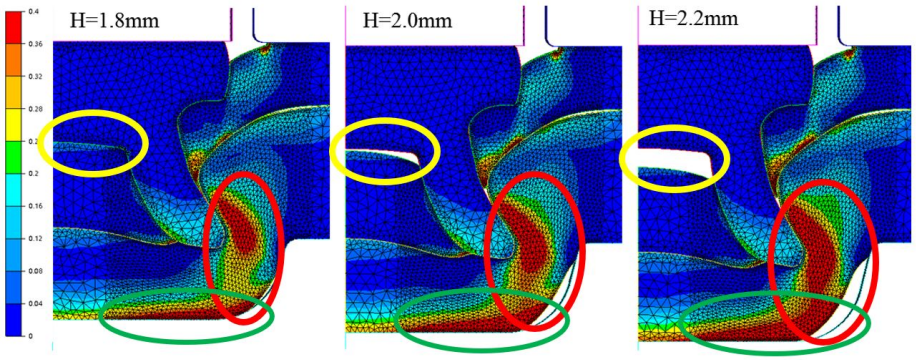

Figure 5.7. The fracture distribution with different die depth

Figure 5.8 shows the variation of force on the punch by using the die with different depth. The curve indicated that the force with different depth showed the minimal difference at initial riveting process. But the die with 1.8 mm depth eventually turned out the largest force required by forming a joint, and the deeper dies needed less the forming force. Because there were more contacts between the bottom sheet and die, the punch was required to have higher force to squeeze and compress the material into the die cavity. The dies with 2.0 mm and 2.2 mm depth with more space in the cavity, the forming force would be lower than 1.8 mm die.

Although there were more remaining space in the deeper die cavity, the bottom sheet did not have sufficient ductility to withstand more plastic deformation. The larger force applied on the deeper dies can lead to more severe cracks formed on the joint button and the top sheet could be damaged at the same time. However, increasing the die depth is an effective method to improve the joint strength by raising the interlock distance if the

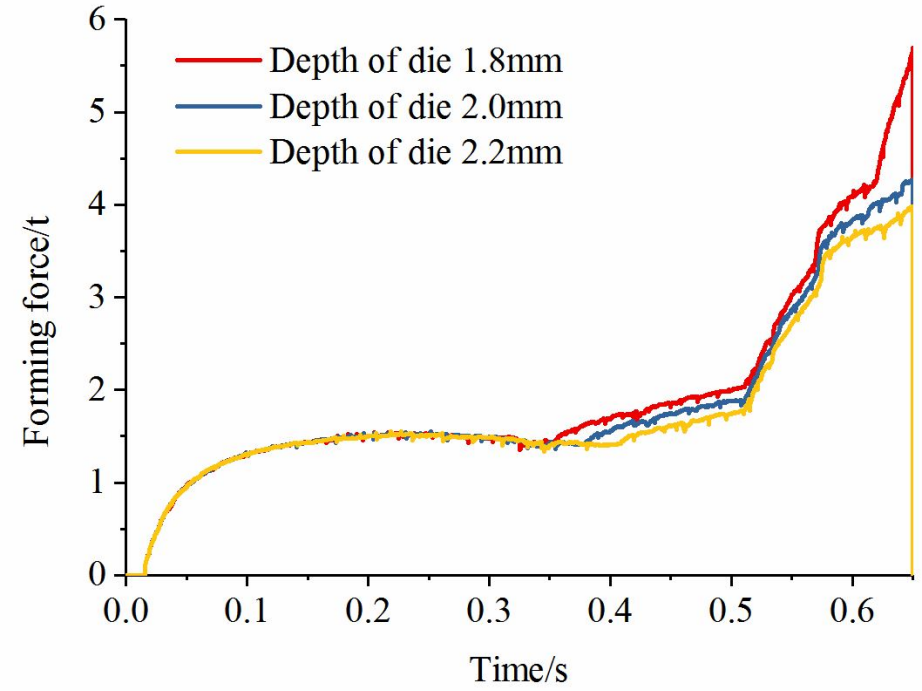

Figure 5.8. The force variation with different die depth

bottom material sheet has enough ductility to deform. In order to use the deeper die without the severe cracks on the joint button, changing the profile of the die cavity could be a solution to reduce the extra plastic deformation on the joint button areas.

5.3 Rivetability improvement by simulation

To reduce the plastic deformation on the joint button, the draft angle of die can be increased to provide more support on the bottom sheet material during the riveting. Figure 5.9 shows the simulation of fracture conditions inside of die cavity with the draft angles (α) of die is 104°. At this condition, the die cavity is almost filled by the bottom sheet material. And the fracture fields are mainly concentrated on the joint button and the area around rivet tip. Based on the previous analysis of fraction root cause during the riveting process, the more tension can be converted into compression if the draft of die can be increased.

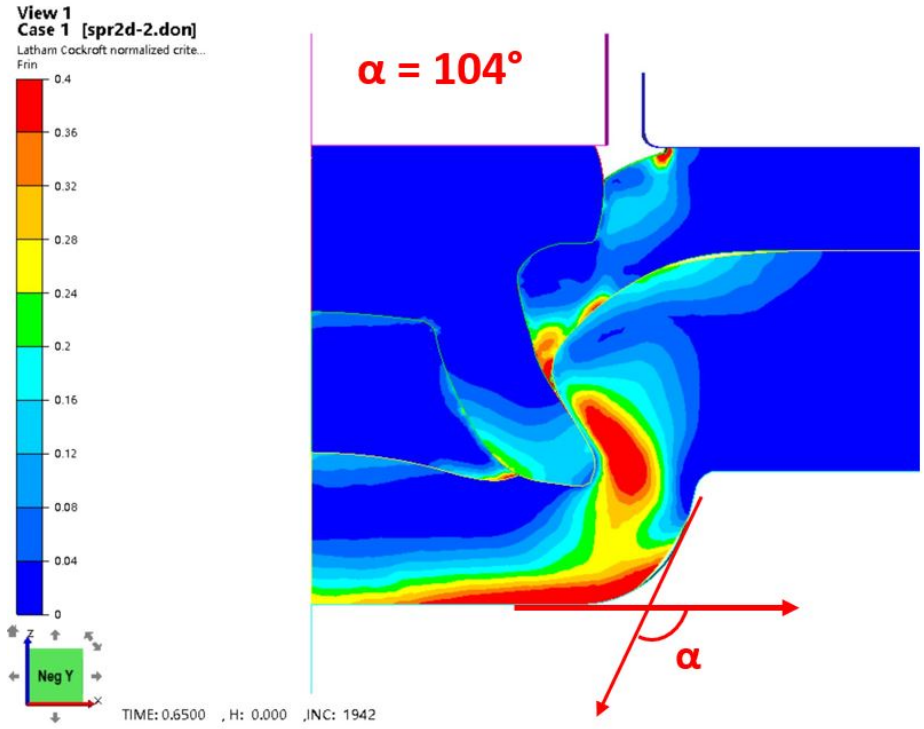

Figure 5.9. The fracture conditions by using 1.8 mm die with 104° draft angle

Once the draft angle of die started to increase to 120°, the magnitude of fracture on the joint button and the fracture area around rivet shank are reduced as shown in figure 5.10. The biggest change of fracture condition concentrates on the joint button area. The red fracture field penetration for the die with 120° draft angle is thinner than 104° draft angle die. It essentially caused by the more amount of material inside of die cavity is compressed instead of shearing. If the draft angle can be further increased, the tension on the joint button area can be further reduced.

After increasing the draft angle to 135°, the fractures around rivet tip and joint button are unexpectedly reduced as shown in figure 5.11. The size of high fracture field around the rivet tip is further decreased compared to 104° and 120° dies. And the thickness of hot zone on joint button become much thinner and shallow. Moreover, the color changed from yellow to green between two fracture hot zone indicated that the connection between two high fracture fields is further reduced by increasing the draft angle.

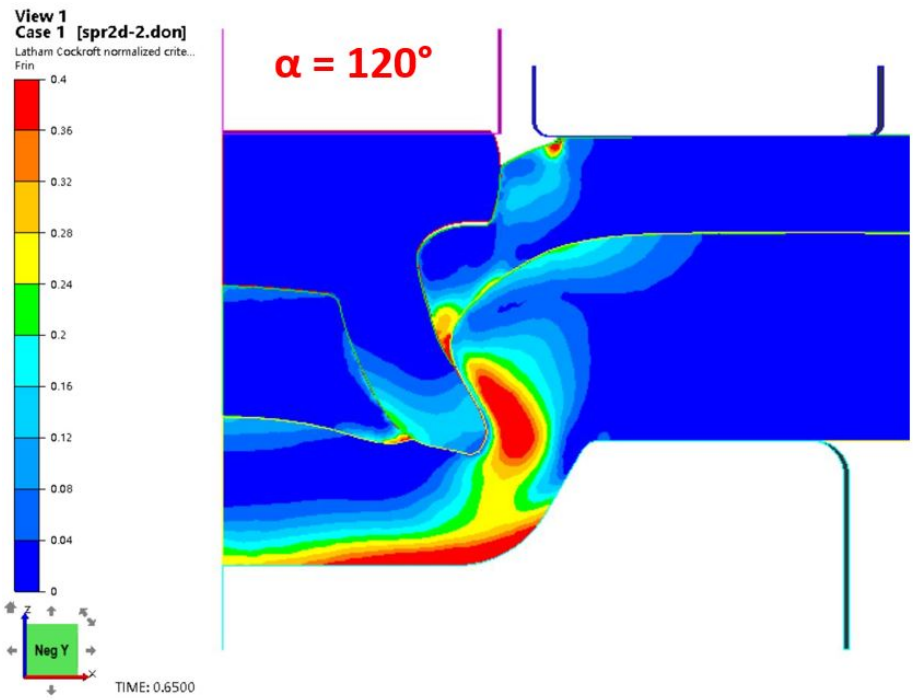

Figure 5.10. The fracture conditions by using 1.8 mm die with 120° draft angle

Figure 5.12 shows the fracture condition with different incline angle by using 2.0 mm die. The die with 2.0 mm depth has more space in the cavity, which can allow the bottom sheet to further deform during the riveting. But the extra plastic deformation for die casting aluminum alloy plays an opposite role to improve the joint strength. The more cracks that may appear on the joint button and the connection between the cracks on the joint button and cracks around rivet shank could lead to lethal failure of the joint. In terms of the simulation results, increasing the incline angle of die cavity sidewall showed the similar improvement as 1.8 mm die. The fracture around rivet shank and the hot zone on joint button were further reduced in magnitude and size. The extra space in die cavity was filled by the bottom sheet material. Meanwhile, the connection between to the two main fracture fields was diminished. In addition, the gaps, which were pointed out by the red circles in the figure, were gradually closed by increasing the incline angle.

To further investigate the influence of incline angle on the fracture condition of joint, the die with 2.2 mm depth was also simulated as shown in Figure 5.13. The hot zones around rivet shank and joint button area were severe. The two main high fracture

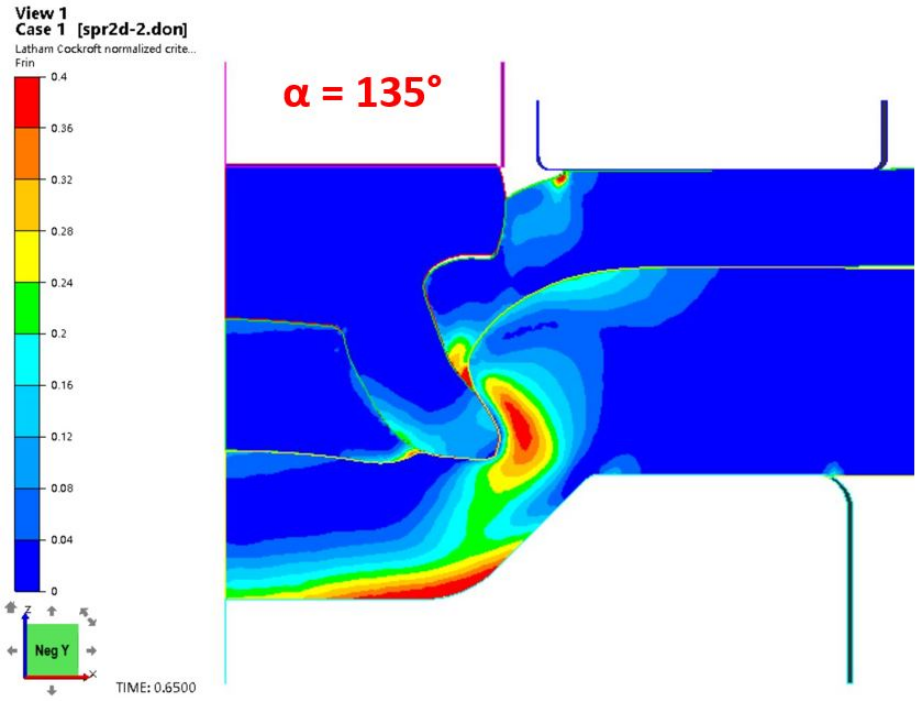

Figure 5.11. The fracture conditions by using 1.8 mm die with 135° draft angle

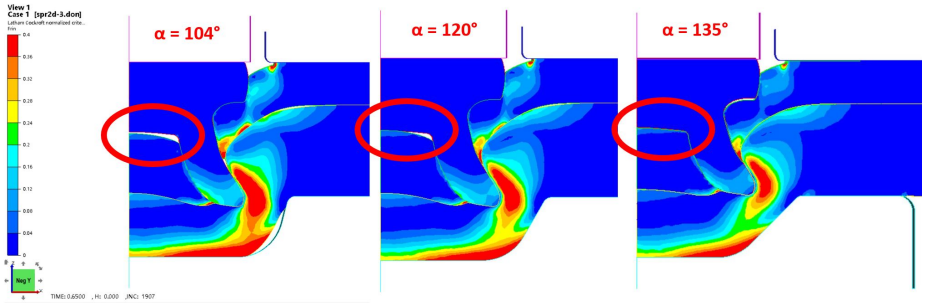

Figure 5.12. The fracture conditions by using different incline angle with 2.0 mm die

fields had built a completed connection with the high magnitude of fracture and the magnitude and size of hot zone were the most severe in three dies. But there was an obvious improvement on fracture reduction when the incline angle increased to 120°. And the more space inside of die cavity was gradually filled by the bottom sheet. The largest improvement on fracture reduction and die cavity filling occurred when the incline angle increased to 135°. The connection between two site hot zones was further reduced and the

die cavity had been filled eventually. Although the gaps between the top sheet and inside of rivet shank was not completely closed up, it still had a drastical improvement compared to the original gap.

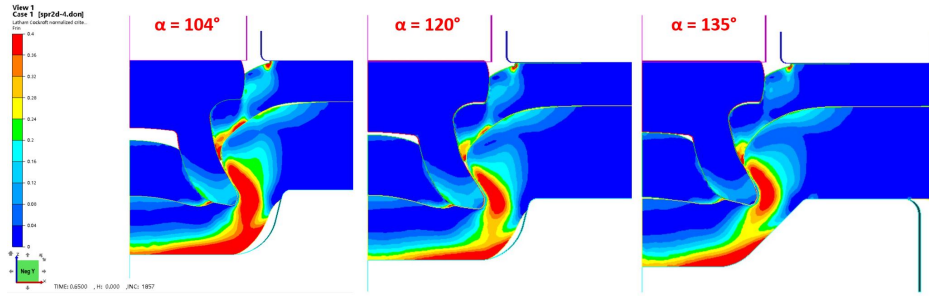

Figure 5.13. The fracture conditions by using different incline angle with 2.2 mm die

In terms of the fracture variation by using different incline angle of die cavity sidewall, the principle of improvement on fracture can be summarized by the perspective of plastic deformation and the form of applied force during the riveting process. Once the incline angle was increased, the space of the die cavity was reduced. Particularly, the plastic deformation around the joint button area was further reduced by the angle variation. The larger inclined angle provided more support to allow the bottom sheet deformation. Furthermore, because of the less ductility of die casting aluminum alloy, the extra deformation around the joint button area was easy to cause the fracture due to the tension effect. The flat sidewall was also able to convert the tension to the compression effect when the incline angle was increased. And the fracture was also further reduced by the increase of the incline angle.

CHAPTER 6. CONCLUSION

Self-Pierce Riveting was designated for joining the ductile materials, but the die casting structural components with relative low ductility also needed to be joined by SPR with the development of automotive industry in recent years. The die casting aluminum alloy has the low rivetability because of the high silicon content and the plate-like eutectic silicon morphology. Ryobi W3 alloy, commercial A380 and commercial A6061 have been used to compare the influence on rivetability in silicon content. In order to modify the eutectic silicon morphology, heat treatment has been used to investigate the microstructure evolution of W3 alloy. The crack formation and propagation mechanism on joint button were summarized based on the variation of silicon morphology. The die depth as a variable has been used for investigating the influence of cracks on joint performance. The comprehensive joint performance was determined and analyzed by the combination of shear test and the crack statistical results. SPR simulation was achieved by FORGE, which was used for investigating and validating the influence of die depth and cracking mechanism. The modification draft angle of die was used to improve the rivetability of die casting aluminum alloy. The specific conclusions from each section are listed in the following:

1. The aluminum alloy with low silicon content was able to improve the rivetability. And the silicon morphology modified by strontium could relatively reduce the cracks on joint button.

2. Under the loading condition, the cracks tended to initiate at eutectic sites and propagate along the silicon network due to the brittleness of eutectic silicon phase.

3. Heat treatment enabled to effectively modify the silicon morphology. Once the heat treatment temperature went to 350°C, the silicon starts to break into pieces. And the silicon phase was spherized at 400°C. The broken silicon network and spherical-like silicon particles led to an obvious crack reduction on joint button.

4. The broken silicon phase would effectively suppress the cracks during riveting process because the spherized silicon phase was hardly to cause the stress concentration and the cracks were hard to propagate because of the broken silicon network.

5. Deeper die would generate more large cracks due to the larger deformation on the joint button area. Heat treatment can dramatically reduce the large cracks initiation and propagation when the temperature goes up to 400°C.

6. The joint strength could be elevated by increasing the die depth. However, the cracks could affect the joint strength in consideration of both shear test results and crack statistical results. W3 alloy combining with 400°C heat treatment and 1.8 mm die depth became to the best option to maximize the SPR joint performance.

7. The simulation results indicated that the high strain concentration areas located at rivet shank field and the contact area between bottom sheet and die. And the high strain fields were mainly caused by the tension during the riveting.

8. Using the strain concentration to determine the fracture was not appropriate. The fracture distribution based on the Normalized Cockcroft & Latham criterion showed the most likely areas that could form the cracks.

9. In terms of the fracture distribution results, increasing the draft angle of die was able to diminish the fracture in magnitude and size by reducing a large amount of plastic deformation.

REFERENCES

Abe, Y., Kato, T., & Mori, K. (2006). Joinability of aluminium alloy and mild steel sheets by self piercing rivet. *Journal of Materials Processing Technology*, *177*(1-3), 417–421.

Abe, Y., Kato, T., & Mori, K. (2009). Self-piercing riveting of high tensile strength steel and aluminium alloy sheets using conventional rivet and die. *Journal of materials processing technology*, *209*(8), 3914–3922.

Atzeni, E., Ippolito, R., & Settineri, L. (2007). Fem modeling of self-piercing riveted joint. In *Key engineering materials* (Vol. 344, pp. 655–662).

Atzeni, E., Ippolito, R., & Settineri, L. (2009). Experimental and numerical appraisal of self-piercing riveting. *CIRP annals*, *58*(1), 17–20.

Audi tt coup 07-body. (2013). `http://www.volkspage.net/technik/ssp/ssp/SSP_383.pdf`. (Online)

Automotive. (2013). `http://www.henrob.com/GB/automotive.php`. (Online)

Blacket, S. (1995). The self pierce riveting process comes of age. *Institute of Metals and Materials Australasia Ltd.(Australia),*, 149–154.

Blundell, N., Han, L., Hewitt, R., et al. (2005). A comparative study between self pierce riveting and spot friction joining. *łŁŁ= Transactions of Society of Automotive Engneers of Japan*, *36*(5), 187–192.

Bokhari, N. (1995). Self-piercing rivetingprocess and equipment. *Weld Met Fabr*, *63*, 186–188.

Bonde, N. (1996). Self-piercing riveting in high-strength steel-a way to increase fatigue life. *IBEC'96–Advanced Technology & Process*, 16–20.

Booth, G., Olivier, C., Westgate, S., Liebrecht, F., & Braunling, S. (2000). *Self-piercing riveted joints and resistance spot welded joints in steel and aluminium* (Tech. Rep.). SAE Technical Paper.

Bouchard, P.-O., Laurent, T., & Tollier, L. (2008). Numerical modeling of self-pierce rivetingfrom riveting process modeling down to structural analysis. *Journal of Materials Processing Technology*, *202*(1-3), 290–300.

Briskham, P., Blundell, N., Han, L., Hewitt, R., Young, K., & Boomer, D. (2006). *Comparison of self-pierce riveting, resistance spot welding and spot friction joining for aluminium automotive sheet* (Tech. Rep.). SAE Technical Paper.

Budde, L., Lappe, W., & Liebrecht, F. (1992). Further developments in the self-piercing rivet technology. *Bleche Rohre Profile*, *39*, 310–314.

Carandente, M., Dashwood, R., Masters, I., & Han, L. (2016). Improvements in numerical simulation of the spr process using a thermo-mechanical finite element analysis. *Journal of Materials Processing Technology*, *236*, 148–161.

Casalino, G., Rotondo, A., & Ludovico, A. (2008). On the numerical modelling of the multiphysics self piercing riveting process based on the finite element technique. *Advances in Engineering Software*, *39*(9), 787–795.

Chrysanthou A, S. X. (2013). *Self-piercing riveting: properties, processing and applications* (Vol. 1). Woodhead, Cambridge.

Clinch rivet tool. (2015). `https://us.tox-pressotechnik.com/us/products/joining-systems/tox-clinch-procedure/tox-clinchrivet.html`. (Online)

Dannbauer, H., Gaier, C., Dutzler, E., & Halaszi, C. (2006). Development of a model for the stiffness and life time prediction of self piercing riveted joints in automotive components. *Materials Testing*, *48*(11-12), 576–581.

Di Franco, G., Fratini, L., & Pasta, A. (2013). Analysis of the mechanical performance of hybrid (spr/bonded) single-lap joints between cfrp panels and aluminum blanks. *International Journal of Adhesion and Adhesives*, *41*, 24–32.

Di Franco, G., Fratini, L., Pasta, A., & Ruisi, A. (2010). On the self-piercing riveting of aluminium blanks and carbon fibre composite panels. *International Journal of Material Forming*, *3*(1), 1035–1038.

Di Franco, G., Fratini, L., Pasta, A., & Ruisi, V. F. (2013). On the self-piercing riveting of aluminium blanks and carbon fibre composite panels. *International journal of material forming*, *6*(1), 137–144.

Doo, R. (1993). Automotive body construction using self-piercing riveting. *Automotive Manufacturing International*.

Duan, H., Han, G., Wang, M., Zhang, X., Liu, Z., & Liu, Z. (2014). Rotation friction pressing riveting of az31 magnesium alloy sheet. *Materials & Design (1980-2015)*, *54*, 414–424.

Durandet, Y., Deam, R., Beer, A., Song, W., & Blacket, S. (2010). Laser assisted self-pierce riveting of az31 magnesium alloy strips. *Materials & Design*, *31*, S13–S16.

Fiore, V., Alagna, F., Di Bella, G., & Valenza, A. (2013). On the mechanical behavior of bfrp to aluminum aa6086 mixed joints. *Composites Part B: Engineering*, *48*, 79–87.

Franco, G. D., Fratini, L., & Pasta, A. (2012). Fatigue behaviour of self-piercing riveting of aluminium blanks and carbon fibre composite panels. *Proceedings of the Institution of Mechanical Engineers, Part L: Journal of Materials: Design and Applications*, *226*(3), 230–241.

Fratini, L., & Ruisi, V. F. (2009). Self-piercing riveting for aluminium alloys-composites hybrid joints. *The International Journal of Advanced Manufacturing Technology*, *43*(1-2), 61.

Fu, M., & Mallick, P. (2003). Fatigue of self-piercing riveted joints in aluminum alloy 6111. *International Journal of Fatigue*, *25*(3), 183–189.

Galtier, A., & Gacel, J.-N. (2002). *Fatigue behavior of mechanical joining for hss grades* (Tech. Rep.). SAE Technical Paper.

Gay, A., Lefebvre, F., Bergamo, S., Valiorgue, F., Chalandon, P., Michel, P., & Bertrand, P. (2015). Fatigue of aluminum/glass fiber reinforced polymer composite assembly joined by self-piercing riveting. *Procedia Engineering*, *133*, 501–507.

Gay, A., Lefebvre, F., Bergamo, S., Valiorgue, F., Chalandon, P., Michel, P., & Bertrand, P. (2016). Fatigue performance of a self-piercing rivet joint between aluminum and glass fiber reinforced thermoplastic composite. *International Journal of Fatigue*, *83*, 127–134.

Gladman, T. (1999). Precipitation hardening in metals. *Materials science and technology*, *15*(1), 30–36.

Hadley, S., Das, S., & Miller, J. (2000). Aluminum r&d for automotive uses and the department of energys role. *Oak Ridge National Laboratory*, 1–28.

Hahn, O., & Horstmann, M. (2007). Mechanical joining of magnesium components by means of inductive heating-realization and capability. In *Materials science forum* (Vol. 539, pp. 1638–1643).

Han, G., Wang, M., Liu, Z., & Wang, P.-C. (2013). A new joining process for magnesium alloys: rotation friction drilling riveting. *Journal of Manufacturing Science and Engineering*, *135*(3), 031012.

Han, L., & Chrysanthou, A. (2008). Evaluation of quality and behaviour of self-piercing riveted aluminium to high strength low alloy sheets with different surface coatings. *Materials & Design*, *29*(2), 458–468.

Han, L., Thornton, M., Li, D., & Shergold, M. (2010). *Effect of setting velocity on self-piercing riveting process and joint behaviour for automotive applications* (Tech. Rep.). SAE Technical Paper.

Han, L., Thornton, M., & Shergold, M. (2010). A comparison of the mechanical behaviour of self-piercing riveted and resistance spot welded aluminium sheets for the automotive industry. *Materials & Design*, *31*(3), 1457–1467.

Han, L., Young, K., Chrysanthou, A., & Osullivan, J. (2006). The effect of pre-straining on the mechanical behaviour of self-piercing riveted aluminium alloy sheets. *Materials & design*, *27*(10), 1108–1113.

Han, L., Young, K., Hewitt, R., Alkahari, M., & Chrysanthou, A. (2006). *Effect of sheet material coatings on quality and strength of self-piercing riveted joints* (Tech. Rep.). SAE Technical Paper.

Haque, R., Beynon, J., & Durandet, Y. (2012). Characterisation of force–displacement curve in self-pierce riveting. *Science and Technology of Welding and joining*, *17*(6), 476–488.

He, X., Gu, F., & Ball, A. (2012). Recent development in finite element analysis of self-piercing riveted joints. *The international journal of advanced manufacturing technology*, *58*(5-8), 643–649.

He, X., Pearson, I., & Young, K. (2008). Self-pierce riveting for sheet materials: state of the art. *Journal of materials processing technology*, *199*(1-3), 27–36.

He, X., Wang, Y., Lu, Y., Zeng, K., Gu, F., & Ball, A. (2015). Self-piercing riveting of similar and dissimilar titanium sheet materials. *The International Journal of Advanced Manufacturing Technology*, *80*(9-12), 2105–2115.

He, X., Zhao, L., Deng, C., Xing, B., Gu, F., & Ball, A. (2015). Self-piercing riveting of similar and dissimilar metal sheets of aluminum alloy and copper alloy. *Materials & Design (1980-2015)*, *65*, 923–933.

Hegde, S., & Prabhu, K. N. (2008). Modification of eutectic silicon in al–si alloys. *Journal of materials science*, *43*(9), 3009–3027.

Hill, H. (1994). Introduction to the self-pierce riveting process and equipment. *IBEC'94-Body Assembly & Manufacturing*, 1–9.

Hoang, N.-H., Hopperstad, O., Langseth, M., & Westermann, I. (2013). Failure of aluminium self-piercing rivets: an experimental and numerical study. *Materials & Design*, *49*, 323–335.

Hoang, N.-H., Porcaro, R., Langseth, M., & Hanssen, A.-G. (2010). Self-piercing riveting connections using aluminium rivets. *International Journal of Solids and Structures*, *47*(3-4), 427–439.

Hou, W., Mangialardi, E., Hu, S., Wang, P., & Menassa, R. (2004). Characterization for quality monitoring of a self-piercing riveting process. In *Aws sheet metal welding conference xi, paper* (pp. 8–3).

Huang, Z., Xue, S., Lai, J., Xia, L., & Zhan, J. (2014). Self-piercing riveting with inner flange pipe rivet. *Procedia Engineering*, *81*, 2042–2047.

Hulbert, J. (1972). Riveting without prepunching. *Machine design*, *44*(8), 73.

Iguchi, H., & Ohmi, Y. (2003). *Joining technologies for aluminum body-improvement of self-piercing riveting* (Tech. Rep.). SAE Technical Paper.

Kaščák, L., & Spišák, E. (2012). Joining materials by self-piercing riveting method. *Transfer inovácií*, *22*, 43–46.

Kato, T., Abe, Y., & Mori, K. (2007). Finite element simulation of self-piercing riveting of three aluminium alloy sheets. In *Key engineering materials* (Vol. 340, pp. 1461–1466).

Khanna, S., Long, X., Krishnamoorthy, S., & Agrawal, H. (2006). Fatigue properties and failure characterisation of self-piercing riveted 6111 aluminium sheet joints. *Science and Technology of Welding and Joining*, *11*(5), 544–549.

Khezri, R., Sjöström, E., & Melander, A. (2000). Self-piercing riveting of high strength steel. *Swedish Institute for Metal Research: Report No.: IM-2000-554*.

Kim, D.-W., Xu, J., Li, W., & Blake, D. (2006). Force characteristics of self-piercing riveting. *Proceedings of the Institution of Mechanical Engineers, Part B: Journal of Engineering Manufacture*, *220*(8), 1259–1266.

King, R. P., OSullivan, J. M., Spurgeon, D., & Bentley, P. (1995). Setting load requirements and fastening strength in the self-pierce riveting process. In *Proceedings of the 11th national conference on manufacturing research* (pp. 57–61).

Krause, A., & Chernenkoff, R. (1995). *A comparative study of the fatigue behavior of spot welded and mechanically fastened aluminum joints* (Tech. Rep.). SAE Technical Paper.

Krishnappa, U. S. (2008). *Numerical investigation of self-piercing riveted dual layer joint*. Unpublished doctoral dissertation, Wichita State University.

Lappe, W., & Budde, L. (1993). Possibilities for monitoring and controlling the mechanical process in sheet metal assembly. *Paderborn University*.

Li, B., & Fatemi, A. (2006). An experimental investigation of deformation and fatigue behavior of coach peel riveted joints. *International journal of fatigue*, *28*(1), 9–18.

Li, D., Chrysanthou, A., Patel, I., & Williams, G. (2017). Self-piercing riveting-a review. *The International Journal of Advanced Manufacturing Technology*, *92*(5-8), 1777–1824.

Li, D., Han, L., Chrysanthou, A., Shergold, M., & Williams, G. (2014). The effect of setting velocity on the static and fatigue strengths of self-piercing riveted joints for automotive applications. In *Tms 2014: 143rd annual meeting & exhibition* (pp. 557–564).

Li, D., Han, L., Thornton, M., & Shergold, M. (2010). *An evaluation of quality and performance of self-piercing riveted high strength aluminium alloy aa6008 for automotive applications* (Tech. Rep.). SAE Technical Paper.

Li, D., Han, L., Thornton, M., & Shergold, M. (2012). Influence of edge distance on quality and static behaviour of self-piercing riveted aluminium joints. *Materials & Design*, *34*, 22–31.

Li, D., Han, L., Thornton, M., Shergold, M., & Williams, G. (2014). The influence of fatigue on the stiffness and remaining static strength of self-piercing riveted aluminium joints. *Materials & Design (1980-2015)*, *54*, 301–314.

Li, D. Z., Han, L., Lu, Z. J., Thornton, M., & Shergold, M. (2012). Influence of die profiles and cracks on joint buttons on the joint quality and mechanical strengths of high strength aluminium alloy joint. In *Advanced materials research* (Vol. 548, pp. 398–405).

Liu, X., Lim, Y. C., Li, Y., Tang, W., Ma, Y., Feng, Z., & Ni, J. (2016). Effects of process parameters on friction self-piercing riveting of dissimilar materials. *Journal of Materials Processing Technology*, *237*, 19–30.

Lou, M., Li, Y., Li, Y., & Chen, G. (2013). Behavior and quality evaluation of electroplastic self-piercing riveting of aluminum alloy and advanced high strength steel. *Journal of Manufacturing Science and Engineering*, *135*(1), 011005.

Lou, M., Li, Y., Wang, Y., Wang, B., & Lai, X. (2014). Influence of resistance heating on self-piercing riveted dissimilar joints of aa6061-t6 and galvanized dp590. *Journal of Materials Processing Technology*, *214*(10), 2119–2126.

Luo, A., Lee, T., & Carter, J. (2011). Self-pierce riveting of magnesium to aluminum alloys. *SAE International Journal of Materials and Manufacturing*, *4*(1), 158–165.

Ma, Y., Lou, M., Yang, Z., & Li, Y. (2015). Effect of rivet hardness and geometrical features on friction self-piercing riveted joint quality. *Journal of Manufacturing Science and Engineering*, *137*(5), 054501.

Madasamy, C., Faruque, O., & Tyan, T. (2002). Experimental study on the crash performance of aluminum and steel rails. In *Asme 2002 international mechanical engineering congress and exposition* (pp. 223–231).

Madasamy, C., Faruque, O., Tyan, T., & Thomas, R. (2001). Static and impact behavior of self-pierced rivet connections in aluminum. *ASME APPLIED MECHANICS DIVISION-PUBLICATIONS-AMD*, *250*, 73–80.

Miller, W., Zhuang, L., Bottema, J., Wittebrood, A., De Smet, P., Haszler, A., & Vieregge, A. (2000). Recent development in aluminium alloys for the automotive industry. *Materials Science and Engineering: A*, *280*(1), 37–49.

Mizukoshi, H., & Okada, H. (1997). Fatigue properties of mechanical fastening joints. In *Materials science forum* (Vol. 242, pp. 231–238).

Mori, K., Abe, Y., & Kato, T. (2012). Mechanism of superiority of fatigue strength for aluminium alloy sheets joined by mechanical clinching and self-pierce riveting. *Journal of Materials Processing Technology*, *212*(9), 1900–1905.

Mori, K., Abe, Y., & Kato, T. (2014). Self-pierce riveting of multiple steel and aluminium alloy sheets. *Journal of Materials Processing Technology*, *214*(10), 2002–2008.

Mori, K., Kato, T., Abe, Y., & Ravshanbek, Y. (2006). Plastic joining of ultra high strength steel and aluminium alloy sheets by self piercing rivet. *CIRP Annals-Manufacturing Technology*, *55*(1), 283–286.

Mortimer, J. (2001). Jaguar uses x350 car to pioneer use of self-piercing rivets. *Industrial Robot: An International Journal*, *28*(3), 192–198.

Mucha, J. (2011). A study of quality parameters and behaviour of self-piercing riveted aluminium sheets with different joining conditions. *Strojniški vestnik-Journal of Mechanical Engineering*, *57*(4), 323–333.

Mucha, J. (2014). The numerical analysis of the effect of the joining process parameters on self-piercing riveting using the solid rivet. *Archives of Civil and Mechanical Engineering*, *14*(3), 444–454.

Mucha, J. (2015). The failure mechanics analysis of the solid self-piercing riveting joints. *Engineering Failure Analysis*, *47*, 77–88.

Mucha, J., Kaščák, L., & Spišák, E. (2013). The experimental analysis of forming and strength of clinch riveting sheet metal joint made of different materials. *Advances in Mechanical Engineering*, *5*, 848973.

Mucha, J., & Witkowski, W. (2013). The experimental analysis of the double joint type change effect on the joint destruction process in uniaxial shearing test. *Thin-Walled Structures*, *66*, 39–49.

Patrick, E., & Sharp, M. (1992). *Joining aluminum auto body structure* (Tech. Rep.). SAE Technical Paper.

Pickin, C., Young, K., & Tuersley, I. (2007). Joining of lightweight sandwich sheets to aluminium using self-pierce riveting. *Materials & design*, *28*(8), 2361–2365.

Porcaro, R., Hanssen, A., Langseth, M., & Aalberg, A. (2006a). The behaviour of a self-piercing riveted connection under quasi-static loading conditions. *International journal of solids and structures*, *43*(17), 5110–5131.

Porcaro, R., Hanssen, A., Langseth, M., & Aalberg, A. (2006b). Self-piercing riveting process: An experimental and numerical investigation. *Journal of Materials Processing Technology*, *171*(1), 10–20.

Presz, W., & Cacko, R. (2010). Analysis of the influence of a rivet yield stress distribution on the micro-spr joint–initial approach. *Archives of civil and mechanical engineering*, *10*(4), 69–75.

Razmjoo, G., & Westgate, S. (1999). Fatigue properties of clinched, self-piercing riveted and spot welded joints in steel and aluminium alloy sheet. *TWI Report*, *680*, 1999.

Riches, S., Westgate, S., Nicholas, E., & Powell, H. (1995). Advanced joining technologies for lightweight vehicle manufacture. In *Proceedings of the materials for lean weight vehicles conference, institute of materials* (pp. 137–146).

Rivet types. (2018). `http://www.henrob.com/products/rivets/rivet-types/`. (Online)

Settineri, L., Atzeni, E., & Ippolito, R. (2010). Self piercing riveting for metal-polymer joints. *International journal of material forming*, *3*(1), 995–998.

Sjöström, E. (2006). *Self piercing riveting and adhesive bonding of cast magnesium to ultra high strength sheet steel.* Kimab, Report No.: IM-2006-501.

Stephens, E. (2014). Mechanical strength of self-piercing riveting (spr). In *Self-piercing riveting* (pp. 11–32). Elsevier.

Sun, X. (2014). Optimization of the strength of self-piercing rivets (sprs). In *Self-piercing riveting* (pp. 149–170). Elsevier.

Sunday, S. P. (1983). *Self-piercing rivets for aluminum components* (Tech. Rep.). SAE Technical Paper.

Svensson, L.-E., & Larsson, J. K. (2002). Welding and joining of high performance car bodies. *Steel world*, *7*, 21–27.

Taylor, G. (1997). Self-piercing riveting in automotive assembly. In *The 30th international symposium on automotive technology and automotation (isata)* (pp. 229–240).

Ueda, M., Miyake, S., Hasegawa, H., & Hirano, Y. (2012). Instantaneous mechanical fastening of quasi-isotropic cfrp laminates by a self-piercing rivet. *Composite Structures*, *94*(11), 3388–3393.

Wang, B., Hao, C., Zhang, J., & Zhang, H. (2006). A new self-piercing riveting process and strength evaluation. *Journal of Manufacturing Science and Engineering*, *128*(2), 580–587.

Wang, J., Liu, Z., Shang, Y., Liu, A., Wang, M., Sun, R., & Wang, P.-C. (2011). Self-piercing riveting of wrought magnesium az31 sheets. *Journal of Manufacturing Science and Engineering*, *133*(3), 031009.

Wang, L., & Shivkumar, S. (1995). Strontium modification of aluminium alloy castings in the expendable pattern casting process. *Journal of materials Science*, *30*(6), 1584–1594.

Weber, A. (2015). Assembling fords aluminum wonder truck. *Assembly (Magazine)*, *58*(3).

Westerberg, C. (2002). Finite element simulation of crash testing of self-piercing rivet joints, peel specimen.

Westgate, S., Doo, R., Liebrecht, F., Braeunling, S., Mattsson, T., & Strömberg, K. (2001). *The development of lightweight self-piercing riveting equipment* (Tech. Rep.). SAE Technical Paper.

Xu, Y. (2006). A close look at self-piercing rivetingcomputer simulation is a noteworthy alternative to physical testing of joints. *The fabricator*.

Zhang, J., & Yang, S. (2015). Self-piercing riveting of aluminum alloy and thermoplastic composites. *Journal of Composite Materials*, *49*(12), 1493–1502.

Zhang, X., He, X., Xing, B., Zhao, L., Lu, Y., Gu, F., & Ball, A. (2016). Influence of heat treatment on fatigue performances for self-piercing riveting similar and dissimilar titanium, aluminium and copper alloys. *Materials & Design*, *97*, 108–117.

APPENDIX A. SHEAR TEST, CRACK CALCULATION AND MECHANICAL PROPERTY OF ALUMINUM ALLOY DATA

Table A.1. Shear test results with different die depth (Unit: N-mm)

	1.8mm	2.0mm	2.2mm
As Cast	22754	17136	12903
200°C	21726	16742	13577
250°C	26909	24407	16394
300°C	22543	16603	18682
350°C	25154	22234	23096
400°C	21296	24202	20320

Table A.2. The large cracks fraction results by using different die depth

	1.8mm	2.0mm	2.2mm
As Cast	0.2779	0.4913	0.5364
200°C	0.3579	0.4317	0.5884
250°C	0.3734	0.3917	0.6134
300°C	0.2955	0.3467	0.3962
350°C	0.1719	0.3229	0.3835
400°C	0.0285	0.1915	0.2632

Table A.3. The results of total energy over larger crack fraction using different die depth (Unit: N-mm)

	1.8mm	2.0mm	2.2mm
As Cast	81878	34879	24055
200°C	60704	38782	23074
250°C	72065	62310	26726
300°C	76288	47889	47153
350°C	146329	68857	60224
400°C	747228	126381	77204

Table A.4. The statistical results of counting cracks on joint button with 1.8 mm die depth

	Small Cracks	Large Cracks	Perimeter	S/P	L/P
As Cast	0	8.404	30.241	0	0.2779
200°C	1	10.488	29.304	0.0341	0.3579
250°C	0	10.977	29.4	0	0.3734
300°C	1	8.576	29.021	0.0345	0.2955
350°C	5	5.121	29.797	0.1678	0.1719
400°C	6	0.866	30.337	0.1978	0.0285

Table A.5. The statistical results of counting cracks on joint button with 2.0 mm die depth

	Small Cracks	Large Cracks	Perimeter	S/P	L/P
As Cast	0	13.954	28.402	0	0.4913
200°C	0	12.466	28.877	0	0.4317
250°C	0	10.991	28.059	0	0.3917
300°C	0	9.845	28.398	0	0.3467
350°C	0	9.614	29.772	0	0.3229
400°C	10	5.696	29.742	0.3362	0.1915

Table A.6. The statistical results of counting cracks on joint button with 2.2 mm die depth

	Small Cracks	Large Cracks	Perimeter	S/P	L/P
As Cast	0	14.967	27.905	0	0.5364
200°C	0	16.649	28.295	0	0.5884
250°C	0	17.602	28.698	0	0.6134
300°C	0	11.076	27.955	0	0.3962
350°C	0	11.113	28.981	0	0.3835
400°C	3	7.493	28.474	0.1054	0.2632

Table A.7. The mechanical property of aluminum alloy under different heat treatment conditions

Aging Temp. and Time	UTS (MPa)	YS (MPa)	Elongation (%)	Hardness (HRF)
0 (As Cast)	260.3	133.7	9.62	74
200°C 3hrs	268.0	173.8	8.57	77
250°C 3hrs	225.5	127.3	10.28	71
300°C 3hrs	212.1	126.7	10.68	65
350°C 3hrs	188.4	102.7	12.28	56
400°C 3hrs	177.0	105.7	18.53	39